EQUATIONS OF STATES FOR WHITE DWARFS AND NEUTRON STARS

By

SOMNATH MUKHOPADHYAY

Enrollment No.: PHYS04201304007

VARIABLE ENERGY CYCLOTRON CENTRE,

1/AF, Bidhannagar, Kolkata 700 064, India.

A Thesis submitted to the

Board of Studies in Physical Sciences

In partial fulfillment of requirements

for the Degree of

DOCTOR OF PHILOSOPHY

of

HOMI BHABHA NATIONAL INSTITUTE

May, 2019.

Homi Bhabha National Institute[1]

Recommendations of the Viva Voce Committee

As members of the Viva Voce Committee, we certify that we have read the dissertation prepared by **Shri Somnath Mukhopadhyay** entitled '**Equations of states for White Dwarfs and Neutron Stars**' and recommend that it may be accepted as fulfilling the thesis requirement for the award of Degree of Doctor of Philosophy.

Chairman - Prof. Jan-e Alam	Jane Alam	**Date:**	24/5/2019
Guide / Convener - Prof. D. N. Basu	DNBasu	**Date:**	24/05/2019
Co-guide - <Name> (if any)		**Date:**	
Examiner - Prof. Rajeev Puri		**Date:**	24/05/2019
Member 1- Prof. Gargi Chaudhuri	Gargi Chaudhuri	**Date:**	29.5.2019
Member 2- Prof. D.Bandyopadhyay	Debades Bandyopadhyay	**Date:**	24.5.2019

Final approval and acceptance of this thesis is contingent upon the candidate's submission of the final copies of the thesis to HBNI.

I/We hereby certify that I/we have read this thesis prepared under my/our direction and recommend that it may be accepted as fulfilling the thesis requirement.

Date: 24/05/2019

Place: Kolkata

<Signature>
Co-guide (if applicable)

DNBasu
Prof. D. N. Basu
Guide

1 This page is to be included only for final submission after successful completion of viva voce.

STATEMENT BY AUTHOR

This dissertation has been submitted in partial fulfillment of requirements for an advanced degree at Homi Bhabha National Institute (HBNI) and is deposited in the Library to be made available to borrowers under rules of the HBNI.

Brief quotations from this dissertation are allowable without special permission, provided that accurate acknowledgement of source is made. Requests for permission for extended quotation from or reproduction of this manuscript in whole or in part may be granted by the Competent Authority of HBNI when in his or her judgment the proposed use of the material is in the interests of scholarship. In all other instances, however, permission must be obtained from the author.

Somnath Mukhopadhyay

Somnath Mukhopadhyay

DECLARATION

I, hereby declare that the investigation presented in the thesis has been carried out by me. The work is original and has not been submitted earlier as a whole or in part for a degree / diploma at this or any other Institution / University.

Somnath Mukhopadhyay

Somnath Mukhopadhyay

List of Publications arising from the thesis

(a) Journals :

[1] *"Nuclear constraints on the core-crust transition and crustal fraction of moment of inertia of neutron stars"*

Debasis Atta, **S Mukhopadhyay**, D.N. Basu

Indian J. Phys **91**, 235 (2017).

⋆ [2] *"Landau Quantization and mass-radius relation of magnetized white dwarfs in general relativity"*

Somnath Mukhopadhyay, Debasis Atta, D.N. Basu

Rom. Rep. Phys **69**, 101 (2017).

⋆ [3] *"Compact bifluid hybrid stars: Hadronic Matter mixed with self-interacting fermionic Asymmetric Dark Matter"*

Somnath Mukhopadhyay, Debasis Atta, Kouser Imam, D.N. Basu, C. Samanta

Eur.Phys.J. C **77**, 440 (2017) ; Erratum: Eur.Phys.J. C **77**, 553(2017).

⋆ [4] *"Gravitational waves from isolated neutron stars: mass dependence of r-mode instability"*

Somnath Mukhopadhyay, Joydev Lahiri, Debasis Atta, Kouser Imam, D.N. Basu

Phys.Rev. C **97**, 065804 (2018).

⋆ [5] *"Rossby modes in neutron stars as sources of gravitational waves"*

Sujan Roy, **Somnath Mukhopadhyay**, Joydev Lahiri, Debasis Atta, Partha Roy Chowdhury, D.N. Basu

arXiv:1905.06158 (2019). (Communicated to Physical Review C)

The papers with ⋆ symbol are included in the present thesis work.

(b) Conferences/Symposia:

⋆ [1] *"Mass radius relation of magnetized white dwarfs"*

Somnath Mukhopadhyay, Debasis Atta, D.N. Basu

Proceedings of the DAE Symposium on Nuclear Physics,

Satya Sai University, Andhra Pradesh, India, **60**, 838-839 (2015).

[2] *"Crustal fraction of moment of inertia of pulsars"*

Debasis Atta, **Somnath Mukhopadhyay**, D.N. Basu

Proceedings of the DAE Symposium on Nuclear Physics,

Satya Sai University, Andhra Pradesh, India, **60**, 854-855 (2015).

⋆ [3] *"Interacting & non-interacting fermionic dark matter and quark matter compact stars"*

Debasis Atta, **Somnath Mukhopadhyay**, D.N. Basu, C. Samanta

Proceedings of the DAE Symposium on Nuclear Physics,

Saha Institute of Nuclear Physics, Kolkata, India, **61**, 890-891 (2016).

⋆ [4] *"Quark matter and fermionic dark matter compact stars"*

C. Samanta, **Somnath Mukhopadhyay**, D. N. Basu

Bull. American Physical Society April meeting, Salt Lake City, Utah (2016).

⋆ [5] *"Formation of hadronic stars mixed with self-interacting fermionic asymmetric Dark Matter"*

C. Samanta, **Somnath Mukhopadhyay**, Debasis Atta, Kouser Imam, D.N. Basu

SFDE17: From Local Clouds to Distant Galaxies, ICISE, Quy Nhon, Vietnam (2017).

⋆ [6] *"Effect of the DDM3Y Nuclear equation of state on the r-mode instability of neutron stars"*

Debasis Atta, **Somnath Mukhopadhyay**, D.N. Basu

13th International Conference on Nucleus-nucleus Collisions, Saitama, Japan (2018).

Somnath Mukhopadhyay

Somnath Mukhopadhyay

Dedicated To

My Parents and my Grandmother

Acknowledgements

I would like to express my deep respect to my Ph.D. supervisor, Prof. D.N. Basu for his support and encouragement during my work with him. This work could not have been successful without his valuable suggestions.

I am thankful to Prof. Amitava Roy, Director of Variable Energy Cyclotron Centre and Prof. Jan-e-Alam, Head of Physics Group for providing all the necessary facilities in the institute. I am also thankful to Prof. Gargi Chaudhuri, Prof. Debades Bandyopadhyay, Head of Astroparticle Physics and Cosmology Division, Saha Institute of Nuclear Physics and Prof. Chhanda Samanta, Virginia Military Institute, for their constant guidance during my thesis work.

I also want to express my gratitude to Dr. Debasis Atta and my seniors and friends of V.E.C.C. for their constant inspiration during my Ph.D. work. Special gratefulness is expressed to all the faculty members and staff of V.E.C.C. for their help and cooperation. Thanks are also due to the staff of the library, canteen, administration and accounts sections of V.E.C.C.

And last but not the least, I would like to express my deepest reverence to my parents and my grandmother for their love, care, affection and motivation without which nothing would have been possible in my life.

Somnath Mukhopadhyay

Somnath Mukhopadhyay

Homi Bhabha National Institute

SYNOPSIS OF Ph. D. THESIS

1. **Name of the Student: Shri Somnath Mukhopadhyay**
2. **Name of the Constituent Institution: Variable Energy Cyclotron Centre**
3. **Enrolment No. : PHYS04201304007**
4. **Title of the Thesis: Equations of states for White Dwarfs and Neutron Stars**
5. **Board of Studies: Physical Science**

SYNOPSIS

(Limited to 10 pages in double spacing)

The recently observed peculiar Type Ia supernovae, e.g. SN2006gz, SN2007if, SN2009dc, SN2003fg, [1, 2, 3, 4, 5] with exceptionally high luminosities do not fit with the explosion of a Chandrasekhar mass white dwarf. Moreover, it has been seen that there is a correlation between the surface magnetic field and the mass of white dwarfs. The magnetic white dwarfs seem to be more massive than their nonmagnetic counterparts [6]. Lastly, predictions from the luminosities reveal that the progenitor white dwarfs had masses significantly higher than the Chandrasekhar limit. It seems that the Chandrasekhar limit may be violated by highly magnetized white dwarfs [7]. To account for these facts, we have calculated theoretically the masses of white dwarfs in presence of such high magnetic fields in the general relativistic formalism.

We consider a completely degenerate relativistic electron gas at zero temperature but embedded in a strong magnetic field. We do not consider any form of interactions with the electrons. Electrons, being charged particles, occupy Landau quantized states in a magnetic field. This changes the Equation of State (EoS), which, in turn, changes the pressure and energy density of the white dwarf. In addition to the matter energy density and pressure, the energy density and pressure due to magnetic field are also taken into account. It is the combined pressure and energy density of matter and magnetic field that determines the mass-radius relation of strongly magnetized white dwarfs. It should be emphasized that protons also, being charged particles, are Landau quantized. But since the proton mass is ~ 2000 times the electron mass their cyclotron energy is ~ 2000 times smaller than that of the electron for the same magnetic field, and hence we neglect it.

We present stable solutions of magnetostatic equilibrium models for super-Chandrasekhar white dwarfs with varying magnetic field profiles which is maximum at the centre and goes to 10^9 gauss at the surface of the star by solving the Tolman-Oppenheimer-Volkoff (TOV) equations [8, 9] . This has been obtained by self-consistently including the effects of the magnetic pressure gradient and total magnetic energy density in a general rela-

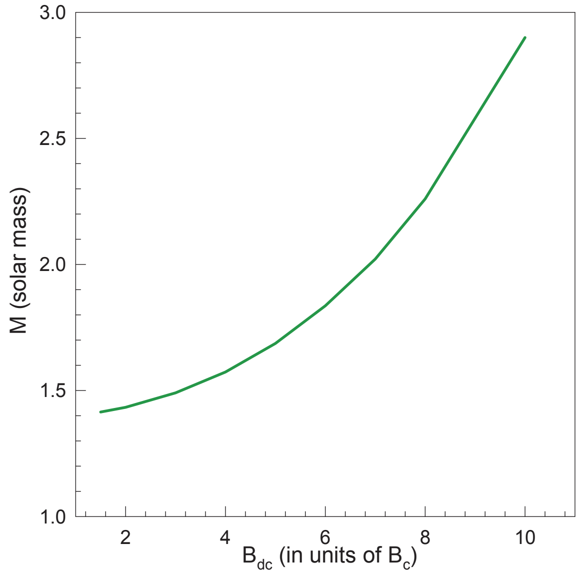

Figure 1: Plot for masses of magnetized white dwarfs as a function of central magnetic field.

tivistic framework. Nevertheless, we have also performed calculations corresponding to very high (single Landau level) and high (multi Landau levels) magnetic field which is constant throughout the star.

In Fig.-1 plot for masses of magnetized white dwarfs are shown as functions of central magnetic field. Present calculations estimate that the maximum stable mass of magnetized white dwarfs could be $\sim 3\ M_{\odot}$. These results are quite useful in explaining the peculiar, overluminous type Ia supernovae that do not conform to the traditional Chandrasekhar mass-limit.

We next consider fermionic Asymmetric Dark Matter (ADM) [10, 11] particles of mass 1 GeV and the self-interaction mediator mass of 100 MeV (low mass implying strong interaction), mixed with rotating and non-rotating neutron stars. Similar hybrid stellar cofigurations have been studied before [12, 13, 14]. ADM, like ordinary baryonic matter, is charge asymmetric with only the dark baryon (or generally only the particle) excess remains after the annihilation of most antiparticles after the Big Bang. Hence

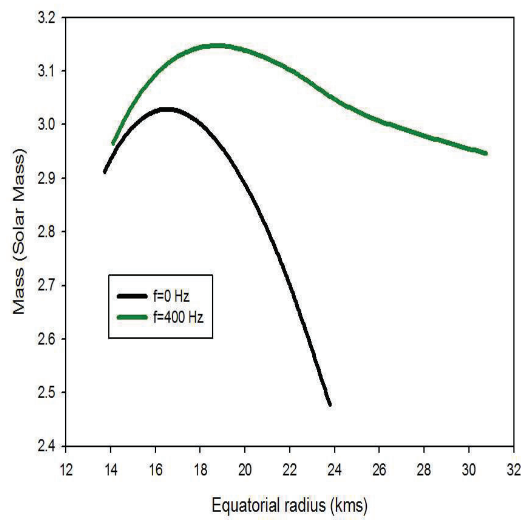

Figure 2: Mass-equatorial radius plots for static and rotating fermionic Asymmetric Dark Matter stars.

these ADM particles are non self-annihilating and behaves like ordinary free particles. The gravitational stability and mass-radius relations of static, rigidly and differentially rotating neutron stars mixed with fermionic ADM are calculated using the LORENE code [15]. It is important to note that we do not allow any phase transition of the nuclear matter and the interaction between nuclear matter and dark matter is only through gravity.

Fig.-2 depicts the plots of mass vs. equatorial radius for static and rotating pure dark stars using self-interacting fermionic dark matter EoS. We see that the maximum mass for non-rotating stars goes to $3.0279M_{\odot}$ with a radius of 16.2349 kms and that for rotating stars with frequency 400 Hz goes to $3.1460M_{\odot}$ with equatorial radius of 19.2173 kms. Now, if we take the dark matter particle mass m_{χ} to be 0.5 GeV, then the maximum mass goes to $\sim 12.6M_{\odot}$ using the relation Mass $\propto 1/m_{\chi}^2$, thus mimicking stellar mass black holes.

To compute the equilibrium models of rotating and non-rotating neutron stars admixed with fermionic ADM, we have used the nuclear matter EoS which is calculated using the isoscalar and the isovector components of M3Y interaction along with density dependence. The density dependence of this DDM3Y effective interaction is completely determined from nuclear matter calculations. The maximum mass of a pure neutron star with DDM3Y effective interaction goes to $1.9227M_{\odot}$ with a radius of 9.7559 kms [16, 17, 18].

We consider two ideal fluids - the nuclear matter and fermionic dark matter with the above two EoSs coupled gravitationally to form the structure of the mixed neutron star.In Fig.-3 the plots of total mass vs. equatorial radius of static, rigidly and differentially rotating neutron stars mixed with fermionic self-interacting dark matter are shown for fixed dark matter central enthalpy ($0.24c^2$) and varying nuclear matter central enthalpies. The maximum mass of the neutron star mixed with strongly self-interacting dark matter goes to $1.3640M_{\odot}$ with a corresponding radius of 6.7523 kms for the case of differential rotation (frequency of dark matter to be 300 Hz and that of nuclear matter to be 700 Hz) as shown in Fig.-3. In Fig.-4 the plots of total mass vs. equatorial radius of static, rigidly and differentially rotating neutron stars mixed with fermionic self-interacting dark matter are shown for fixed nuclear matter central enthalpy ($0.24c^2$) and varying dark matter central enthalpies. In this case the maximum mass goes to $1.9355M_{\odot}$ with a corresponding radius of 10.3717 kms for the case of differential rotation (frequency of dark matter to be 700 Hz and that of nuclear matter to be 300 Hz) as shown in Fig.-4.

We also find that the dark matter dominated neutron star behaves differently than the nuclear matter dominated one that show characteristics similar to low mass self-bound strange stars. This is because of the very strong two-body repulsive interactions of dark matter which is dominant in the low mass region where it counteracts gravity effectively to make radius much smaller. Thus, while the nuclear matter dominance induces gravitational binding, dark matter dominant low mass neutron star becomes more compact. However, if the dark matter particle mass is small compared to the nucleon mass the maximum mass may well be above $2M_{\odot}$, provided no phase transition from nuclear to quark matter occurs.

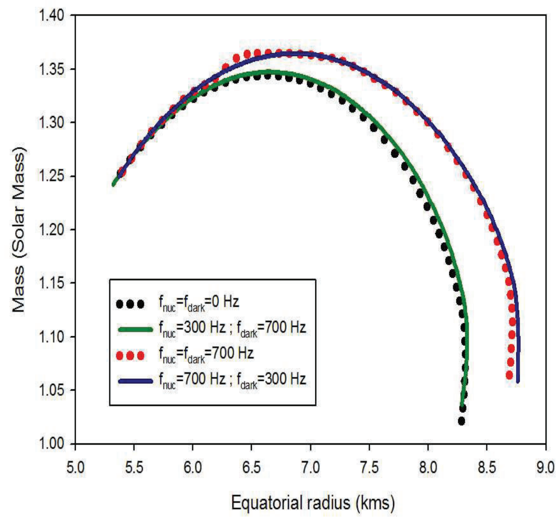

Figure 3: Plots of total mass vs. equatorial radius of static, rigidly rotating and differentially rotating neutron stars mixed with interacting fermionic Asymmetric Dark Matter with fixed dark matter central enthalpy ($0.24c^2$) and varying nuclear matter central enthalpies.

Rotational instabilities in NSs come in different flavours, but they have one general feature in common: they can be directly associated with unstable modes of oscillation [19]. In the present work the r-mode instability has been discussed with reference to the EoS obtained using the density dependent M3Y (DDM3Y) effective nucleon-nucleon (NN) interaction. The discovery of r-mode oscillation in neutron star (NS) by Anderson [19] and confirmed by Friedman and Morsink [20] opened the window for study of the gravitational wave emitted by NSs by using advance detecting system. Also it provides the possible explanation for the spin down mechanism in the hot young NSs as well as in spin up cold old accreting NSs.

The concern here is to study the evolution of the r-modes due to the competition of gravitational radiation and dissipative influence of viscosity.The instability in the mode

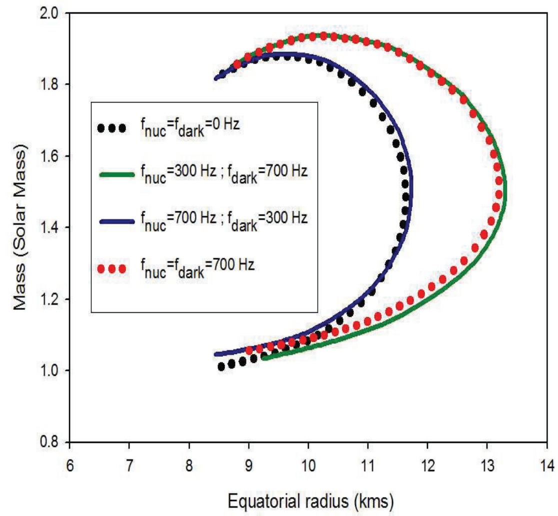

Figure 4: Plots of total mass vs. equatorial radius of static, rigidly rotating and differentially rotating neutron stars mixed with interacting fermionic Asymmetric Dark Matter with fixed nuclear matter central enthalpy ($0.24c2$) and varying dark matter central enthalpies.

grows because of gravitational wave emission which is opposed by the viscosity. For the instability to be relevant, it must grow fast than it is damped out by the viscosity. So the time scale for gravitationally driven instability needs to be sufficiently short to the viscous damping time scale. The shear viscosity time scale is obtained by considering the shear dissipation in the viscous boundary layer between solid crust and the liquid core with the assumption that the crust is rigid and hence static in rotating frame [21].

Bildsten and Ushomirsky [22] have first estimated this effect of solid crust on r-mode instability and shown that the shear dissipation in this viscous boundary layer decreases the viscous damping time scale by more than 10^5 in old acreting neutron stars and more than 10^7 in hot, young neutron stars. Moreover, the bulk viscous dissipation is not significant for temperature of the star below 10^{10} K and in this range of temperature the shear viscosity is the dominant dissipative mechanism, We have restricted our study in

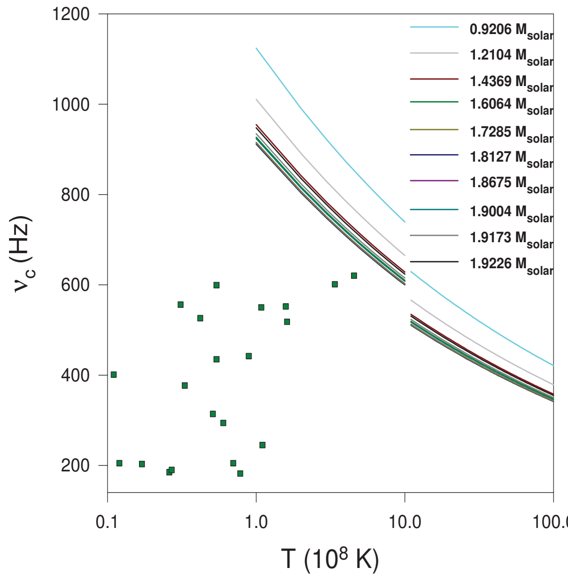

Figure 5: Plots of critical frequency with temperature for different masses of neutron stars. The square dots represent observational data [25].

this work to the range of the temperature $T < 10^{10}$ K and included only shear dissipative mechanism. The studies is similar to the one done by Moustakidis [23], where we have mainly examined the influence of neutron star EoS and the gravitational mass on the instability boundary and other relevant quantities, such as, critical frequency and temperature, etc. for a neutron star using the DDM3Y effective interaction [24].

In Fig.-5, the critical frequency is shown as a function of temperature T for several masses of neutron stars for the DDM3Y EoS. The square dots represent observed Low Mass X-ray Binaries(LMXBs) and Millisecond Radio Pulsars (MSRPs).The plots act as boundaries of the r-mode instability windows. Neutron stars lying above the plots (whose angular frequency is greater than the critical frequency) possess unstable r-modes and hence emit gravitational waves, thus reducing their angular frequencies. Once their angular velocities reach the critical frequency they enter the region below the plots, where the r-modes become stable and hence stop emitting gravitational radiation. From Fig.-5, it is interesting to note that according to our model of the EoS with a rigid crust and a relatively small r-mode amplitude, all of the observed neutron stars lie in the stable r-mode region which is consistent with the lack of observation of gravitational radiation due to r-mode instability. We have also pointed out the fact that the critical frequency depends on the EoS through the radius and the symmetry energy slope parameter L. If the dissipation of r-modes from shear viscosity acts along the boundary layer of the crust-core interface then the r-mode instability region is enlarged to lower values of L.

Bibliography

[1] D. Andrew Howell et al., Nature **443**, 308 (2006).

[2] R. A. Scalzo et al., Astrophys. J. **713**, 1073 (2010).

[3] M. Hicken et al., Astrophys. J. **669**, L17 (2007).

[4] M. Yamanaka et al., Astrophys. J. **707**, L118 (2009).

[5] Jeffrey M. Silverman et al., Mon. Not. R. Astron. Soc., **410**, 1 (2011).

[6] Lilia Ferrario, Domitilla deMartino, Boris T. Gansicke, arXiv: 1504.08072v1 (2015).

[7] U. Das and B. Mukhopadhyay, Phys. Rev. **D 86**, 042001 (2012).

[8] R. C. Tolman, Phys. Rev. **55**, 364 (1939).

[9] J. R. Oppenheimer and G. M. Volkoff Phys. Rev. **55**, 374 (1939).

[10] Gianfranco Bertone, Dan Hooper and Joseph Silk *Physics Reports* **405**, 279 (2005).

[11] George R. Blumenthal, S. M. Faber, Joel R. Primack and Martin J. Rees, *Nature* **311**, 517 (1984).

[12] A. de Lavallaz and M. Fairbairn, *Phys. Rev.* **D 81**, 123521 (2010).

[13] C. Kouvaris and P. Tinyakov, *Phys. Rev.* **D 82**, 063531 (2010).

[14] C. Kouvaris and P. Tinyakov, *Phys. Rev.* **D 83**, 083512 (2011).

[15] Eric Gourgoulhon *arXiv:1003.5015v2* (2011).

[16] D. Atta, S. Mukhopadhyay and D. N. Basu, *Indian J. Phys.*, **91**, 235 (2017).

[17] Debasis Atta and D. N. Basu, *Phys. Rev.* **C 90**, 035802 (2014).

[18] W. M. Seif and D. N. Basu, *Phys. Rev.* **C 89**, 028801 (2014).

[19] N. Andersson, Astrophys. J. **502**, 708 (1998).

[20] J. L. Friedman and S. M. Morsink, Astrophys. J. **502**, 714 (1998).

[21] L. Lindblom, B. J. Owen, and G. Ushomirsky, Phys. Rev. **D 62**, 084030 (2000).

[22] L. Bildsten and G. Ushomirsky, Astrophys. J. Lett. **529**, L33(2000).

[23] Ch. Moustakidis, Phys. Rev. **C 91**,035804 (2015).

[24] D. N. Basu, P. Roy Chowdhury and C. Samanta, Nucl. Phys. **A 811**, 140 (2008).

[25] B. Haskell, N. Degenaar and W. C. G. Ho, Mon. Not. R. Astron. Soc. **424**, 93 (2012).

Publications in Refereed Journal:

a. Published

1) Landau Quantization and mass-radius relation of magnetized white dwarfs in general relativity.

Somnath Mukhopadhyay, Debasis Atta, D.N. Basu, **Rom. Rep. Phys 69, 101 (2017)**.

2) Nuclear constraints on the core-crust transition and crustal fraction of moment of inertia of neutron stars.

Debasis Atta, **Somnath Mukhopadhyay**, D.N. Basu , **Ind. J. Phys. 91, 235-242 (2017).**

3) Compact bifluid hybrid stars: hadronic matter mixed with self-interacting fermionic asymmetric dark matter.

Somnath Mukhopadhyay, Debasis Atta, K. Imam, D.N. Basu, C. Samanta, **Eur. Phys. J. C. 77, 440 (2017).**

4) Gravitational waves from isolated neutron stars: mass dependence of r-mode instability.

Somnath Mukhopadhyay, Joydev Lahiri, Debasis Atta, Kouser Imam, D.N. Basu, **Phys.Rev. C 97, 065804 (2018).**

b. Accepted: NA

c. Communicated: NA

Other Publications:

a. Book/Book Chapter : NA

b. Conference/Symposium :

1) Mass radius relation of magnetized white dwarfs.
Somnath Mukhopadhyay, Debasis Atta, D.N. Basu, Proceedings of the DAE Symposium on Nuclear Physics, Satya Sai University, Andhra Pradesh, India, 60, 838-839 (2015).

2) Crustal fraction of moment of inertia of pulsars.
Debasis Atta, **Somnath Mukhopadhyay**, D.N. Basu, Proceedings of the DAE Symposium on Nuclear Physics, Satya Sai University, Andhra Pradesh, India, 60, 854-855 (2015).

3) Interacting & non-interacting fermionic dark matter and quark matter compact stars.
Debasis Atta, **Somnath Mukhopadhyay**, D.N. Basu, C. Samanta, Proceedings of the DAE Symposium on Nuclear Physics, Saha Institute of Nuclear Physics, Kolkata, India, 61, 890-891 (2016).

4) Quark matter and fermionic dark matter compact stars.
C. Samanta, **Somnath Mukhopadhyay,** D. N. Basu, Bull. American Physical Society April meeting, April 16-19, Salt Lake City, Utah (2016).

5) Formation of hadronic stars mixed with self-interacting fermionic Asymmetric Dark Matter.
Chhanda Samanta, **Somnath Mukhopadhyay**, Debasis Atta, Kouser Imam, D. N. Basu, SFDE17: From Local Clouds to Distant Galaxies, ICISE, Quy Nhon, Vietnam (2017).

Somnath Mukhopadhyay
Signature of Student:

Date: 31.08.2018.

Based on the scientific content of the lecture delivered by the candidate in the seminar, his capability to answer several questions raised in the seminar and his publications in refereed journals, Sri Somnath Mukhopadhyay may be permitted to write his thesis.

Doctoral Committee:

S. No.	Name	Designation	Signature	Date
1.	Prof. Jan-e Alam	Chairman	Jane Alam	31/8/18
2.	Prof. D. N. Basu	Guide/ Convener	D N Basu	31/08/2018
3.		Co-guide (if any)		
4.	Prof. Gargi Chaudhuri	Member	Gargi Chaudhuri	31.8.18
5.	Prof. D.Bandyopadhyay(SINP)	Member	Debades Bandyopadhyay	31.8.18
6.		Member		

Contents

List of Figures

List of Tables

Chapter 1

INTRODUCTION

Compact stars are exotic astrophysical objects formed as stellar remnants when a normal star runs out of nuclear fuel. Compact stars are of three types, namely, white dwarfs, neutron stars and black holes. A star shines and thus loses its nuclear energy reservoir in a finite time. When a star has exhausted all its energy, the gas pressure of the hot interior can no longer support the weight of the star and the star collapses to a denser state. The formation of the different types of compact stars depends on the mass of the normal star prior to the gravitational collapse. Stars with masses less than $10M_\odot$ at the end of their lifetime collapse into white dwarfs, those with $\sim 10-20M_\odot$ form neutron stars and those with masses greater than $20M_\odot$ form black holes.

A White Dwarf is a compact star whose mean mass is of the order of a Solar mass and mean radius of the order of 1000 kms. Hence its mean density is $\sim 10^9$ gms/cc, making a white dwarf one of the densest objects in the Universe. A white dwarf's interior is degenerate, and it is supported against gravitational collapse by the pressure of the extremely relativistic free electron gas. Since electrons are fermions and they are degenerate inside a white dwarf, at such densities they have extremely large kinetic energies and hence large pressure which is enough to support them against gravity. The atomic nuclei contributes mainly to the gravitational mass of a white dwarf. The composition of white dwarfs depends on the final product of nuclear fusion in the star before collapse. Very low mass stars produce helium white dwarfs, low to intermediate stars such as the Sun produce carbon-oxygen white dwarfs and slightly higher mass stars produce oxygen-neon-magnesium white dwarfs. White dwarfs have a maximum possible mass of $\sim 1.44M_{\odot}$, known as the Chandrasekhar limit, beyond which it is gravitationally unstable [1]. If a white dwarf's mass surpasses the Chandrasekhar limit, its interior undergoes runaway nuclear fusion which makes the white dwarf explode in a Type Ia supernova explosion.

Ultrahigh magnetic fields in nature are known to be associated with white dwarfs, neutron stars and black holes. Of these, the largest magnetic fields are found on the surfaces of magnetars, Anomalous X-ray Pulsars (AXPs) and Soft Gamma Repeaters (SGRs), certain classes of neutron stars, with an order of magnitude of 10^{15} gauss. Recently, a strong magnetic field of the same order of magnitude as that of a magnetar has been found at the jet base of a supermassive black hole PKS 1830-211 [2]. These strong magnetic fields drastically modify the Equation of State (EoS) of a compact star and its stability. Hence, studying the EoS and equilibria of compact stars in presence of high magnetic fields is an important and rapidly growing field of research in theoretical astrophysics. In this study we have incorporated the Landau quantization of electron gas embedded in a density-dependent magnetic field inside white dwarfs, consistent with observations, and showed that such ultramagnetized white dwarfs have masses well above the Chandrasekhar limit. These white dwarfs are hence called Super-Chandrasekhar white dwarfs.

Another class of compact stars are called Neutron Stars. A neutron star's mass is of the order of one solar mass but in contrast to a white dwarf, its radius is of the order of only 10 km. Hence the mean density of a neutron star is $\sim 10^{15}$ gms/cc, making a neutron star's interior to be the densest matter in the Cosmos. A neutron star is born from the violent core-collapse supernova explosion of a massive star generally known as

Type II supernova. At the pre-supernova stage, the massive star consists of a white dwarf-like iron core and surrounded by layers of less processed material from nuclear shell burning. The iron core doesn't fuse due to its highest binding energy per nucleon. As a result when mass is added to the core by shell burning, the core mass surpasses the Chandrasekhar limit,becomes unstable and collapses. During the collapse, the lepton content decreases due to net electron capture on nuclei and free protons. But when the core density approaches $\sim 10^{12}$ gms/cc, the neutrinos can no longer escape from the core on the dynamical time-scale. The core continues to collapse until the rapidly increasing pressure reverses the collapse at a bounce density of a few times nuclear density. This bounce results in a shock which is largely dissipated by the energy required to dissociate massive nuclei in the still infalling matter of the original iron core. The shock wave expels the outer layers of gas forming a supernova and the resultant supernova remnant becomes the newly born neutron star.

A neutron star's interior is enriched with a plethora of exotic phases of dense matter which makes its composition or the Equation of State (EoS) a total mystery till today. The interior can be broadly divided into three regions : the outer crust, the inner crust and the core. The outer crust consists of a lattice of atomic nuclei of iron-peak elements - iron, cobalt and nickel immersed in a relativistic degenerate electron gas. It envelops the inner crust which extends from the neutron drip density to a transition density $\sim 1.7 \times 10^{14}$ gms/cc. The inner crust consists of neutron-rich nuclei immersed in a free neutron and electron gas. Some recent results also predict presence of nuclear "pasta" phases in the inner crust [3]. Beyond the inner crust lies the core, where as a result of increasing density, all the atomic nuclei melt into their constituents, protons and neutrons to form a phase of uniform nuclear matter. Due to the high Fermi energies of the nucleons in the core, more exotic baryons such as hyperons as well as a gas of free up, down and strange quarks can form [4, 5]. Moreover, studies have also shown the existence of pion and kaon condensates

[6, 7].

To predict the mass-radius relationship of a neutron star, one needs to know the EoS, which is the fundamental problem of neutron star research. The neutron star crustal EoS has been somewhat calculated with an accuracy, sufficient to construct neutron star models. The theories are based on reliable experimental data on atomic nuclei, nucleon scattering, and on the well elaborated theory of strongly coupled high density Coulomb plasmas. Examples are the Feynman-Metropolis-Teller (FMT) [8], Baym-Pethick-Sutherland (BPS) [9] and Baym-Bethe-Pethick (BBP) [10] EoSs. The core EoS is much more difficult to treat since such superdense matter cannot be reproduced in laboratories and there is a lack of the precise relativistic many-body theory of strongly interacting particles at such densities. Instead, there are numerous theoretical effective models of the core EoS. Modern models for the EoS of the core fall into two main categories: nonrelativistic variational approximation and relativistic field theoretic approaches. Some of the EoSs based on the nonrelativistic nuclear potentials are the Skyrme-Lyon(SLy) [11, 12], APR [13], FPS [14], BPAL12 [15] etc. The Relativistic Mean Field (RMF) EoS is based on relativistic field theory of particles [16].

Neutron stars are home to the strongest magnetic fields of the Universe. Their surface field strengths lie in the range of $\sim 10^{10} - 10^{15}$ gauss. Highly magnetized rapidly rotating neutron stars are called pulsars. The magnetic field of a pulsar is dipolar and the magnetic dipole moment axis, being misaligned with the rotation axis, a pulsar emits electromagnetic radiation from its north and south magnetic poles. When this beam of radiation intersects our line of sight we observe a pulse. Observations show that the pulses are very periodic over millions of years, which means that the rotational frequency is almost constant. Hence pulsars can be considered as precise clocks.

But sometimes sudden jumps in rotational frequencies ω which may be as large as $\frac{\Delta\omega}{\omega} \sim 10^{-6} - 10^{-9}$ have been observed for many pulsars. This phenomenon is called pulsar glitch. The hypothesis of experience of glitches [17] by all radio pulsars is substantiated by observation of glitches. A glitch is a sudden increase in the frequency rotation of a rotation-powered pulsar, which, due to braking provided by the emission of radiation and high-energy particles, generally decreases steadily. This sudden increase in the rotational frequency of pulsar is due to a short time coupling of the faster-spinning superfluid core of the pulsar to its crust, which are usually decoupled. The transfer of angular momentum from core to the surface caused by this brief coupling decreases the measured time period. It is envisaged that the breaking of the magnetic dipole of pulsar ensues coupling which applies a twisting force to the crust causing a brief coupling. The inner crust consists of a crystal lattice of nuclei immersed in a neutron superfluid [18] where core to crust transition occurs. With a regular array of rotational vortices created due to rotation of the pulsar, the superfluid consisting of neutrons (both deeper inside the star and within the inner crust) is entangled. The reason that the rotational frequency of a superfluid is proportional to the density of vortices, as the pulsar slows down these vortices need to gradually move outwards. Although in the crust the vortices are pinned by their interaction with the nuclear lattice, in the star's deep inside this process is freely allowed. Various theoretical models [19, 20, 21, 22, 23] differ in important aspects of the stress release mechanism of glitch which are associated with pinned vortices. The crust may get rearranged due to the breaking of vortices or a cluster of vortices may move macroscopically outward by overcoming the pinning force suddenly. This phenomenon results in a glitch due to sudden decrease in the angular momentum of the superfluid within the crust causing a sudden increase in angular momentum of the rigid crust itself. The common feature of all the models is that they agree that the fundamental requirement is the presence of a rigid structure which impedes the motion of rotational vortices present in a superfluid and which encompasses enough of the volume of the pulsar to contribute significantly to the total moment of inertia.

The effective interactions are either of microscopic origin such as M3Y forces [24, 25] or of phenomenological origin such as Seyler-Blanchard [26, 27, 28, 29, 30], Skyrme [31, 32, 33] and simple effective interactions [34, 35, 36]. Based upon the characterization of nuclear matter described by the two-body density dependent M3Y effective interaction [24, 25] (DDM3Y) based on the Brueckner-Goldstone G-matrix elements of the Reid-Elliott NN interaction, a systematic description of the spin and isospin symmetric nuclear matter (SNM) and the dependence of bulk behavior of isospin asymmetric nuclear matter (IANM) on isospin have been provided. In the present work, the EoS used is obtained from the density dependent M3Y effective nucleon-nucleon (NN) interaction (DDM3Y) for which the incompressibility K_∞ for the SNM, nuclear symmetry energy $E_{sym}(\rho_0)$ at saturation density ρ_0, the isospin dependent part K_τ of the isobaric incompressibility and the slope L are in excellent agreement with the constraints extracted from measured isotopic dependence of the giant monopole resonances in even-A Sn isotopes, from the neutron skin thickness of nuclei recently, and from analyses of experimental data on isospin diffusion and isotopic scaling in intermediate energy heavy-ion collisions [37, 38]. The core-crust transition in neutron stars is determined [39] by analyzing the stability of the β-equilibrated dense nuclear matter with respect to the thermodynamic stability conditions [40, 41, 42, 43, 44]. The mass-radius relation for neutron stars is obtained by solving the Tolman-Oppenheimer-Volkoff Equation (TOV) [45, 46] and then the crustal fraction of moment of inertia is determined using pressure and density at core-crust transition. Since in the Vela pulsar the angular momentum requirements of glitches indicate that 1.4% of the star's moment of inertia drives these events, the allowed region for masses and radii for Vela pulsar is determined from the condition that the crustal fraction of the total moment of inertia $\frac{\Delta I}{I} > 0.014$ which sets a limit for its radius.

Since neutron stars are very compact they are sources of high gravity. Gravitational waves emitted from isolated and binary neutron stars are efficient informers about the interior characteristics of neutron stars. Nowadays gravitational wave astronomy with pulsars has grown into a rich topic of study. The tidal deformabilities and gravitational wave profiles of neutron stars in binary systems are directly connected to the EoS. The only limitation is the extreme smallness of the wave amplitude on the Earth ($\sim 10^{-21}$). But on August 17, 2017, the first gravitational wave signal of two colliding neutron stars, named as GW170817, was detected by the Laser Interferometer Gravitational-Wave Observatory (LIGO), Virgo and some 70 ground- and space-based observatories [47]. The inspiralling objects were 1.1 to $1.6 M_{\odot}$.

Rapidly rotating neutron stars also suffer from various rotational instabilities. Quasi-normal modes of rapidly rotating isolated and accreting compact stars also act as sensitive probes for general relativistic effects such as gravitational waves and of the properties of ultradense matter. Temporal changes in the rotational period of neutron stars can reveal the internal changes of the stars with time. Albeit orders of magnitude smaller than the gravitational waves emitted from neutron stars in binary systems, waves emitted from rotational instabilities can be detected in future by the advanced LIGO, advanced Virgo, Einstein, Large Interferometer Space Antenna (LISA) and the Square Kilometer Array (SKA) telescopes. In this work we have studied one type of rotational instability, known as the r-mode (Rossby mode) instability using the DDM3Y EoS and calculated the spin-down and spin-down rates.

Next, we consider neutron stars with dark matter cores. Neutron stars and white dwarfs being very compact and dense, can accrete and efficiently capture dark matter particles and become dark matter admixed compact stars. Even main-sequence stars can accumulate dark matter particles within them throughout their lifetime and at the end of their lifetimes end up as dark matter admixed compact stars. The accumulation process of dark matter can be different for different models of dark matter. Such “hybrid” stars can show drastically different mass-radius relationships based on the amount and properties of dark matter particles inside them. Their observational characteristics have been put forward by several studies [48, 49, 50, 51, 52, 53, 54]. Hence compact stars admixed with dark matter can act as sensitive probes of not only the nature of superdense baryonic matter but also of the properties of dark matter itself.

We have considered pure hadronic stars with the DDM3Y effective nucleon-nucleon interaction admixed with strongly self-interacting fermionic Asymmetric Dark Matter with particle mass of 1 GeV, consistent with dark matter observations. The Asymmetric Dark Matter EoS is calculated theoretically based on the massive vector field theory similar to the meson exchange of nuclear interaction. The mass of the mediator of the interaction is taken to be 100 MeV. We have considered equal and different rotational frequencies of nuclear and dark matter and have employed the two-fluid formalism to calculate the mass-radius relations. We have found that the maximum mass of a pure dark matter star goes to $\sim 3M_{\odot}$ while that of a neutron star admixed with dark matter to be $\sim 1.94M_{\odot}$ with a radius of ~ 10.4 kms.

Chapter 2

EQUATION OF STATE FOR NON-MAGNETIZED AND MAGNETIZED WHITE DWARF MATTER

The magnitude of magnetic fields of white dwarfs is constrained by the virial theorem:

$$\left(\frac{4}{3}\pi R^3\right)\frac{B^2}{8\pi} = \frac{3}{5}\frac{GM^2}{R}, \tag{2.1}$$

which gives

$$B_{max} = B_{\odot}\left(\frac{M}{M_{\odot}}\right)\left(\frac{R}{R_{\odot}}\right)^{-2}. \tag{2.2}$$

Here, $B,\ B_{\odot},\ M,\ M_{\odot},\ R,\ R_{\odot}$ are the magnetic field, mass and radius of the white dwarf and sun respectively. Using $B_{\odot} = 2 \times 10^8$ gauss, $M = 1.4\ M_{\odot}$ and $R = 0.0086\ R_{\odot}$, we get the order of magnitude as $B_{max} \sim 10^{12}$ gauss.

The recently observed peculiar Type Ia supernovae, e.g. SN2006gz, SN2007if, SN2009dc, SN2003fg, [55, 56, 57, 58, 59] with exceptionally high luminosities do not fit with the explosion of a Chandrasekhar mass white dwarf. Moreover, it has been seen that there is a correlation between the surface magnetic field and the mass of white dwarfs. The magnetic white dwarfs seem to be more massive than their nonmagnetic counterparts [60]. Lastly, predictions from the luminosities reveal that the progenitor white dwarfs had masses significantly higher than the Chandrasekhar limit. It seems that the Chandrasekhar limit may be violated by highly magnetized white dwarfs. To account for these facts, we have calculated theoretically the masses of white dwarfs in presence of such high magnetic fields in the general relativistic formalism.

2.1 The Equation of State for non-magnetic White Dwarfs

We consider a relativistic, completely degenerate Fermi gas at zero temperature and neglect any form of interactions between the fermions. By the Pauli exclusion principle, no quantum state can be occupied by more than one fermion with an identical set of quantum numbers. Thus a noninteracting Fermi gas, unlike a Bose gas, is prohibited from condensing into a Bose-Einstein condensate. The total energy of the Fermi gas at absolute zero is larger than the sum of the single-particle ground states because the Pauli principle implies a degeneracy pressure that keeps fermions separated and moving. For this reason, the pressure of a Fermi gas is non-zero even at zero temperature, in contrast to that of a classical ideal gas. This so-called degeneracy pressure stabilizes a white dwarf (a Fermi gas of electrons) against the inward pull of gravity, which would ostensibly collapse the star into a Black Hole. However if a star is sufficiently massive to overcome the degeneracy pressure, it collapse into a singularity due to gravity. While the pressure inside a white dwarf is entirely due to electrons, its mass comes mostly from the atomic nuclei.

2.1.1 Completely degenerate free electron Gas

The non-interacting assembly of fermions at zero temperature exerts pressure because of kinetic energy from different states filled up to Fermi level. Since pressure is force per unit area which means rate of momentum transfer per unit area, it is given by

$$P_e = \frac{1}{3}\int pvn_p d^3p = \frac{1}{3}\int \frac{p^2c^2}{\sqrt{(p^2c^2+m_e^2c^4)}} n_p d^3p \tag{2.3}$$

where m_e is the rest mass, v is the velocity of the particles with momentum $\vec{p}$ and $n_p d^3p$ is the number of particles per unit volume having momenta between $\vec{p}$ and $\vec{p}+d\vec{p}$. The factor $\frac{1}{3}$ accounts for the fact that, on average, only $\frac{1}{3}$rd of total particles $n_p d^3p$ are moving in a particular direction. For fermions having spin $\frac{1}{2}$, degeneracy $= 2$, $n_p d^3p = \frac{8\pi p^2 dp}{h^3}$ and hence number density $n_e$is given by

$$n_e = \int_0^{p_F} n_p d^3p = \frac{8\pi p_F^3}{3h^3} = \frac{x_F^3}{3\pi^2\lambda_e^3} \tag{2.4}$$

where p_F is the Fermi momentum which is maximum momentum possible at zero temperature, $x_F = \frac{p_F}{m_e c}$ is a dimensionless quantity and $\lambda_e = \frac{\hbar}{m_e c}$ is the Compton wavelength. The energy density ε_e is given by

$$\varepsilon_e = \int_0^{p_F} En_p d^3p = \int_0^{p_F} \sqrt{(p^2c^2+m_e^2c^4)}\frac{8\pi p^2 dp}{h^3} \tag{2.5}$$

which along with Eq.(2.3) turns out upon integration to be

$$\varepsilon_e = \frac{m_e c^2}{\lambda_e^3}\chi(x_F); \qquad P_e = \frac{m_e c^2}{\lambda_e^3}\phi(x_F), \tag{2.6}$$

where

$$\chi(x) = \frac{1}{8\pi^2}[x\sqrt{1+x^2}(1+2x^2) - \ln(x+\sqrt{1+x^2})] \tag{2.7}$$

and

$$\phi(x) = \frac{1}{8\pi^2}[x\sqrt{1+x^2}(\frac{2x^2}{3} - 1) + \ln(x+\sqrt{1+x^2})]. \tag{2.8}$$

2.1.2 Contribution of atomic nuclei to the energy density

For the EoS for non-magnetic White Dwarfs, the pressure is provided by the relativistic electrons only and therefore, pressure P is given by

$$P = P_e = \frac{m_e c^2}{\lambda_e^3}\phi(x_F), \tag{2.9}$$

whereas for energy density ε both electrons (with its kinetic energy) and atomic nuclei contribute, so that

$$\varepsilon = \varepsilon_e + n_e(m_p + f m_n)c^2 = \frac{m_e c^2}{\lambda_e^3}\chi(x_F) + n_e(m_p + f m_n)c^2 \tag{2.10}$$

where m_n and m_p are the masses of neutron and proton, respectively and f is the number of neutrons per electron. Commonly, electron-degenerate stars consist of helium, carbon, oxygen, etc., for which $f = 1$. To be precise, one should in fact also subtract $n_e(1+f)$ times binding energy per nucleon from the second term on the right hand side of the above equation. Obviously, this correction is composition dependent and its contribution being quite small, e.g. in case of helium star it is about 0.7% to the second term, it is not considered in calculations. Since the kinetic energy of electrons in the above equation contributes negligibly, the mass density for $f = 1$ white dwarfs can be expressed in units of 2×10^9 gms/cc by multiplying number density of electrons n_e expressed in units of fm^{-3} by the factor 1.6717305×10^6.

2.2 The Equation of State for magnetized White Dwarfs

Like the former case, here also we consider a completely degenerate relativistic electron gas at zero temperature but embedded in a strong magnetic field. We do not consider any form of interactions with the electrons. Electrons, being charged particles, occupy Landau quantized states in a magnetic field. This changes the EoS, which, in turn, changes the pressure and energy density of the white dwarf. In addition to the matter energy density and pressure, the energy density and pressure due to magnetic field are also taken into account. It is the combined pressure and energy density of matter and magnetic field that determines the mass-radius relation of strongly magnetized white dwarfs. It should be emphasized that protons also, being charged particles, are Landau quantized. But since the proton mass is ~ 2000 times the electron mass their cyclotron energy is ~ 2000 times smaller than that of the electron for the same magnetic field, and hence we neglect it.

2.2.1 Landau quantization and EoS for free electron gas in magnetic field

In order to calculate the thermodynamic quantities like the energy density and pressure of an electron gas in a magnetic field, we need to know the density of states and the dispersion relation. The quantum mechanics of a charged particle in a magnetic field is presented in many texts (e.g. Sokolov and Ternov (1968) [61], Landau and Lifshitz (1977) [62], Canuto and Ventura (1977) [63] Mészáros (1992) [64]). Here we summarize the basics needed for our later discussion. Let us first consider the motion of a charged particle (charge q and mass m_e) in a uniform magnetic field B assumed to be along the z-axis. In classical physics, the particle gyrates in a circular orbit with radius and angular frequency (cyclotron frequency) given by

$$r_c = \frac{m_e c v_\perp}{qB}; \qquad \omega_c = \frac{qB}{m_e c} \tag{2.11}$$

where $v_\perp$ is the velocity perpendicular to the magnetic field. The hamiltonian of the system is given by

$$H = \frac{1}{2m_e}\Big(\vec{p} - \frac{q\vec{A}}{c}\Big)^2 \tag{2.12}$$

where $\vec{B} = \nabla \times \vec{A}$ with $\vec{A}$ being the electromagnetic vector potential. To have magnetic field in z-direction with magnitude B one must have

$$\vec{A} = \begin{pmatrix} 0 \\ Bx \\ 0 \end{pmatrix} \tag{2.13}$$

and therefore

$$H = \frac{1}{2m_e}[p_x^2 + \Big(p_y - \frac{qBx}{c}\Big)^2 + p_z^2] \tag{2.14}$$

The operator $\hat{p}_y$ commutes with this hamiltonian since the operator y is absent. Thus operator $\hat{p}_y$ can be replaced by its eigenvalue $\hbar k_y$.Using cyclotron frequency $\omega_c = \frac{qB}{m_e c}$ one obtains

$$H = \frac{p_x^2}{2m_e} + \frac{1}{2}m_e\omega_c^2\Big(x - \frac{\hbar k_y}{m_e\omega_c}\Big)^2 + \frac{p_z^2}{2m_e}, \tag{2.15}$$

the first two terms of which is exactly the quantum harmonic oscillator with the minimum of the potential shifted in co-ordinate space by $x_0 = \frac{\hbar k_y}{m_e\omega_c}$. Noting that translating harmonic oscillator potential does not affect the energies, energy eigenvalues can be given by

$$E_{n,p_z} = (n + \frac{1}{2})\hbar\omega_c + \frac{p_z^2}{2m_e}, \qquad n = 0, 1, 2.... \tag{2.16}$$

The energy does not depend on the quantum number k_y, so there will be degeneracies. Each set of wave functions with same value of n is called a Landau Level. Each Landau level is degenerate due to the second quantum number k_y. If periodic boundary condition is assumed k_y can take values $k_y = \frac{2\pi N}{l_y}$ where N is another integer and l_x, l_y, l_z being the dimensions of the system. The allowed values of N are further restricted by the condition that the centre of the force of the oscillator x_0 must physically lie within the system, $0 \leq x_0 \leq l_x$ which implies $0 \leq N \leq \frac{l_x l_y m_e \omega_c}{2\pi\hbar} = \frac{qBl_x l_y}{hc}$. Hence for electrons with spin s and charge $q = -|e|$, the maximum number of particles per Landau level per unit area is $\frac{|e|B(2s+1)}{hc}$. On solving Schrödinger's equation for electrons with spin in an external magnetic field in z-direction which is uniform and static, Eq.(2.16) modifies to

$$E_{\nu,p_z} = \nu\hbar\omega_c + \frac{p_z^2}{2m_e}, \qquad \nu = n + \frac{1}{2} + s_z. \tag{2.17}$$

Clearly for the lowest Landau level ($\nu = 0$) the spin degeneracy $g_\nu = 1$ (since only $n = 0$, $s_z = -\frac{1}{2}$ is allowed) and for all other higher Landau levels ($\nu \neq 0$), $g_\nu = 2$ (for $s_z = \pm\frac{1}{2}$).

For extremely strong magnetic fields such that $\hbar\omega_c \geq m_e c^2$ the motion perpendicular to the magnetic field still remains quantized but becomes relativistic. The solution of the Dirac equation in a constant magnetic field [65] is given by the energy eigenvalues

$$E_{\nu,p_z} = \left[p_z^2 c^2 + m_e^2 c^4 \left(1 + 2\nu B_D\right)\right]^{\frac{1}{2}} \tag{2.18}$$

where the dimensionless magnetic field defined as $B_D = B/B_c$ is introduced with B_c given by $\hbar\omega_c = \hbar\frac{|e|B_c}{m_e c} = m_e c^2 \Rightarrow B_c = \frac{m_e^2 c^3}{|e|\hbar} = 4.414 \times 10^{13}$ gauss. Obviously, the density of states in presence of magnetic field gets modified to

$$\sum_{\nu} \frac{2|e|B}{hc} g_\nu \int \frac{dp_z}{h} \tag{2.19}$$

where the sum is on all Landau levels ν. At zero temperature the number density of electrons is given by

$$n_e = \sum_{\nu=0}^{\nu_m} \frac{2|e|B}{h^2 c} g_\nu \int_0^{p_F(\nu)} dp_z = \sum_{\nu=0}^{\nu_m} \frac{2|e|B}{h^2 c} g_\nu p_F(\nu) \tag{2.20}$$

where $p_F(\nu)$ is the Fermi momentum in the νth Landau level and ν_m is the upper limit of the Landau level summation. The Fermi energy E_F of the νth Landau level is given by

$$E_F^2 = p_F^2(\nu)c^2 + m_e^2 c^4 \left(1 + 2\nu B_D\right) \tag{2.21}$$

and ν_m can be found from the condition $[p_F(\nu)]^2 \geq 0$ or

$$\nu \leq \frac{\epsilon_F^2 - 1}{2B_D} \quad \Rightarrow \quad \nu_m = \frac{\epsilon_{Fmax}^2 - 1}{2B_D}, \tag{2.22}$$

where $\epsilon_F = \frac{E_F}{m_e c^2}$ is the dimensionless Fermi energy and $\epsilon_{Fmax} = \frac{E_{Fmax}}{m_e c^2}$ the dimensionless maximum Fermi energy of a system for a given B_D and ν_m. Obviously, very small B_D corresponds to large number of Landau levels leading to the familiar non-magnetic EoS. ν_m is taken to be the nearest lowest integer. Like the former case, if we define a dimensionless Fermi momentum $x_F(\nu) = \frac{p_F(\nu)}{m_e c}$ then Eqs.(2.20) and (2.21) may be written as

$$n_e = \frac{2B_D}{(2\pi)^2 \lambda_e^3} \sum_{\nu=0}^{\nu_m} g_\nu x_F(\nu) \tag{2.23}$$

and

$$\epsilon_F = \left[x_F^2(\nu) + 1 + 2\nu B_D\right]^{\frac{1}{2}} \tag{2.24}$$

or

$$x_F(\nu) = \left[\epsilon_F^2 - (1 + 2\nu B_D)\right]^{\frac{1}{2}}. \tag{2.25}$$

The electron energy density is given by

$$\begin{aligned}
\varepsilon_e &= \frac{2B_D}{(2\pi)^2\lambda_e^3}\sum_{\nu=0}^{\nu_m} g_\nu \int_0^{x_F(\nu)} E_{\nu,p_z} d\left(\frac{p_z}{m_e c}\right) \\
&= \frac{2B_D}{(2\pi)^2\lambda_e^3} m_e c^2 \sum_{\nu=0}^{\nu_m} g_\nu (1 + 2\nu B_D)\psi\left(\frac{x_F(\nu)}{(1 + 2\nu B_D)^{1/2}}\right),
\end{aligned} \tag{2.26}$$

where

$$\psi(z) = \int_0^z (1 + y^2)^{1/2} dy = \frac{1}{2}[z\sqrt{1 + z^2} + \ln(z + \sqrt{1 + z^2})] \tag{2.27}$$

The pressure of the electron gas is given by

$$\begin{aligned}
P_e &= n_e^2 \frac{d}{dn_e}\left(\frac{\varepsilon_e}{n_e}\right) = n_e E_F - \varepsilon_e \\
&= \frac{2B_D}{(2\pi)^2\lambda_e^3} m_e c^2 \sum_{\nu=0}^{\nu_m} g_\nu (1 + 2\nu B_D)\eta\left(\frac{x_F(\nu)}{(1 + 2\nu B_D)^{1/2}}\right),
\end{aligned} \tag{2.28}$$

where

$$\eta(z) = z\sqrt{1 + z^2} - \psi(z) = \frac{1}{2}[z\sqrt{1 + z^2} - \ln(z + \sqrt{1 + z^2})]. \tag{2.29}$$

2.2.2 Contributions of magnetic field and atomic nuclei

In the present case of magnetic White Dwarfs, the explicit contributions from the energy density $\varepsilon_B = \frac{B^2}{8\pi}$ and pressure $P_B = \frac{1}{3}\varepsilon_B$ arising due to magnetic field need to be added to the matter energy density and pressure as

$$
\begin{aligned}
P = & \quad P_e + P_B \\
= & \quad \frac{2B_D}{(2\pi)^2\lambda_e^3} m_e c^2 \sum_{\nu=0}^{\nu_m} g_\nu (1 + 2\nu B_D)\eta \left(\frac{x_F(\nu)}{(1 + 2\nu B_D)^{1/2}} \right) \\
& + \frac{B^2}{24\pi},
\end{aligned}
\tag{2.30}
$$

and

$$
\begin{aligned}
\varepsilon = & \quad \varepsilon_e + n_e(m_p + f m_n)c^2 + \varepsilon_B \\
= & \quad \frac{2B_D}{(2\pi)^2\lambda_e^3} m_e c^2 \sum_{\nu=0}^{\nu_m} g_\nu (1 + 2\nu B_D)\psi \left(\frac{x_F(\nu)}{(1 + 2\nu B_D)^{1/2}} \right) \\
& + n_e(m_p + f m_n)c^2 + \frac{B^2}{8\pi}.
\end{aligned}
\tag{2.31}
$$

2.3 Coulomb corrections to White Dwarf EoS: The Feynman-Metropolis-Teller Approach

The Feynman-Metropolis-Teller treatment of compressed atom [66] is extended to the relativistic regime. Each atomic configuration is confined by a Wigner-Seitz cell and is characterized by a positive electron Fermi energy. The nonrelativistic treatment assumes a pointlike nucleus and infinite values of the electron Fermi energy can be attained. In the relativistic treatment, there exists a limiting configuration, reached when the Wigner-Seitz cell radius equals the radius of the nucleus with a maximum value of the electron Fermi energy. FMT treatment with Coulomb screening in presence of strong quantizing magnetic field has been applied in this work to develop the Equation of State(EoS). The Mass-Radius relations for magnetized WDs are obtained by solving the Tolman-Oppenheimer-Volkoff equations.

We consider a compressed atom as a Wigner-Seitz cell consisted of a finite sized nucleus at the center of the cell and completely degenerate relativistic electron gas embedded in a strong magnetic field. We consider here the interaction between the nucleus and the electrons. Electrons, being charged particles, occupy Landau quantized states in a magnetic field. Electrons with spin s and charge $q = -|e|$, the maximum number of particles per Landau level per unit area is $\frac{|e|B(2s+1)}{hc}$ in magnetic field B. On solving Dirac's with spin in an external magnetic field B in z-direction which is uniform and static, energy eigenvalues are given by

$$E_{\nu,p_z} = \left[p_z^2c^2 + m_e^2c^4\left(1+2\nu B_D\right)\right]^{\frac{1}{2}} - m_ec^2 - eV(r) \tag{2.32}$$

where ν=n+$\frac{1}{2}$+s_z, the Landau quantum number, m_e is electron rest mass and the dimensionless magnetic field defined as B_D=B/B_c is introduced with B_c given by $\hbar\omega_c$=$\hbar\frac{|e|B_c}{m_ec}$=$m_ec^2 \Rightarrow$ B_c=$\frac{m_e^2c^3}{|e|\hbar}$=$4.414\times10^{13}$ gauss. A constant distribution of protons confined in a radius given by R_c=$r_0A^{\frac{1}{3}}$ with r_0=$1.2fm$ is assumed. Using Landau quantization, electronic number density is given by

$$\begin{aligned} n_e = & \frac{2B_D}{(2\pi)^2\lambda_e^3}\sum_{\nu=0}^{\nu_m} g_\nu \frac{p_zc}{m_ec^2} \\ p_zc = & \left[\widehat{V}^2\left(1-\frac{\nu}{\nu_m}\right) + 2m_ec^2\widehat{V}\left(1-\frac{\nu}{\nu_m}\right)\right]^{\frac{1}{2}}, \end{aligned} \tag{2.33}$$

where $\widehat{V} = eV + E_{\nu,p_z}$ and Eq.(2.32) is used for its evaluation. ν_m is the upper limit of Landau level can be found from the condition $p_z^2 \geq 0$ and is given by $\nu_m = \frac{\widehat{V}^2+2\widehat{V}m_ec^2}{2B_Dm_e^2c^4}$. The overall Coulomb potential outside the nucleus satisfies the poisson equation

$$\begin{aligned} \nabla^2V(r) = & \ 4\pi en_e(r) \\ \Rightarrow \frac{1}{x}\frac{d^2\chi(x)}{dx^2} = & \ \frac{8\pi e^2B_D}{4\pi^2c\hbar}\frac{m_\pi}{m_e}\left(\frac{\lambda_\pi}{\lambda_e}\right)^3 \\ & \sum_{\nu=0}^{\nu_m} g_\nu\left(1-\frac{\nu}{\nu_m}\right)^{\frac{1}{2}}\left[\left(\frac{\chi(x)}{x}\right)^2 + \frac{\chi(x)}{x}\frac{2m_e}{m_\pi}\right]^{\frac{1}{2}}, \end{aligned} \tag{2.34}$$

where dimensionless quantities $x=\frac{r}{\lambda_\pi}, \frac{\chi}{r}=\frac{\widehat{V}(r)}{c\hbar}$ have been introduced. Solving Eq.(3) we find the electrostatic potential and the electronic distribution. Hence the potential energy density ε_p, kinetic energy density ε_k are found. The energy density ε and pressure P expressions are given by,

$$
\begin{aligned}
\varepsilon_p = & \quad -en_e(r)V(r) \\
\varepsilon_k = & \quad \frac{2B_D m_e c^2}{4\pi^2\lambda_e^3}\sum_{\nu=0}^{\nu_m} g_\nu\left(1+2\nu B_D\right) \\
& \quad \psi\left(\frac{x_F(\nu)}{(1+2\nu B_D)^{1/2}}\right) \\
\varepsilon = & \quad \varepsilon_p+\varepsilon_k+\rho m_B c^2+\frac{B^2}{8\pi}
\end{aligned}
\tag{2.35}
$$

$$
\begin{aligned}
P = & \quad P_B + P_e \\
= & \quad \frac{B^2}{24\pi}+\frac{2B_D m_e c^2}{4\pi^2\lambda_e^3} \\
& \quad \sum_{\nu=0}^{\nu_m} g_\nu\left(1+2\nu B_D\right)\eta\left(\frac{x_F(\nu)}{(1+2\nu B_D)^{1/2}}\right)
\end{aligned}
\tag{2.36}
$$

where $x_F(\nu)=p_z/m_e c$, $\lambda_e=\frac{\hbar}{m_e c}$, $\lambda_\pi=\frac{\hbar}{m_\pi c}$, m_π is the pion mass, ρ is the baryonic number density, m_B is the baryonic mass. The magnetic energy contribution is $\varepsilon_B=\frac{B^2}{8\pi}$ while $P_B=\frac{\varepsilon_B}{3}$ is the magnetic contribution to pressure and

$$
\begin{aligned}
\psi\left(z\right) = & \quad \int_0^z \left(1+y^2\right)^{\frac{1}{2}} \\
= & \quad \frac{1}{2}\left[z\sqrt{1+z^2}+ln\left(z+\sqrt{1+z^2}\right)\right] \\
\eta\left(z\right) = & \quad z\sqrt{1+z^2}-\psi\left(z\right)
\end{aligned}
\tag{2.37}
$$

We perform calculations with varying magnetic field inside WD given by the form [67]

$$
B_d = B_s + B_0[1-\exp\{-\beta(\rho/\rho_0)^\gamma\}]
\tag{2.38}
$$

where B_d (in units of B_c) is the magnetic field at baryonic density ρ, B_s (in units of B_c) is the surface magnetic field and ρ_0 is taken as ρ(r=0)/10 and β, γ are constants. We choose constants β=0.8, γ=0.9, rather arbitrarily but the central and surface magnetic fields once fixed the variations of its profile do not alter the gross results. The maximum central magnetic field strength is kept at $10B_c$ which is 4.414×10^{14} gauss [68] and surface magnetic field at $\sim 10^9$ gauss estimated by observations.

Chapter 3

MASSES & RADII OF WHITE DWARFS

If rapidly rotating compact stars were non-axisymmetric, they would emit gravitational waves in a very short time scale and settle down to axisymmetric configurations. Therefore, we need to solve for rotating and axisymmetric configurations in the framework of general relativity. For the matter and the spacetime the following assumptions are made. The matter distribution and the spacetime are axisymmetric, the matter and the spacetime are in a stationary state, the matter has no meridional motions, the only motion of the matter is a circular one that is represented by the angular velocity, the angular velocity is constant as seen by a distant observer at rest and the matter can be described as a perfect fluid. To study the rotating stars the following metric is used

$$\begin{aligned} ds^2 = &-e^{(\gamma+\rho)}dt^2 + e^{2\alpha}(dr^2 + r^2 d\theta^2) \\ &+e^{(\gamma-\rho)}r^2 \sin^2\theta(d\phi - \omega dt)^2 \end{aligned} \tag{3.1}$$

where the gravitational potentials γ, ρ, α and ω are functions of polar coordinates r and θ only.

3.1 Tolman-Oppenheimer-Volkoff Equation and its numerical solution for White Dwarfs

The Einstein's field equations for the three potentials γ, ρ and α can be solved using the Green's-function technique [69] and the fourth potential ω can be determined from other potentials. All the physical quantities may then be determined from these potentials. Rotational frequency of stars is limited by Kepler's frequency which is the mass shedding limit. For very compact stars such as neutron stars the Kepler's frequency is very high and can go up to millisecond order [70, 71] whereas white dwarfs being about thousand times bigger in size and much less dense, Kepler's frequency is very small and one may safely use the zero frequency limit [72] to the Einstein's field equations. Obviously, at the zero frequency limit corresponding to the static solutions of the Einstein's field equations for spheres of fluid, the present formalism yields the results for the solution of the Tolman-Oppenheimer-Volkoff (TOV) equation [45, 46] given by

$$\frac{dP(r)}{dr} = -\frac{G}{c^4}\frac{[\varepsilon(r)+P(r)][m(r)c^2+4\pi r^3 P(r)]}{r^2[1-\frac{2Gm(r)}{rc^2}]} \tag{3.2}$$

$$\text{where} \quad \varepsilon(r)=\rho(r)c^2 \quad \text{and} \quad m(r)c^2=\int_0^r \varepsilon(r')d^3r'$$

which can be easily solved numerically using Runge-Kutta method for masses and radii. The quantities $\varepsilon(r)$ and $P(r)$ are the energy density and pressure at a radial distance r from the centre, and are given by the equation of state. The mass of the star contained within a distance r is given by $m(r)$. The size of the star is determined by the boundary condition $P(r) = 0$ and the total mass M of the star integrated up to the surface R is given by $M = m(R)$ [73]. The single integration constant needed to solve the TOV equation is P_c, the pressure at the center of the star calculated at a given central density ρ_c.

Recently, there are some important calculations for masses and radii of magnetized white dwarfs using non-relativistic Lane-Emden equation assuming a constant magnetic field throughout which provided masses up to 2.3-2.6 $M_\odot$ [74], a mass significantly greater than the Chandrasekhar limit. However, because of the structure of the Lane-Emden equation, pressure arising due to constant magnetic field do not contribute while for the general relativistic TOV equation case is not the same. Moreover, the EoS needed to be fitted to a polytropic form. In order to derive a mass limit for magnetized white dwarfs (similar to the mass limit of $\sim$1.4 $M_\odot$ obtained by Chandrasekhar [1] for non-magnetic white dwarfs), the same authors, under certain approximations, have been able to reduce the EoS to a polytropic form with index $1 + 1/n = 2$ for which analytic solution of Lane-Emden equation exists ($\theta(\xi) = sin\xi/\xi$ where $\rho = \rho_c\theta^n$ with ρ and ρ_c being density and central density, respectively) and avoiding the energy density $\varepsilon_B = \frac{B^2}{8\pi}$ and pressure $P_B = \frac{1}{3}\varepsilon_B$ arising due to magnetic field by assuming it to be constant throughout, they were able to set a mass limit of 2.58 $M_\odot$ [75, 76]. In the present work, we have calculated masses and radii of white dwarfs by solving the general relativistic TOV equation both for non-magnetic and magnetized white dwarfs using the exact EoS without resorting to fit it to a polytropic form.

3.1.1 Chandrasekhar limit for White Dwarfs

We verify Chandrasekhar limit [1] for masses of white dwarfs by actually solving TOV equation for non-magnetic white dwarfs. The masses and radii of such white dwarfs are listed in Table-3.1. It is interesting to note that considering a very high central density of 3.343×10^{10} gms/cc for $f = 1$ white dwarfs, one can asymptotically reach the Chandrasekhar mass limit. It is important to mention that beyond this density at $\sim 4.3\times10^{11}$ gms/cc, the neutron drip point [77], the nuclei become so neutron rich that with increasing density the continuum neutron states begin to be filled, and the lattice of neutron-rich nuclei becomes permeated by a sea of neutrons. In Table-3.1, masses and radii of non-magnetic white dwarfs as a function of central density are provided. In Fig.-3.1 plot for masses of non-magnetic white dwarfs is shown as a function of central density whereas in Fig.-3.2 mass-radius relationship of non-magnetic white dwarfs is provided. These results for non-magnetic white dwarfs do conform to the traditional Chandrasekhar mass-limit.

Table 3.1: Variations of masses and radii of non-magnetic white dwarfs with central number density of electrons which can be expressed in units of 2×10^9 gms/cc for mass density by multiplying with 1.6717305×10^6.

n_e (r=0)	Radius	Mass
fm^{-3}	Kms	$M_\odot$
1.0×10^{-5}	917.87	1.3904
5.0×10^{-6}	1126.83	1.3905
4.0×10^{-6}	1202.53	1.3896
3.8×10^{-6}	1220.55	1.3893
3.6×10^{-6}	1239.80	1.3890
3.4×10^{-6}	1260.43	1.3887
3.2×10^{-6}	1282.65	1.3883
3.0×10^{-6}	1306.67	1.3878
2.8×10^{-6}	1332.78	1.3873
2.6×10^{-6}	1361.33	1.3866
2.4×10^{-6}	1392.75	1.3859
2.2×10^{-6}	1427.62	1.3850
2.0×10^{-6}	1466.67	1.3839

n_e (r=0)	Radius	Mass
fm^{-3}	Kms	$M_\odot$
1.8×10^{-6}	1510.90	1.3825
1.6×10^{-6}	1561.69	1.3809
1.4×10^{-6}	1621.01	1.3788
1.2×10^{-6}	1691.86	1.3761
1.0×10^{-6}	1779.00	1.3724
8.0×10^{-7}	1890.72	1.3673
6.0×10^{-7}	2043.29	1.3594
4.0×10^{-7}	2275.36	1.3457
2.0×10^{-7}	2721.16	1.3138
1.0×10^{-7}	3233.63	1.2692
1.0×10^{-8}	5482.58	1.0051
1.0×10^{-9}	8721.75	0.5949

3.1.2 Super-Chandrasekhar White Dwarfs

As mentioned in the beginning of this section that unlike non-relativistic Lane-Emden equation, pressure arising due to constant magnetic field does contribute to the general relativistic TOV equation. Presence of high constant magnetic field do not provide valid solutions to the TOV equations. Hence, we present stable solutions of magnetostatic equilibrium models for super-Chandrasekhar white dwarfs with varying magnetic field profiles which is maximum at the centre and goes to 10^9 gauss at the surface of the star. This has been obtained by self-consistently including the effects of the magnetic pressure gradient and total magnetic density in a general relativistic framework. Nevertheless, we have also performed calculations corresponding to very high (single Landau level) and

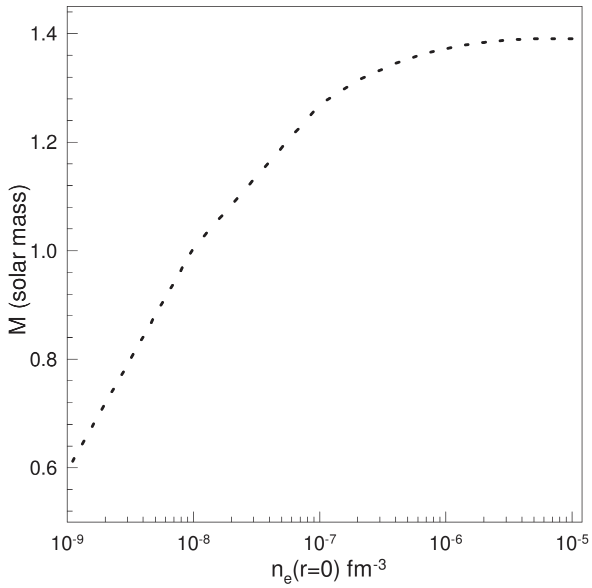

Figure 3.1: Plot for masses of non-magnetic white dwarfs as a function of central density.

high (multi Landau levels) magnetic field which is constant throughout the star in order to compare with the results from solutions of Lane-Emden equation described above, but for these cases we have to ignore the explicit contributions from energy density ε_B and pressure P_B arising due to magnetic field. Results of such calculations are provided in Tables-3.2 & 3.3 for magnetized white dwarfs with single and multiple Landau levels, respectively.

Now we perform the actual calculations with varying magnetic field including the effects of energy density and pressure arising due to magnetic field in a general relativistic framework. The variation of magnetic field [67] inside white dwarf is taken to be of the form

$$B_d = B_s + B_0[1 - \exp\{-\beta(n_e/n_0)^\gamma\}] \tag{3.3}$$

where B_d (in units of B_c) is the magnetic field at electronic number density n_e, B_s (in units of B_c) is the surface magnetic field and n_0 is taken as n_e(r=0)/10 and β, γ are constants. Once central magnetic field is fixed, B_0 can be determined from above equation. We

Table 3.2: Variations of masses and radii of uniformly magnetized white dwarfs with central number density of electrons which can be expressed in units of 2×10^9 gms/cc for mass density by multiplying with 1.6717305×10^6. The minimum magnetic field B_{dmin} corresponding to the central density required to make single Landau level throughout is listed in units of B_c.

n_e (r=0)	Radius	Mass	B_{dmin}
fm^{-3}	Kms	$M_\odot$	in units of B_c
5.0×10^{-6}	592.28	2.4521	253
4.0×10^{-6}	636.54	2.4508	218
3.0×10^{-6}	698.11	2.4461	180
2.0×10^{-6}	792.71	2.4204	138
1.0×10^{-6}	989.84	2.4149	86.5

Table 3.3: Variations of masses and radii of uniformly magnetized white dwarfs with central number density of electrons which can be expressed in units of 2×10^9 gms/cc for mass density by multiplying with 1.6717305×10^6. The magnetic field B_d ($< B_{dmin}$ for the central density) is also listed which generates multiple Landau levels.

n_e (r=0)	Radius	Mass	B_d
fm^{-3}	Kms	$M_\odot$	in units of B_c
4.6736×10^{-6}	1149.77	1.3925	1.5
3.5147×10^{-6}	663.58	2.4491	200

Table 3.4: Variations of masses and radii of magnetized white dwarfs with central number density of electrons which can be expressed in units of 2×10^9 gms/cc for mass density by multiplying with 1.6717305×10^6. The maximum magnetic field B_{dc} at the centre is listed in units of B_c whereas the surface magnetic field B_s is taken to be 10^9 gauss.

n_e (r=0)	Radius	Mass	B_{dc}
fm^{-3}	Kms	$M_\odot$	in units of B_c
4.674017×10^{-6}	1285.91	1.4146	1.5
4.673846×10^{-6}	1344.46	1.4236	1.75
4.674209×10^{-6}	1349.45	1.4339	2.0
4.675374×10^{-6}	1388.04	1.4906	3.0
4.672188×10^{-6}	1438.94	1.5731	4.0
4.670830×10^{-6}	1503.64	1.6863	5.0
4.678118×10^{-6}	1581.27	1.8353	6.0
4.677677×10^{-6}	1663.86	2.0217	7.0
4.665741×10^{-6}	1758.40	2.2601	8.0
4.661657×10^{-6}	1954.44	2.8997	10.

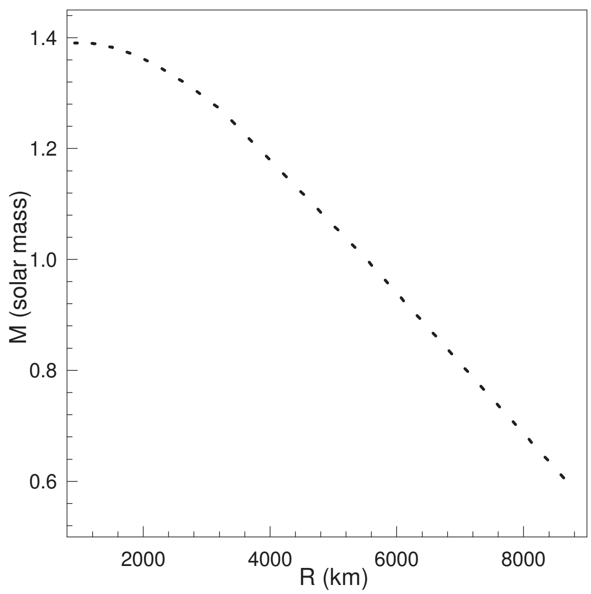

Figure 3.2: Plot for mass-radius relationship of non-magnetic white dwarfs.

choose constants $\beta = 0.8$ and $\gamma = 0.9$, rather arbitrarily by using unequal non-unity values, which provides stable solutions of magnetostatic equilibrium models for super-Chandrasekhar white dwarfs. Nevertheless, the magnetic field is not taken completely in ad hoc manner, because central and surface magnetic fields once fixed the variations of its profile do not alter the gross results. Moreover, we have kept maximum central magnetic field strength at $10B_c$ which is 4.414×10^{14} gauss, near to the lower of the maximum limit suggested by N. Chamel et al. [68] and surface magnetic field $\sim 10^9$ gauss estimated by observations. In Table-3.4 the results of these realistic calculations are listed. In Figs.-3.3,3.4 plots for masses and radii of magnetized white dwarfs are shown as functions of central magnetic field. Present calculations estimate that the maximum stable mass of magnetized white dwarfs could be $\sim 3\ M_\odot$. These results are quite useful in explaining the peculiar, overluminous type Ia supernovae that do not conform to the traditional Chandrasekhar mass-limit.

The EoS for magnetized WD in presence of Coulomb screening has been explored as further refinement and tabulated in Table 3.5. We find that the inclusion of Coulomb

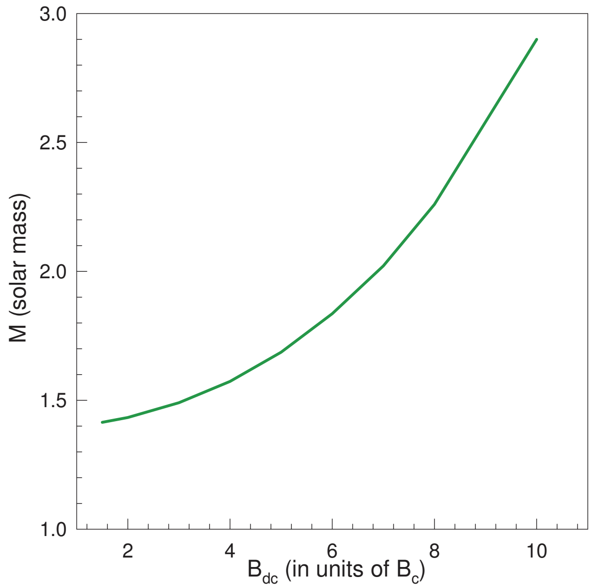

Figure 3.3: Plot for masses of magnetized white dwarfs as a function of central magnetic field.

interaction modifies the masses of WD further upward and significantly greater than Chandrasekhar limit.

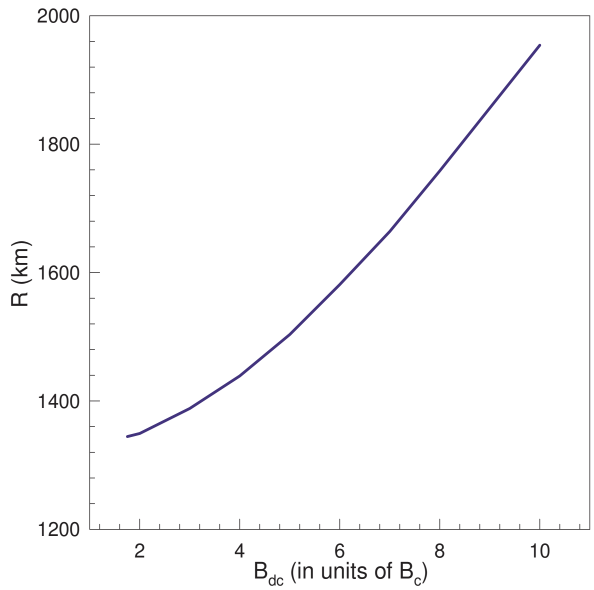

Figure 3.4: Plot for radii of magnetized white dwarfs as a function of central magnetic field.

Table 3.5: Variations of masses and radii of magnetized WD with coulomb interaction. The maximum magnetic field B_{dc} at the centre is listed in units of B_c.

ρ (r=0)	Radius	Mass	B_{dc}
fm^{-3}	Kms	$M_\odot$	B_c
4.674×10^{-7}	3572.24	2.2653	1.5
4.674×10^{-7}	3142.19	1.8405	1.2
4.674×10^{-7}	2801.06	1.5725	0.9
4.675×10^{-6}	2110.46	3.2624	8.0
4.672×10^{-6}	1659.09	2.0178	5.0
4.671×10^{-6}	1369.83	1.5157	2.0

Chapter 4

EQUATION OF STATE FOR NEUTRON STAR MATTER

The basic equation in neutron star matter research is the shape of the relationship between the pressure and energy density $P = P(\varepsilon)$, usually called the equation of state. At the zero temperature, the state of neutron star matter should be uniquely described by the quantities that are conserved by the process leading to equilibrium. Stable high density nuclear matter must be in chemical equilibrium for all types of reactions including the weak interactions, while the beta decay and orbital electron capture takes place simultaneously. For the β-equilibrated neutron star matter we have free neutron decay $n \rightarrow p + \beta^- + \overline{\nu_e}$ which are governed by weak interaction and the electron capture process $p + \beta^- \rightarrow n + \nu_e$. Both types of reactions change the electron fraction and thus affect the EoS. Here we assume that neutrinos generated in these reactions leave the system. The absence of neutrino has a dramatic effect on the equation of state and mainly induces a significant change on the values of proton fraction x_p.

4.1 Nuclear Equation of State

The EoS for nuclear matter is obtained by using the isoscalar and the isovector [78] components of M3Y effective NN interaction along with its density dependence. The nuclear matter calculation is then performed which enables complete determination of this density dependence. The minimization of energy per nucleon determines the equilibrium density of the symmetric nuclear matter (SNM). The variation of the zero range potential with energy, over the entire range of the energy per nucleon ϵ, is treated properly by allowing it to vary freely with the kinetic energy part ϵ^{kin} of ϵ. This treatment is more plausible as well as provides excellent result for the SNM incompressibility K_∞. Moreover, the EoS for SNM is not plagued with the superluminosity problem.

Employing various forms of density dependence [79, 80, 81], the EoS for nuclear matter has also been derived using explicitly the direct and finite range exchange contributions. Moreover, using finite range M3Y interaction, Hartree-Fock approximation has been used to compute properties of nuclear matter and finite nuclei [82, 83, 84]. In the limiting case of constant density, which holds true for infinite nuclear matter, the exchange integral reduces to a constant leading to an 'effective' exchange interaction of $J_{00}(\epsilon)\delta(s)$ type [85], typically the zero range potential used in the present calculations to evaluate the exchange term.

The energy per nucleon ϵ for IANM can be derived within a Fermi gas model of interacting neutrons and protons as [86]

$$\epsilon(\rho, X) = [\frac{3\hbar^2 k_F^2}{10m}]F(X) + (\frac{\rho J_v C}{2})(1 - \beta\rho^n) \tag{4.1}$$

where isospin asymmetry $X = \frac{\rho_n - \rho_p}{\rho_n + \rho_p}$, $\rho = \rho_n + \rho_p$ with ρ_n, ρ_p and ρ being the neutron, proton and nucleonic densities respectively, m is the nucleonic mass, k_F=$(1.5\pi^2\rho)^{\frac{1}{3}}$ which equals Fermi momentum in case of SNM, $\epsilon^{kin} = [\frac{3\hbar^2 k_F^2}{10m}]F(X)$ with $F(X)$=$[\frac{(1+X)^{5/3}+(1-X)^{5/3}}{2}]$

and J_v=$J_{v00} + X^2 J_{v01}$, J_{v00} and J_{v01} represent the volume integrals of the isoscalar and the isovector parts of the M3Y interaction. The isoscalar and isovector components t_{00}^{M3Y} and t_{01}^{M3Y} of the M3Y effective NN interaction are given by $t_{00}^{M3Y}(s,\epsilon) = 7999\frac{\exp(-4s)}{4s} - 2134\frac{\exp(-2.5s)}{2.5s} + J_{00}(1-\alpha\epsilon)\delta(s)$ and $t_{01}^{M3Y}(s,\epsilon) = -4886\frac{\exp(-4s)}{4s} + 1176\frac{\exp(-2.5s)}{2.5s} + J_{01}(1-\alpha\epsilon)\delta(s)$, respectively, with J_{00}=-276 MeVfm^3, J_{01}=228 MeVfm^3, $\alpha = 0.005\text{MeV}^{-1}$. The DDM3Y effective NN interaction is given by $v_{0i}(s,\rho,\epsilon) = t_{0i}^{M3Y}(s,\epsilon)g(\rho)$ where $g(\rho) = C(1-\beta\rho^n)$ is the density dependence with C and β being the constants of density dependence. This form of density dependence was originally taken by Myers in the single folding calculation [87] and it also has a physical meaning for $n = 2/3$ because then β can be interpreted as the 'in medium' effective NN interaction cross section.

Differentiating Eq.(4.1) with respect to ρ one obtains equation for $X = 0$:

$$\frac{\partial\epsilon}{\partial\rho} = [\frac{\hbar^2 k_F^2}{5m\rho}] + \frac{J_{v00}C}{2}[1-(n+1)\beta\rho^n] - \alpha J_{00}C[1-\beta\rho^n][\frac{\hbar^2 k_F^2}{10m}]. \tag{4.2}$$

The saturation condition $\frac{\partial\epsilon}{\partial\rho} = 0$ at $\rho = \rho_0$, $\epsilon = \epsilon_0$, determines the equilibrium density of the cold SNM. Then for fixed values of the saturation energy per nucleon ϵ_0 and the saturation density ρ_0 of the cold SNM, Eq.(4.1) and Eq.(4.2) with the saturation condition can be solved simultaneously to obtain the values of β and C which are given by

$$\beta = \frac{[(1-p)+(q-\frac{3q}{p})]\rho_0^{-n}}{[(3n+1)-(n+1)p+(q-\frac{3q}{p})]} \tag{4.3}$$

$$\text{where} \quad p = \frac{[10m\epsilon_0]}{[\hbar^2 k_{F_0}^2]},\ q = \frac{2\alpha\epsilon_0 J_{00}}{J_{v00}^0} \tag{4.4}$$

where $J_{v00}^0 = J_{v00}(\epsilon_0^{kin})$ which means J_{v00} is evaluated at $\epsilon^{kin} = \epsilon_0^{kin}$, the kinetic energy part of the saturation energy per nucleon of SNM, $k_{F_0} = [1.5\pi^2\rho_0]^{1/3}$ and

$$C = -\frac{[2\hbar^2 k_{F_0}^2]}{5mJ_{v00}^0\rho_0[1-(n+1)\beta\rho_0^n - \frac{q\hbar^2 k_{F_0}^2(1-\beta\rho_0^n)}{10m\epsilon_0}]}, \tag{4.5}$$

respectively. Obviously, the constants C and β determined by this methodology depend upon ϵ_0, ρ_0, the index n of the density dependent part and through the volume integral J^0_{v00}, on the strengths of the M3Y interaction .

The calculations have been carried out by using the values of saturation density $\rho_0 = 0.1533$ fm^{-3} [29] and saturation energy per nucleon $\epsilon_0 = -15.26$ MeV [88] for the SNM. ϵ_0 is the co-efficient a_v of the volume term of Bethe-Weizsäcker mass formula, calculated by fitting the recent experimental and estimated Audi-Wapstra-Thibault atomic mass excesses [89]. This term has been obtained by minimizing the mean square deviation incorporating correction for the electronic binding energy [90]. In a similar work, including surface symmetry energy term, Wigner term, shell correction and also the proton form factor correction to Coulomb energy, a_v turns out to be 15.4496 MeV [91] ($a_v = 14.8497$ MeV when A^0 and $A^{1/3}$ terms are also included). Using the standard values of $\alpha = 0.005$ MeV^{-1} for the parameter of energy dependence of the zero range potential and n=2/3, the values deduced for the constants C and β and the SNM incompressibility K_∞ are, respectively, 2.2497, 1.5934 fm^2 and 274.7 MeV. The term ϵ_0 is a_v and its value of -15.26 ± 0.52 MeV encompasses, more or less, the entire range of values. For this value of a_v now the values of the constants of density dependence are $C = 2.2497 \pm 0.0420$, $\beta = 1.5934 \pm 0.0085$ fm^2 and the SNM incompressibility K_∞ turns out to be 274.7 ± 7.4 MeV.

4.1.1 Symmetric and isospin asymmetric nuclear matter

The EoSs of the SNM and the IANM which describes energy per nucleon ϵ as a function of nucleonic density ρ can be obtained by setting isospin asymmetry $X = 0$ and $X \neq 0$, respectively, in Eq.(4.1). It is observed that the energy per nucleon ϵ for SNM is negative (bound) up to nucleonic density of $\sim 2\rho_0$ while for pure neutron matter (PNM) $\epsilon > 0$ and is always unbound by nuclear forces.

The compression modulus or incompressibility of the SNM, which is a measure of the curvature of an EoS at saturation density and is defined as $k_F^2 \frac{\partial^2 \epsilon}{\partial k_F^2} \mid_{k_F = k_{F_0}}$. It measures the stiffness of an EoS and can be theoretically obtained by using Eq.(4.1) for X=0. The IANM incompressibilities are evaluated at saturation densities ρ_s with the condition of vanishing pressure which is $\frac{\partial \epsilon}{\partial \rho}|_{\rho=\rho_s} = 0$. The incompressibility K_s for IANM is therefore expressed as

$$
\begin{aligned}
K_s = &-\frac{3\hbar^2 k_{F_s}^2}{5m} F(X) - \frac{9 J_v^s C n(n+1)\beta \rho_s^{n+1}}{2} \\
&-9\alpha J C[1-(n+1)\beta\rho_s^n][\frac{\rho_s \hbar^2 k_{F_s}^2}{5m}]F(X) \\
&+[\frac{3\rho_s \alpha J C(1-\beta\rho_s^n)\hbar^2 k_{F_s}^2}{10m}]F(X),
\end{aligned} \tag{4.6}
$$

where k_{F_s} implies that the k_F is calculated at saturation density ρ_s. The term $J_v^s = J_{v00}^s + X^2 J_{v01}^s$ is J_v evaluated at $\epsilon^{kin} = \epsilon_s^{kin}$ which is the kinetic energy part of the saturation energy per nucleon ϵ_s and $J = J_{00} + X^2 J_{01}$.

In Table-4.1, IANM incompressibility K_s as a function of X, for the standard value of $n = 2/3$ and energy dependence parameter $\alpha = 0.005$ MeV^{-1}, is provided. The magnitude of the IANM incompressibility K_s decreases with X due to lowering of the saturation densities ρ_s with the isospin asymmetry X as well as decrease in the EoS curvature. At high values of X, the IANM does not have a minimum which signify that it can never be bound by itself due to interaction of nuclear force. However, the β equilibrated nuclear matter which is a highly neutron rich IANM exists in the core of the neutron stars since its energy per nucleon is lower than that of SNM at high densities. Although it is unbound by the nuclear interaction but can be bound due to very high gravitational field that can be realized inside neutron stars.

Table 4.1: IANM incompressibility at different isospin asymmetry X using the usual values of $n = \frac{2}{3}$ and $\alpha = 0.005$ MeV^{-1}.

X	ρ_s	K_s
	fm^{-3}	MeV
0.0	0.1533	274.69
0.1	0.1525	270.44
0.2	0.1500	257.68
0.3	0.1457	236.64
0.4	0.1392	207.62
0.5	0.1300	171.16
0.6	0.1170	127.84
0.7	0.0980	78.38

It is worthwhile to mention that the RMF-NL3 incompressibility for SNM is 271.76 MeV [92, 93] which is very close to 274.7±7.4 MeV obtained from the present calculation. In spite of the fact that the parameters of the density dependence of DDM3Y interaction have been tuned to reproduce the saturation energy per nucleon ϵ_0 and the saturation density ρ_0 of the cold SNM that are obtained from finite nuclei, the agreement of the present EoS [94] with the experimental flow data [95], where the high density behavior looks phenomenologically confirmed, justifies its extrapolation to high density.

The SNM incompressibility is experimentally determined from the compression modes isoscalar giant monopole resonance (ISGMR) and isoscalar giant dipole resonance (ISGDR) of nuclei. The violations of self consistency in HF-RPA calculations [96] of the strength functions of ISGMR and ISGDR cause shifts in the calculated values of the centroid energies. These shifts may be larger in magnitude than the current experimental uncertainties. In fact, due to the use of a not fully self-consistent calculations with Skyrme interactions [96], the low values of K_∞ in the range of 210-220 MeV were predicted. Skyrme parmetrizations of SLy4 type predict K_∞ values lying in the range of 230-240 MeV [96] when this drawback is corrected. Besides that bona fide Skyrme forces can be built so that the K_∞ for SNM is rather close to the relativistic value of $\sim$ 250-270 MeV. Conclusion may, therefore, be drawn from the ISGMR experimental data that the magnitude of $K_\infty \approx 240 \pm 20$ MeV.

The lower values [97, 98] for K_∞ are usually predicted by the ISGDR data. However, it is generally agreed upon that the extraction of K_∞ in this case more problematic for various reasons. Particularly, for excitation energies [96] above 30 and 26 MeV for ^{116}Sn and ^{208}Pb, respectively, the maximum cross-section for ISGDR at high excitation energy decreases very strongly and can even fall below the range of current experimental sensitivity. The upper limit of the recent values [99] for the nuclear incompressibility K_∞ for SNM extracted from experiments is rather close to the present non-relativistic

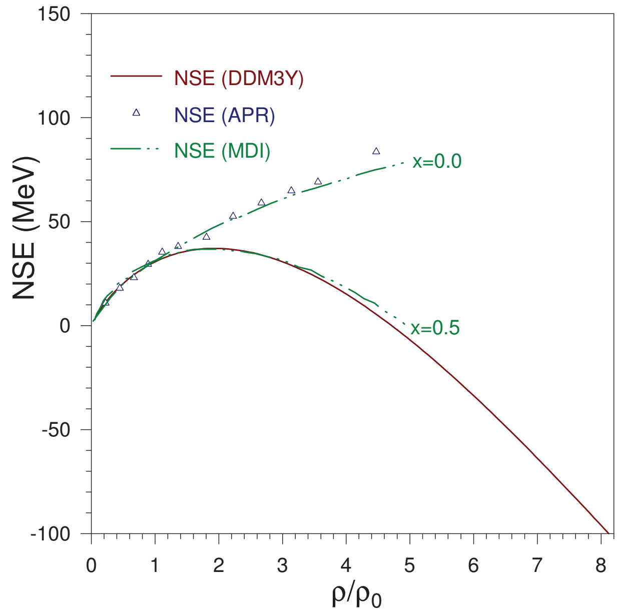

Figure 4.1: (Color online) Plots of the nuclear symmetry energy NSE is as a function of ρ/ρ_0 for the present calculation using DDM3Y interaction and its comparison, with those for Akmal-Pandharipande-Ravenhall (APR) [13] and the MDI interactions for the variable x=0.0, 0.5 defined in Ref. [105].

mean field model estimate employing DDM3Y interaction which is also in agreement with the theoretical estimates of relativistic mean field (RMF) models. With Gogny effective interactions [100], which include nuclei where pairing correlations are important, the results of microscopic calculations reproduce experimental data on heavy nuclei for K_∞ in the range about 220 MeV [101]. It may, therefore, be concluded that the calculated value of 274.7±7.4 MeV is a good theoretical result and is only slightly too high compared to the recent acceptable value [102, 103] of K_∞ for SNM in the range of 250-270 MeV.

4.1.2 Nuclear symmetry energy & its slope, incompressibility and isobaric incompressibility

The EoS of IANM, given by Eq.(4.1) can be expanded, in general, as

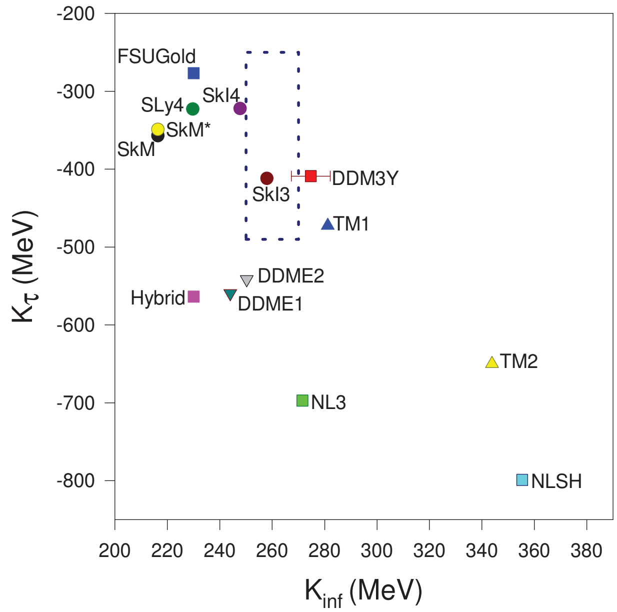

Figure 4.2: (Color online) The plots of K_τ versus K_∞ (K_{inf}). Present calculation (DDM3Y) is compared with other predictions as tabulated in Refs. [118, 120] and the dotted rectangular region encompasses the values of $K_\infty = 250 - 270$ MeV [103] and $K_\tau = -370 \pm 120$ MeV [37].

$$\epsilon(\rho, X) = \epsilon(\rho, 0) + E_{sym}(\rho)X^2 + O(X^4) \tag{4.7}$$

where $E_{sym}(\rho) = \frac{1}{2}\frac{\partial^2 \epsilon(\rho,X)}{\partial X^2} \mid_{X=0}$ is termed as the nuclear symmetry energy (NSE). The exchange symmetry between protons and neutrons in nuclear matter when one neglects the Coulomb interaction and assumes the charge symmetry of nuclear forces results in the absence of odd-order terms in X in Eq.(4.7). To a good approximation, the density-dependent NSE $E_{sym}(\rho)$ can be obtained using the following equation [104]

$$E_{sym}(\rho) = \epsilon(\rho, 1) - \epsilon(\rho, 0) \tag{4.8}$$

as the higher-order terms in X are negligible. The above equation can be obtained using Eq.(4.1). It represents a penalty levied on the system as it departs from the symmetric limit of equal number of protons and neutrons. Thus, it can be defined as the energy required per nucleon to change the SNM to PNM. In Fig.-4.1 the plot of NSE as a function of ρ/ρ_0 is shown for the present calculation (DDM3Y) and compared with those for Akmal-Pandharipande-Ravenhall [13] and MDI interactions [105].

A constraint on the NSE at nuclear saturation density $E_{sym}(\rho_0)$ is provided by the volume symmetry energy coefficient S_v which can be extracted from measured atomic mass excesses. The theoretical estimate for value of the NSE at saturation density $E_{sym}(\rho_0)$=30.71±0.26 MeV obtained from the present calculations (DDM3Y) is reasonably close to the value of S_v=30.048 ±0.004 MeV extracted [106] from the measured atomic mass excesses of 2228 nuclei. The value of NSE at ρ_0 remains mostly the same which is 30.03±0.26 MeV if one uses the mathematical definition of $E_{sym}(\rho) = \frac{1}{2}\frac{\partial^2 \epsilon(\rho,X)}{\partial X^2}\mid_{X=0}$ alternatively. The value of $E_{sym}(\rho_0) \approx 30$ MeV [107, 108, 109] appears well established empirically. The different parameterizations of RMF models, which fit observables of isospin symmetric nuclei nicely, steers to a comparatively wide range of predictions of 24-40 MeV for $E_{sym}(\rho_0)$ theoretically. Our present result (DDM3Y) of 30.71±0.26 MeV is reasonably close to that obtained using Skyrme interaction SkMP (29.9 MeV) [110], Av18+δv+UIX* variational calculation (30.1 MeV) [13].

The NSE $E_{sym}(\rho)$ can be expanded around the nuclear matter saturation density ρ_0 as

$$E_{sym}(\rho) = E_{sym}(\rho_0) + \frac{L}{3}\Big(\frac{\rho-\rho_0}{\rho_0}\Big) + \frac{K_{sym}}{18}\Big(\frac{\rho-\rho_0}{\rho_0}\Big)^2 \tag{4.9}$$

up to second order in density where L and K_{sym} represents the slope and curvature parameters of NSE at ρ_0 and hence $L = 3\rho_0\frac{\partial E_{sym}(\rho)}{\partial \rho}\mid_{\rho=\rho_0}$ and $K_{sym} = 9\rho_0^2\frac{\partial^2 E_{sym}(\rho)}{\partial \rho^2}\mid_{\rho=\rho_0}$. The K_{sym} and L highlights the density dependence of NSE around ρ_0 and carry important information at both high and low densities on the properties of NSE. Particularly, it is found that the slope parameter L correlate linearly with neutron-skin thickness of heavy nuclei and it can be obtained from the measured thickness of neutron skin of heavy nuclei [111, 112, 113]. Although there are large uncertainties in the experimental measurements, this has been possible [114] recently.

Differentiation of Eq.(4.8) twice with respect to the nucleonic density ρ using Eq.(4.1) provides [115]

$$
\begin{aligned}
&\frac{\partial E_{sym}}{\partial \rho} = \frac{2}{5}(2^{2/3}-1)\frac{E_F^0}{\rho}(\frac{\rho}{\rho_0})^{2/3} + \frac{C}{2}[1-(n+1)\beta\rho^n] \\
&\times J_{v01}(\epsilon^{kin}_{X=1}) - \frac{\alpha J_{01} C}{5} E_F^0 (\frac{\rho}{\rho_0})^{2/3}[1-\beta\rho^n]F(1) \\
&-(2^{2/3}-1)\frac{\alpha J_{00} C}{5} E_F^0 (\frac{\rho}{\rho_0})^{2/3}[1-\beta\rho^n] \\
&-\frac{3}{10}(2^{2/3}-1)\alpha J_{00} C E_F^0 (\frac{\rho}{\rho_0})^{2/3}[1-(n+1)\beta\rho^n]
\end{aligned} \tag{4.10}
$$

$$
\begin{aligned}
&\frac{\partial^2 E_{sym}}{\partial \rho^2} = -\frac{2}{15}(2^{2/3}-1)\frac{E_F^0}{\rho^2}(\frac{\rho}{\rho_0})^{2/3} - \frac{C}{2}n(n+1)\beta\rho^{n-1} \\
&\times J_{v01}(\epsilon^{kin}_{X=1}) - \frac{2\alpha J_{01} C}{5}\frac{E_F^0}{\rho}(\frac{\rho}{\rho_0})^{2/3}[1-(n+1)\beta\rho^n]F(1) \\
&+\frac{\alpha J_{01} C}{15}\frac{E_F^0}{\rho}(\frac{\rho}{\rho_0})^{2/3}[1-\beta\rho^n]F(1) \\
&+(2^{2/3}-1)\frac{\alpha J_{00} C}{15}\frac{E_F^0}{\rho}(\frac{\rho}{\rho_0})^{2/3}[1-\beta\rho^n] \\
&-\frac{2}{5}(2^{2/3}-1)\alpha J_{00} C \frac{E_F^0}{\rho}(\frac{\rho}{\rho_0})^{2/3}[1-(n+1)\beta\rho^n] \\
&+\frac{3}{10}(2^{2/3}-1)\alpha J_{00} C E_F^0 (\frac{\rho}{\rho_0})^{2/3} n(n+1)\beta\rho^{n-1}.
\end{aligned} \tag{4.11}
$$

Here the Fermi energy is $E_F^0 = \frac{\hbar^2 k_{F_0}^2}{2m}$ for the SNM at ground state and to evaluate the values of L and K_{sym}, the definitions of which are provided after Eq.(4.9), along with Eqs.(4.10,4.11) at ρ=ρ_0 have been used.

The isobaric incompressibility $K_\infty(X)$ for infinite IANM can be expanded in the power series of isospin asymmetry parameter X as $K_\infty(X) = K_\infty + K_\tau X^2 + K_4 X^4 + O(X^6)$. Compared to K_τ [37] the magnitude of the higher-order K_4 parameter is quite small in general. The former essentially characterizes the isospin dependence of the incompressibility at ρ_0 and expressed as $K_\tau = K_{sym} - 6L - \frac{Q_0}{K_\infty} L = K_{asy} - \frac{Q_0}{K_\infty} L$ where the third-order derivative parameter of SNM at ρ_0 is Q_0, given by

$$Q_0 = 27\rho_0^3 \frac{\partial^3 \epsilon(\rho, 0)}{\partial \rho^3} \mid_{\rho=\rho_0} . \tag{4.12}$$

One obtains, using Eq.(4.1), the following

$$\begin{aligned}
&\frac{\partial^3 \epsilon(\rho, X)}{\partial \rho^3} = -\frac{C J_v(\epsilon^{kin}) n(n+1)(n-1)\beta\rho^{n-2}}{2} \\
&+\frac{8}{45}\frac{E_F^0}{\rho^3} F(X)(\frac{\rho}{\rho_0})^{\frac{2}{3}} + \frac{3\alpha JC}{5} n(n+1)\beta\rho^{n-1}\frac{E_F^0}{\rho} \\
&\times F(X)(\frac{\rho}{\rho_0})^{\frac{2}{3}} + \frac{\alpha JC}{5}[1-(n+1)\beta\rho^n]\frac{E_F^0}{\rho^2} F(X)(\frac{\rho}{\rho_0})^{\frac{2}{3}} \\
&-\frac{4\alpha JC}{45}[1-\beta\rho^n]\frac{E_F^0}{\rho^2} F(X)(\frac{\rho}{\rho_0})^{\frac{2}{3}}
\end{aligned} \tag{4.13}$$

where the Fermi energy $E_F^0 = \frac{\hbar^2 k_{F_0}^2}{2m}$ for the SNM at ground state, $k_{F_0} = (1.5\pi^2\rho_0)^{\frac{1}{3}}$ and $J = J_{00} + X^2 J_{01}$. Thus

$$\begin{aligned}
&\frac{\partial^3 \epsilon(\rho, 0)}{\partial \rho^3} \mid_{\rho=\rho_0} = -\frac{C J_{v00}(\epsilon_0^{kin}) n(n+1)(n-1)\beta\rho_0^{n-2}}{2} \\
&+\frac{8}{45}\frac{E_F^0}{\rho_0^3} + \frac{3\alpha J_{00} C}{5} n(n+1)\beta\rho_0^{n-1}\frac{E_F^0}{\rho_0} + \frac{\alpha J_{00} C}{5} \\
&\times[1-(n+1)\beta\rho_0^n]\frac{E_F^0}{\rho_0^2} - \frac{4\alpha J_{00} C}{45}[1-\beta\rho_0^n]\frac{E_F^0}{\rho_0^2}.
\end{aligned} \tag{4.14}$$

For the calculations of K_∞, $E_{sym}(\rho_0)$, L, K_{sym} and K_τ, the values of ρ_0=0.1533 fm^{-3}, $\epsilon_0 = -15.26 \pm 0.52$ MeV for the SNM and $n = \frac{2}{3}$ [116] have been used. Using the improved quantum molecular dynamics transport model, the collisions involving ^{112}Sn and ^{124}Sn nuclei can be simulated to reproduce isospin diffusion data from two different observables and the ratios of proton and neutron spectra. The constraints on the density dependence of the NSE at subnormal density can be obtained [117] by comparing these data to calculations performed over a range of NSEs at ρ_0 and different representations of the density dependence of the NSE. The results for K_∞, L, $E_{sym}(\rho_0)$ and density dependence of $E_{sym}(\rho)$ [116] of the present calculations are consistent with these constraints [117]. In Table-4.2, the values of K_∞, $E_{sym}(\rho_0)$, L, K_{sym} and K_τ are tabulated and compared with the corresponding quantities obtained from the RMF models [118]. The range of values of the ten constraints (experimental and empirical) provided in Table-I of Ref.[119] compare well with the theoretical values listed in Table-4.2 and Fig.-4.2 except incompressibility which is only slightly overestimated.

What is a reasonable value of incompressibility [96] remains controversial. In the following we present our results in the backdrop of others, without justifying any particular value for K_∞, but for an objective view of the current situation which, we stress, is still progressing. In Fig.-4.2, the plot of K_τ versus K_∞ for the present calculation (DDM3Y) has been compared with the predictions of SkI3, SkI4, SLy4, SkM, SkM*, FSUGold, NL3, Hybrid [118], NLSH, TM1, TM2, DDME1 and DDME2 as given in Table-I of Ref. [120]. The recent values of $K_\infty = 250 - 270$ MeV [103] and $K_\tau = -370 \pm 120$ MeV [37] are enclosed by the dotted rectangular region. Though both DDM3Y and SkI3 are within the above region, unlike DDM3Y the L value for SkI3 is 100.49 MeV which is much above the acceptable limit of 58.9 ± 16 MeV [121, 122, 123, 124]. Another recent review [125] also finds that $E_{sym}(\rho_0) = 31.7 \pm 3.2$ MeV and $L = 58.7 \pm 28.1$ MeV with an error for L that is considerably larger than that for $E_{sym}(\rho_0)$. However, DDME2 is reasonably close to the rectangular region which has $L = 51$ MeV. It is worthwhile to mention here that the DDM3Y interaction with the same ranges, strengths and density dependence that provides $L = 45.11 \pm 0.02$, allows good descriptions of elastic and inelastic scattering, proton radioactivity [86] and α radioactivity of superheavy elements [126, 127]. The present NSE increases initially with nucleonic density up to about $2\rho_0$ and then decreases monotonically (hence 'soft') and becomes negative at higher densities (about $4.7\rho_0$) [86, 116] (hence 'super-soft'). It is consistent with the recent evidence for a soft NSE at suprasaturation densities [105] and with the fact that the super-soft nuclear symmetry energy preferred by the FOPI/GSI experimental data on the π^+/π^- ratio in relativistic heavy-ion reactions can readily keep neutron stars stable if the non-Newtonian gravity proposed in the grand unification theories is considered [128].

Table 4.2: Comparison of the present results obtained using DDM3Y effective interaction with those of RMF models [118] for SNM incompressibility K_∞, NSE at saturation density $E_{sym}(\rho_0)$, slope L and the curvature K_{sym} parameters of NSE, K_{asy} and isobaric incompressibility K_τ of IANM (all in MeV).

Model	K_∞	$E_{sym}(\rho_0)$	L	K_{sym}	K_{asy}	Q_0	K_τ
This work	274.7	30.71	45.11	-183.7	-454.4	-276.5	-408.97
	± 7.4	± 0.26	± 0.02	± 3.6	± 3.5	± 10.5	± 3.01
FSUGold	230.0	32.59	60.5	-51.3	-414.3	-523.4	-276.77
NL3	271.5	37.29	118.2	$+100.9$	-608.3	$+204.2$	-697.36
Hybrid	230.0	37.30	118.6	$+110.9$	-600.7	-71.5	-563.86

4.2 Equation of state of β-equilibrated nuclear matter

The β-equilibrated nuclear matter EoS is obtained by evaluating the asymmetric nuclear matter EoS at the isospin asymmetry X determined from the β-equilibrium proton fraction $x_p = \frac{\rho_p}{\rho}$, obtained approximately by solving

$$\hbar c(3\pi^2\rho x_p)^{1/3} = 4E_{sym}(\rho)(1-2x_p). \qquad (4.15)$$

The exact way of obtaining β-equilibrium proton fraction is by solving

$$\hbar c(3\pi^2\rho x_p)^{1/3} = -\frac{\partial\epsilon(\rho, x_p)}{\partial x_p} = +2\frac{\partial\epsilon}{\partial X}, \tag{4.16}$$

where isospin asymmetry $X = 1 - 2x_p$.

The stability of the β-equilibrated dense matter in neutron stars is investigated and the location of the inner edge of their crusts and core-crust transition density and pressure are determined using the DDM3Y effective nucleon-nucleon interaction [39]. The stability of any single phase, also called intrinsic stability, is ensured by the convexity of $\epsilon(\rho, x_p)$. The thermodynamical inequalities allow us to express the requirement in terms of $V_{thermal} = \rho^2\Big[2\rho\frac{\partial\epsilon}{\partial\rho}+\rho^2\frac{\partial^2\epsilon}{\partial\rho^2}-\rho^2\frac{(\frac{\partial^2\epsilon}{\partial\rho\partial x_p})^2}{\frac{\partial^2\epsilon}{\partial x_p^2}}\Big]$. The condition for core-crust transition is obtained by making $V_{thermal} = 0$. The results for the transition density, pressure and proton fraction at the inner edge separating the liquid core from the solid crust of neutron stars are calculated for various n. The symmetric nuclear matter incompressibility K_∞, nuclear symmetry energy at saturation density $E_{sym}(\rho_0)$, the slope L and isospin dependent part K_τ of the isobaric incompressibility are already tabulated in Table-4.2 and these are all in excellent agreement with the constraints recently extracted from measured isotopic dependence of the giant monopole resonances in even-A Sn isotopes, from the neutron skin thickness of nuclei, and from analyses of experimental data on isospin diffusion and isotopic scaling in intermediate energy heavy-ion collisions.

The rigorous way of dealing with core-crust transition is producing a unified EoS and evaluating the density where the clustered phase becomes energetically disfavored with respect to the homogeneous solution [129]. It should be clarified here that the crustal region of the compact star in the present work consists of FMT+BPS+BBP up to number density of 0.0582 fm^{-3} and β-equilibrated neutron star matter up to core-crust transition number density of 0.0938 fm^{-3} which is far beyond 0.0582 fm^{-3}, otherwise we would have taken a unified EoS. The three different methods to calculate the transition density are the thermodynamical spinodal (the method used in this work), the dynamical spinodal within the Vlasov formalism and the relativistic random phase approximation. It was shown that the last two methods [130] give similar results, confirming previous studies [131, 132]. The thermodynamical method also gives a good estimate of the transition density [130, 133] and involves simpler calculations.

4.3 Crustal fraction of moment of inertia in neutron stars

The moment of inertia of a neutron star can be calculated by assuming it to be rotating slowly with a uniform angular velocity Ω [134, 135]. The angular velocity $\bar{\omega}(r)$ of a point in the star measured with respect to the angular velocity of the local inertial frame is determined by the equation

$$\frac{1}{r^4}\frac{d}{dr}\left[r^4 j \frac{d\bar{\omega}}{dr}\right] + \frac{4}{r}\frac{dj}{dr}\bar{\omega} = 0 \tag{4.17}$$

where

$$j(r) = e^{-\phi(r)}\sqrt{1 - \frac{2Gm(r)}{rc^2}}. \tag{4.18}$$

The function $\phi(r)$ is constrained by the condition

$$e^{\phi(r)}\mu(r) = \text{constant} = \mu(R)\sqrt{1 - \frac{2GM}{Rc^2}} \tag{4.19}$$

where the chemical potential $\mu(r)$ is defined as

$$\mu(r) = \frac{\varepsilon(r) + P(r)}{\rho(r)}. \tag{4.20}$$

Using these relations, Eq.(4.17) can be solved subject to the boundary conditions that $\bar{\omega}(r)$ is regular as $r \to 0$ and $\bar{\omega}(r) \to \Omega$ as $r \to \infty$. The moment of inertia of the star can then be calculated using the definition $I = J/\Omega$, where the total angular momentum J is given by

$$J = \frac{c^2}{6G} R^4 \frac{d\bar{\omega}}{dr}\Big|_{r=R}. \tag{4.21}$$

The crustal fraction of the moment of inertia $\frac{\Delta I}{I}$ can be expressed as a function of gravitational mass of the star M and its radius R by the following approximate expression [18]

$$\begin{aligned} \frac{\Delta I}{I} &\approx \frac{28\pi \mathrm{P}_t R^3}{3Mc^2} \left(\frac{1 - 1.67\xi - 0.6\xi^2}{\xi} \right) \\ &\times \left(1 + \frac{2\mathrm{P}_t}{\rho_t m_b c^2} \frac{(1+7\xi)(1-2\xi)}{\xi^2} \right)^{-1} \end{aligned} \tag{4.22}$$

where $\xi = \frac{GM}{Rc^2}$, ρ_t and P_t are the density and the pressure, respectively, at the core to crust transition. As obvious from the above equation the major dependence is on the value of P_t, since ρ_t enters only as a correction term. The fact that from the observations of pulsar glitches the crustal fraction of the moment of inertia can be inferred, makes it particularly interesting [136].

It has been shown that the glitches show a self-sustaining instability for which the star prepares over a waiting time [18]. The glitches in the Vela pulsar suggests that the angular momentum should be such that more than 1.4% of the moment of inertia drives these events. Therefore, if glitches originate in the liquid of the inner crust, it would imply that $\frac{\Delta I}{I} > 1.4\%$.

4.4 Theoretical Calculations and Results

The values of the saturation density ρ_0 and the saturation energy per baryon ϵ_0 of SNM used in the calculations are 0.1533 fm^{-3} [29] and -15.26 MeV [88], respectively. The co-efficient of the volume term a_v of the liquid drop model mass formula represents the saturation energy per baryon and can be determined by fitting the atomic mass excesses (experimental and estimated) from Audi-Wapstra-Thibault atomic mass table [89] by minimizing the mean square deviation. In such calculations the corrections for the electronic binding energy [90] are included. In a recent work that includes surface symmetry energy term, Wigner term, shell correction and proton form factor correction to Coulomb energy also, a_v turns out to be 15.4496 MeV and when A^0 and $A^{1/3}$ terms are also included [91] it turns out to be 14.8497 MeV. Using the usual value of $\alpha = 0.005$ MeV^{-1} for the parameter of energy dependence of the zero range potential and $n = \frac{2}{3}$, the values obtained for the constants of density dependence C and β and the SNM incompressibility K_∞ are 2.2497, 1.5934 fm^2 and 274.7 MeV, respectively. The value of -15.26±0.52 MeV of the saturation energy per baryon, more or less, covers the entire range for which the values of C=2.2497±0.0420, β=1.5934±0.0085 fm^2 and the SNM incompressibility K_∞=274.7±7.4 MeV [86] are obtained.

The stability of the β-equilibrated dense matter in neutron stars is investigated and the location of the inner edge of their crusts and core-crust transition density and pressure are determined using the DDM3Y effective NN interaction. The results for the transition density, pressure and proton fraction at the inner edge separating the liquid core from the solid crust of neutron stars are calculated and presented in Table-4.3 for $n = \frac{2}{3}$. The symmetric nuclear matter incompressibility K_∞, nuclear symmetry energy at saturation density $E_{sym}(\rho_0)$, the slope L and isospin dependent part K_τ of the isobaric incompressibility are also tabulated since these are all in excellent agreement with the recently extracted constraints from the measured isotopic dependence of the giant monopole resonances in even-A Sn isotopes [137], from the neutron skin thickness of nuclei, and from analyses of experimental data on isospin diffusion and isotopic scaling in intermediate energy heavy-ion collisions.

The calculations for masses and radii are performed using the EoS covering the crustal region of a compact star which are Feynman-Metropolis-Teller (FMT) [8], Baym-Pethick-Sutherland (BPS) [9] and Baym-Bethe-Pethick (BBP) [10] upto number density of 0.0582 fm^{-3} and β-equilibrated neutron star matter beyond. The values of I obtained by solving Eq.(4.17) subject to the boundary conditions stated earlier are listed in Table-4.4 along with masses M, radii R and crustal thickness ΔR of neutron stars. Once masses and radii are determined, $\frac{\Delta I}{I}$ are obtained from Eq.(4.22) and listed in Table-4.4. In Fig.-4.3, variation of mass with central density is plotted for slowly rotating neutron stars for the present nuclear EoS. In Fig.-4.4, the mass-radius relation of slowly rotating neutron stars is shown. Using Eq.(4.22) again the mass-radius relation is obtained for fixed values of $\frac{\Delta I}{I}$, ρ_t and P$_t$. This is then plotted in the same figure for $\frac{\Delta I}{I}$ equal to 0.014. For Vela pulsar, the constraint $\frac{\Delta I}{I} > 1.4\%$ implies that allowed mass-radius lie to the right of the line defined by $\frac{\Delta I}{I} = 0.014$ (for $\rho_t = 0.0938$ fm^{-3}, P$_t = 0.5006$ MeV fm^{-3}). This condition is given by the inequality $R \geq 4.10 + 3.36 M/M_\odot$ km.

The calculations are performed for five different n values that correspond to SNM incompressibility ranging from ~180-330 MeV. For each case, the constants C and β obtained by reproducing the ground state properties of SNM become different leading to five different sets of these three parameters. We certainly cannot change strengths and ranges of the M3Y interaction. In Table-4.5, the variations of the core-crust transition density, pressure and proton fraction for β-equilibrated neutron star matter, symmetric nuclear matter incompressibility K_∞, isospin dependent part K_τ of isobaric incompressibility, neutron star's maximum mass with corresponding radius and crustal thickness with parameter n are listed along with corresponding Vela pulsar constraints. It is important to mention here that recent observations of the binary millisecond pulsar J1614-2230 by P. B. Demorest et al. [138] suggest that the masses lie within 1.97$\pm$0.04 $M_\odot$ where $M_\odot$ is the solar mass. Recently the radio timing measurements of the pulsar PSR J0348 + 0432 and its white dwarf companion have confirmed the mass of the pulsar to be in the range 1.97-2.05 $M_\odot$ at 68.27% or 1.90-2.18 $M_\odot$at 99.73% confidence [139]. The observed 1.97$\pm$0.04 $M_\odot$ neutron star rotates with 3.1 ms and results quoted in Table 2 are for non-rotating case. Similar work using M3Y effective interaction using the so called CDM3Y6 [140] density dependence can predict $\sim$2 $M_\odot$ neutron stars. For rotating stars [72] present EoS predict masses higher than the lower limit of 1.93 $M_\odot$ for maximum mass of neutron stars. We used the same value of ρ_0 =0.1533 fm^{-3} since we wanted to keep consistency with all our previous works on nuclear matter. We would like to mention that if instead we would have used the value of 0.16 fm^{-3} [141] for ρ_0, the value of K_∞ would have been slightly higher by $\sim$2 MeV and correspondingly maximum mass of neutron stars by $\sim$0.01 $M_\odot$.

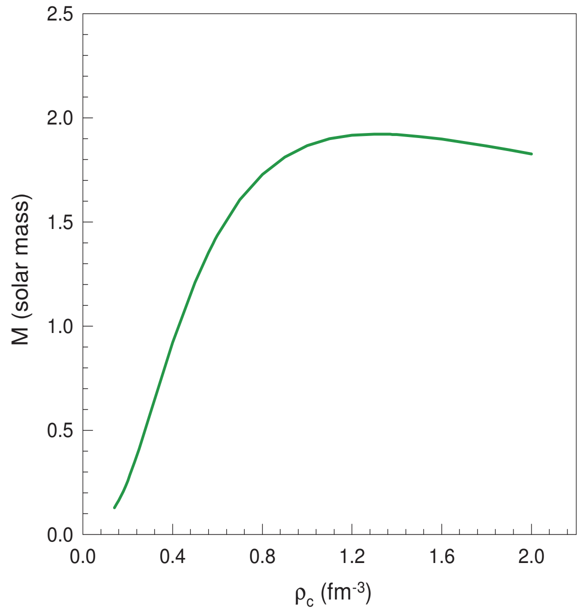

Figure 4.3: Variation of mass with central density for slowly rotating neutron stars for the present nuclear EoS.

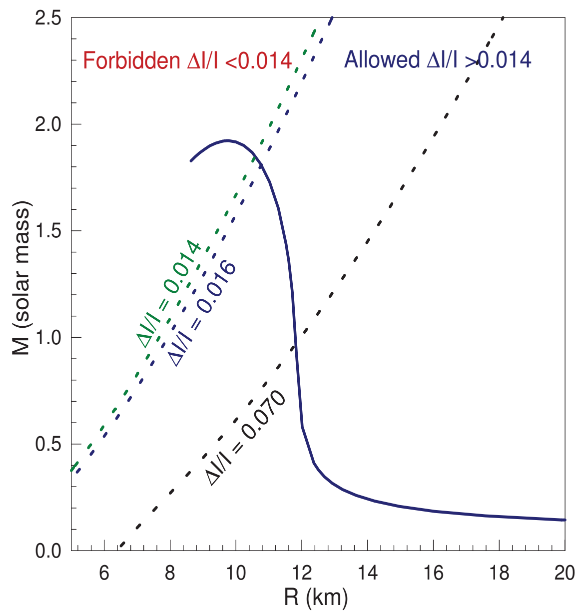

Figure 4.4: The mass-radius relation of slowly rotating neutron stars for the present nuclear EoS. The constraint of $\frac{\Delta I}{I} > 1.4\%$ $(1.6\%, 7\%)$ for the Vela pulsar implies that to the right of the line defined by $\frac{\Delta I}{I} = 0.014$ $(0.016, 0.07)$ (for $\rho_t = 0.0938$ fm^{-3}, $\mathrm{P}_t = 0.5006$ MeV fm^{-3}), allowed masses and radii lie.

Table 4.3: Results of present calculations for $n=\frac{2}{3}$ of symmetric nuclear matter incompressibility K_∞, nuclear symmetry energy at saturation density $E_{sym}(\rho_0)$, the slope L and isospin dependent part K_τ of the isobaric incompressibility (all in MeV) [38] are tabulated along with the density, pressure and proton fraction at the core-crust transition for β-equilibrated neutron star matter and corresponding Vela pulsar constraint.

K_∞	$E_{sym}(\rho_0)$	L	K_τ
274.7 ± 7.4	30.71 ± 0.26	45.11 ± 0.02	-408.97 ± 3.01
$\rho_t(\mathrm{fm}^{-3})$	$\mathrm{P}_t(\mathrm{MeVfm}^{-3})$	$x_{p(t)}$	Vela pulsar R(km)
0.0938	0.5006	0.0308	$R \geq 4.10 + 3.36 M/M_\odot$

Table 4.4: Radii, masses, total & crustal fraction of moment of inertia and crustal thickness as functions of central density ρ_c.

ρ_c	R	M	I	$\frac{\Delta I}{I}$	ΔR
fm^{-3}	km	$M_\odot$	$M_\odot$km^2	fraction	km
2.00	8.6349	1.8277	70.88	0.0055	0.2462
1.90	8.7598	1.8467	73.83	0.0057	0.2523
1.80	8.8957	1.8651	77.00	0.0060	0.2598
1.70	9.0444	1.8824	80.38	0.0063	0.2696
1.60	9.2052	1.8980	83.97	0.0067	0.2806
1.50	9.3810	1.9109	87.70	0.0072	0.2951
1.40	9.5710	1.9197	91.52	0.0079	0.3121
1.39	9.5911	1.9203	91.91	0.0080	0.3144
1.38	9.6109	1.9208	92.29	0.0080	0.3161
1.37	9.6314	1.9213	92.67	0.0081	0.3185
1.36	9.6514	1.9217	93.05	0.0082	0.3203
1.35	9.6718	1.9220	93.43	0.0083	0.3222
1.34	9.6928	1.9223	93.81	0.0084	0.3248
1.33	9.7141	1.9225	94.18	0.0085	0.3275
1.32	9.7349	1.9226	94.55	0.0085	0.3296

ρ_c	R	M	I	$\frac{\Delta I}{I}$	ΔR
fm^{-3}	km	$M_\odot$	$M_\odot\mathrm{km}^2$	fraction	km
1.31	9.7559	1.9227	94.93	0.0086	0.3318
1.30	9.7770	1.9226	95.30	0.0087	0.3340
1.20	9.9995	1.9173	98.85	0.0098	0.3620
1.10	10.2371	1.9004	101.88	0.0112	0.3970
1.00	10.4902	1.8675	103.94	0.0132	0.4441
0.90	10.7544	1.8127	104.42	0.0158	0.5066
0.80	11.0239	1.7285	102.47	0.0197	0.5929
0.70	11.2865	1.6064	97.04	0.0255	0.7148
0.60	11.5245	1.4369	87.06	0.0344	0.8952
0.59	11.5456	1.4170	85.78	0.0356	0.9175
0.58	11.5666	1.3965	84.44	0.0368	0.9411
0.57	11.5874	1.3753	83.04	0.0381	0.9663
0.56	11.6073	1.3536	81.58	0.0394	0.9924
0.55	11.6262	1.3313	80.07	0.0408	1.0193
0.50	11.7135	1.2104	71.65	0.0492	1.1792

ρ_c	R	M	I	$\frac{\Delta I}{I}$	ΔR
fm^{-3}	km	$M_\odot$	$M_\odot \mathrm{km}^2$	fraction	km
0.45	11.7830	1.0734	61.88	0.0602	1.3897
0.40	11.8388	0.9206	51.00	0.0752	1.6801
0.30	12.0129	0.5808	28.54	0.1249	2.7618
0.25	12.3703	0.4103	19.24	0.1686	3.9149
0.24	12.5113	0.3779	17.73	0.1805	4.2542
0.23	12.6944	0.3464	16.35	0.1942	4.6511
0.22	12.9314	0.3159	15.14	0.2103	5.1189
0.21	13.2434	0.2867	14.12	0.2296	5.6802
0.20	13.6576	0.2587	13.31	0.2537	6.3643
0.19	14.2131	0.2323	12.74	0.2847	7.2125
0.18	14.9725	0.2075	12.47	0.3265	8.2904
0.17	16.0398	0.1845	12.59	0.3863	9.7057
0.16	17.5771	0.1634	13.25	0.4767	11.6254
0.15	19.8913	0.1445	14.77	0.6254	14.3634
0.14	23.5740	0.1278	17.88	0.8972	18.5215

Table 4.5: Variations of the core-crust transition density, pressure and proton fraction for β-equilibrated neutron star matter, symmetric nuclear matter incompressibility K_∞ and isospin dependent part K_τ of isobaric incompressibility with parameter n.

n	ρ_t	P_t	$x_{p(t)}$	K_∞	K_τ	Maximum Mass	Radius	Crustal Thickness
	fm^{-3}	$MeVfm^{-3}$		MeV	MeV	$M_\odot$	km	km
Expt.	values	- - $\rightarrow$	$\rightarrow$	250-270	-370±120	1.97±0.04		
1/6	0.0797	0.4134	0.0288	182.13	-293.42	1.4336	8.5671	0.4009
				R(km) $\geq$	4.48 +	$3.37M/M_\odot$		
1/3	0.0855	0.4520	0.0296	212.98	-332.16	1.6002	8.9572	0.3743
				R(km) $\geq$	4.31 +	$3.36M/M_\odot$		
1/2	0.0901	0.4801	0.0303	243.84	-370.65	1.7634	9.3561	0.3515
				R(km) $\geq$	4.19 +	$3.36M/M_\odot$		
2/3	0.0938	0.5006	0.0308	274.69	-408.97	1.9227	9.7559	0.3318
				R(km) $\geq$	4.10 +	$3.36M/M_\odot$		
1	0.0995	0.5264	0.0316	336.40	-485.28	2.2335	10.6408	0.3088
				R(km) $\geq$	3.99 +	$3.36M/M_\odot$		

Chapter 5

R-MODE INSTABILITY IN NEUTRON STARS

Rotational instabilities in NSs come in different flavours, but they have one general feature in common: they can be directly associated with unstable modes of oscillation [142, 143, 144, 145, 146, 147]. In the present work the r-mode instability has been discussed with reference to the EoS obtained using the density dependent M3Y (DDM3Y) effective nucleon-nucleon (NN) interaction. The discovery of r-mode oscillation in neutron star (NS) by Anderson [142] and confirmed by Friedman and Morsink [144] opened the window for study of the gravitational wave emitted by NSs by using advance detecting system. Also it provides the possible explanation for the spin down mechanism in the hot young NSs as well as in spin up cold old accreting NSs.

The r-mode oscillation is analogous to Rossby wave in the ocean and results from perturbation in velocity field of the star with little disturbance in the star's density. In a non-rotating star the r-modes are neutral rotational motions. In a rotating star Coriolis effects provide a weak restoring force that gives them genuine dynamics. The r-mode frequency always has different signs in the inertial and rotating frames. That is, although the modes appear retrograde in the rotating system, an observer in the inertial frame shall view them as prograde. To the leading order, the pattern speed of the mode is [148, 149]

$$\sigma = \frac{(l-1)\,(l+2)}{l\,(l+1)}\Omega \tag{5.1}$$

Since, $0 < \sigma < \Omega$ for all $l \geq 2$, where Ω is the angular velocity of the star in the inertial frame, the r-modes are destabilized by the standard Chandrasekhar-Friedman-Schutz (CFS) mechanism and are unstable because of the emission of gravitational waves. The gravitational radiation that the r-modes emit comes from their time-dependent mass currents. This is the gravitational analogue of magnetic monopole radiation. The quadrupole $l = 2$ r-mode is more strongly unstable to gravitational radiation than any other mode in neutron stars. Further, these modes exist with velocity perturbation if and only if $l = m$ mode [145, 148]. This emission in gravitational waves causes a growth in the mode energy E_{rot} in the rotating frame, despite decrease in the inertial-frame energy $E_{inertial}$. This puzzling effect can be understood from the relation between the two energies,

$$E_{rot} = E_{inertial} - \Omega J \tag{5.2}$$

where the angular momentum of the star is J. From this it is clear that E_{rot} may increase if both $E_{inertial}$ and J decrease. The frequencies of these r-modes, in the lowest order terms in an expansion in terms of angular velocity Ω is [149, 150]

$$\omega = -\frac{(l-1)\,(l+2)}{l+1}\Omega. \tag{5.3}$$

The instability in the mode grows because of gravitational wave emission which is opposed by the viscosity [151]. For the instability to be relevant, it must grow fast than it is damped out by the viscosity. So the time scale for gravitationally driven instability needs to be sufficiently short to the viscous damping time scale. The amplitude of r-modes evolves with time dependence $e^{i\omega t - t/\tau}$ as a consequence of ordinary hydrodynamics and the influence of the various dissipative processes. The imaginary part of the frequency $1/\tau$ is determined by the effects of gravitational radiation, viscosity, etc. [150, 152, 153]. The time-scale associated with the different process involve the actual physical parameters of the neutron star. In computing these physical parameters the role of nuclear physics comes into picture, where one gets a platform to constrain the uncertainties existing in the nuclear EoS. The present knowledge on nuclear EoS under highly isospin asymmetric dense situation is quite uncertain. So correlating the predictions of the EoSs obtained under systematic variation of the physical properties, to the r-mode observables can be of help in constraining the uncertainity associated with the EoS.

5.1 Dissipative time scales and stability of the r-modes

The concern here is to study the evolution of the r-modes due to the competition of gravitational radiation and dissipative influence of viscosity. For this purpose it is necessary to consider the effects of radiation on the evolution of mode energy. This is expressed as the integral of the fluid perturbation [150, 154],

$$\widetilde{E} = \frac{1}{2}\int \left[\rho \delta\vec{v}.\delta\vec{v}^{*} + \left(\frac{\delta p}{\rho} - \delta\Phi\right)\delta\rho^{*}\right] d^3r, \tag{5.4}$$

with ρ being the mass density profile of the star, $\delta\vec{v}$, δp, $\delta\Phi$ and $\delta\rho$ are perturbations in the velocity, pressure, gravitational potential and density due to oscillation of the mode respectively. The dissipative time scale of an r-mode is [150],

$$\frac{1}{\tau_i} = -\frac{1}{2\widetilde{E}}\left(\frac{d\widetilde{E}}{dt}\right)_i, \tag{5.5}$$

where the index 'i' refers to the various dissipative mechanisms, i.e., gravitational wave emissions and viscosity (bulk and shear).

For the lowest order expressions for the r-mode $\delta\vec{v}$ and $\delta\rho$ the expression for energy of the mode in Eq.(5.4) can be reduced to a one-dimensional integral [150, 155]

$$\widetilde{E} = \frac{1}{2}\alpha_r^2 R^{-2l+2}\Omega^2 \int_0^R \rho(r) r^{2l+2} dr, \tag{5.6}$$

where R is the radius of the NS, α_r is the dimensionless amplitude of the mode, Ω is the angular velocity of the NS and $\rho(r)$ is the radial dependance of the mass density of NS. Since the expression of $(\frac{d\widetilde{E}}{dt})$ due to gravitational radiation [153, 156] and viscosity [152, 153, 157] are known, Eq.(5.5) can be used to evaluate the imaginary part $\frac{1}{\tau}$. It is convenient to decompose $\frac{1}{\tau}$ as

$$\frac{1}{\tau(\Omega,T)} = \frac{1}{\tau_{GR}(\Omega,T)} + \frac{1}{\tau_{BV}(\Omega,T)} + \frac{1}{\tau_{SV}(\Omega,T)}, \tag{5.7}$$

where $1/\tau_{GR}$, $1/\tau_{BV}$ and $1/\tau_{SV}$ are the contributions from gravitational radiation, bulk viscosity and shear viscosity, respectively, and are given by [152, 153]

$$\begin{aligned} \frac{1}{\tau_{GR}} = -\frac{32\pi G\Omega^{2l+2}}{c^{2l+3}} \frac{(l-1)^{2l}}{[(2l+1)!!]^2} \left(\frac{l+2}{l+1}\right)^{(2l+2)} \\ \times \int_0^{R_c} \rho(r) r^{2l+2} dr, \end{aligned} \tag{5.8}$$

$$\begin{aligned} \frac{1}{\tau_{SV}} = \left[\frac{1}{2\Omega}\frac{2^{l+3/2}(l+1)!}{l(2l+1)!!I_l}\sqrt{\frac{2\Omega R_c^2\rho_c}{\eta_c}}\right]^{-1} \\ \times \left[\int_0^{R_c} \frac{\rho(r)}{\rho_c}\left(\frac{r}{R_c}\right)^{2l+2}\frac{dr}{R_c}\right]^{-1}, \end{aligned} \tag{5.9}$$

where G and c are the gravitational constant and velocity of light respectively; R_c, ρ_c, η_c in Eq.(5.9) are the radius, density and shear viscosity of the fluid at the outer edge of the core respectively.

The shear viscosity time scale in Eq.(5.9) is obtained by considering the shear dissipation in the viscous boundary layer between solid crust and the liquid core with the assumption that the crust is rigid and hence static in rotating frame [152].

The motion of the crust due to mechanical coupling to the core effectively increases τ_{SV} by $(\frac{\Delta v}{v})^{-2}$, where $\frac{\Delta v}{v}$ is the difference in the velocities in the inner edge of the crust and outer edge of the core divided by the velocity of the core [158].

Bildsten and Ushomirsky [159] have first estimated this effect of solid crust on r-mode instability and shown that the shear dissipation in this viscous boundary layer decreases the viscous damping time scale by more than 10^5 in old acreting neutron stars and more than 10^7 in hot, young neutron stars. I_l in Eq.(5.9) has the value $I_2 = 0.80411$, for $l = 2$ [152].

Moreover, the bulk viscous dissipation is not significant for temperature of the star below 10^{10} K and in this range of temperature the shear viscosity is the dominant dissipative mechanism, We have restricted our study in this work to the range of the temperature $T < 10^{10}$ K and included only shear dissipative mechanism. The studies is similar to the one done by Moustakidis [160], where we have mainly examined the influence of neutron star EoS and the gravitational mass on the instability boundary and other relevant quantities, such as, critical frequency and temperature, etc. for a neutron star using the DDM3Y effective interaction [86].

As mentioned above, we have studied the instability within $T \leq 10^{10}$ K, the dominant dissipation mechanism is the shear viscosity in the boundary layer for which the time scale is given in Eq.(5.7), where η_c is the viscosity of the fluid. In the temperature range $T \geq 10^9$ K, the dominant contribution to shear is from neutron-neutron (nn) scattering and below $T \leq 10^9$, it is the electron-electron (ee) scattering that contributes to shear primarily [152]. Therefore,

$$\frac{1}{\tau_{SV}} = \frac{1}{\tau_{ee}} + \frac{1}{\tau_{nn}}, \tag{5.10}$$

where τ_{ee} and τ_{nn} can be obtained from Eq.(5.9) using the corresponding value of η_{SV}^{ee}

and η_{SV}^{nn}. These are given by [161, 162]

$$\eta_{SV}^{ee} = 6 \times 10^6 \rho^2 T^{-2} \qquad (\mathrm{g\ cm^{-1}\ s^{-1}}), \tag{5.11}$$

$$\eta_{SV}^{nn} = 347 \rho^{9/4} T^{-2} \qquad (\mathrm{g\ cm^{-1}\ s^{-1}}), \tag{5.12}$$

where all the quantities are given in CGS units and T is measured in K. In order to have transparent visualisation of the role of angular velocity and temperature on various time scales, it is useful to factor them out by defining fiducial time scales. Thus, we define fiducial shear viscous time scale $\widetilde{\tau}_{SV}$ such that [150, 152],

$$\tau_{SV} = \widetilde{\tau}_{SV} \left(\frac{\Omega_0}{\Omega}\right)^{1/2} \left(\frac{T}{10^8 K}\right), \tag{5.13}$$

and fiducial gravitational radiation time scale $\widetilde{\tau}_{GR}$ is defined through the relation [150, 152],

$$\tau_{GR} = \widetilde{\tau}_{GR} \left(\frac{\Omega_0}{\Omega}\right)^{2l+2}, \tag{5.14}$$

where $\Omega_0 = \sqrt{\pi G \bar{\rho}}$ and $\bar{\rho} = 3M/4\pi R^3$ is the mean density of NS having mass M and radius R. Thus Eq.(5.7) (neglecting bulk viscosity contributions) becomes

$$\frac{1}{\tau(\Omega, T)} = \frac{1}{\widetilde{\tau}_{GR}} \left(\frac{\Omega}{\Omega_0}\right)^{2l+2} + \frac{1}{\widetilde{\tau}_{SV}} \left(\frac{\Omega}{\Omega_0}\right)^{1/2} \left(\frac{10^8 K}{T}\right). \tag{5.15}$$

Dissipative effects cause the mode to decay exponentially as $e^{-t/\tau}$ i.e. the mode is stable, as long as $\tau > 0$. From Eq.(5.8) and Eq.(5.9) it can be seen that $\widetilde{\tau}_{SV} > 0$, while $\widetilde{\tau}_{GR} < 0$. Thus gravitational radiation drives these modes towards instability while viscosity tries to stabilize them. For small Ω the gravitational radiation contribution to $1/\tau$ is very small since it is proportional to Ω^{2l+2}. Thus for sufficiently small angular velocity, viscosity dominates and the mode is stable. But for sufficiently large Ω gravitational radiation will dominate and drive the mode unstable. For a given temperature and mode l the equation for critical angular velocity Ω_c is obtained from the condition $\frac{1}{\tau(\Omega_c,T)} = 0$. At a given T and mode l, the equation for the critical velocity is a polynomial of order $l+1$ in Ω_c^2 and thus each mode has its own characteristic Ω_c. Since the smallest of these, i.e. $l = 2$, is the dominant contributor, study is being done for this mode only. The critical angular velocity Ω_c for this mode is obtained to be

$$\left(\frac{\Omega_c}{\Omega_0}\right) = \left(-\frac{\tilde{\tau}_{GR}}{\tilde{\tau}_{SV}}\right)^{2/11} \left(\frac{10^8 K}{T}\right)^{2/11}. \tag{5.16}$$

The angular velocity of a neutron star can never exceed the Kepler velocity $\Omega_K \approx \frac{2}{3}\Omega_0$. Thus, there is a critical temperature below which the gravitational radiation is completely suppressed by viscosity. This critical temperature is given by [152]

$$\frac{T_c}{10^8 K} = \left(\frac{\Omega_0}{\Omega_c}\right)^{11/2} \left(-\frac{\tilde{\tau}_{GR}}{\tilde{\tau}_{SV}}\right) \approx (3/2)^{11/2} \left(-\frac{\tilde{\tau}_{GR}}{\tilde{\tau}_{SV}}\right). \tag{5.17}$$

The critical angular velocity is now expressed in terms of critical temperature from Eq.(5.13) and Eq.(5.14) as

$$\left(\frac{\Omega_c}{\Omega_0}\right) = \frac{\Omega_K}{\Omega_0} \left(\frac{T_c}{T}\right)^{2/11} \approx (2/3) \left(\frac{T_c}{T}\right)^{2/11}. \tag{5.18}$$

So, once the neutron star EoS is ascertained, then all physical quantities necessary for the calculation of r-mode instability can be performed.

Further, following the work of Owen et al. [153] the evolution of the angular velocity, as the angular momentum is radiated to infinity by the gravitational radiation is given by

$$\frac{d\Omega}{dt} = \frac{2\Omega}{\tau_{GR}} \frac{\alpha_r^2 Q}{1 - \alpha_r^2 Q}, \tag{5.19}$$

where α_r is the dimensionless r-mode amplitude and $Q = 3\tilde{J}/2\tilde{I}$ with,

$$\widetilde{J} = \frac{1}{MR^4} \int_0^R \rho(r) r^6 dr \tag{5.20}$$

and

$$\widetilde{I} = \frac{8\pi}{3MR^2} \int_0^R \rho(r) r^4 dr. \tag{5.21}$$

α_r is treated as free parameter whose value varies within a wide range $1 - 10^{-8}$. Under the ideal consideration that the heat generated by the shear viscosity is same as that taken out by the emission of neutrinos [160, 163], Eq.(5.19) can be solved for the angular frequency $\Omega(t)$ as

$$\Omega(t) = \left(\Omega_{in}^{-6} - Ct\right)^{-1/6}, \tag{5.22}$$

where

$$C = \frac{12\alpha_r^2 Q}{\widetilde{\tau}_{GR}\left(1 - \alpha_r^2 Q\right)} \frac{1}{\Omega_0^6}, \tag{5.23}$$

and Ω_{in} is considered as a free parameter whose value corresponds to be the initial angular velocity. The spin down rate can be obtained from Eq.(5.19) to be,

$$\frac{d\Omega}{dt} = \frac{C}{6}\left(\Omega_{in}^{-6} - Ct\right)^{-7/6}. \tag{5.24}$$

The neutron star spin shall decrease continually until it approaches its critical angular velocity Ω_c. The time t_c taken by neutron star to evolve from its initial value Ω_{in} to its minimum value Ω_c is given by

$$t_c = \frac{1}{C}\left(\Omega_{in}^{-6} - \Omega_c^{-6}\right). \tag{5.25}$$

Table 5.1: Spin frequencies and core temperatures (measurements and upper limits) of observed Low Mass X-ray Binaries (LMXBs) and Millisecond Radio Pulsars (MSRPs) [164].

Source	ν (Hz)	$T_{core}(10^8 K)$
Aql X-1	550	1.08
4U 1608-52	620	4.55
KS 1731-260	526	0.42
MXB 1659-298	556	0.31
SAX J1748.9-2021	442	0.89
IGR 00291+5934	599	0.54
SAX J1808.4-3658	401	< 0.11
XTE J1751-305	435	< 0.54
XTE J0929-314	185	< 0.26
XTE J1807-294	190	< 0.27
XTE J1814-338	314	< 0.51
EXO 0748-676	552	1.58
HETE J1900.1-2455	377	< 0.33
IGR J17191-2821	294	< 0.60
IGR J17511-3057	245	< 1.10
SAX J1750.8-2900	601	3.38
NGC 6440 X-2	205	< 0.12
Swift J1756-2508	182	< 0.78
Swift J1749.4-2807	518	< 1.61
J2124-3358	203	< 0.17
J0030+0451	205	< 0.70

5.2 Theoretical Calculations

The quantity which is of crucial importance in the evaluation of various times scales, as can be seen from Eq.(5.8) and Eq.(5.9), is the integral $\int_0^{R_c} \rho(r) r^6 dr$. This integral can be re-written in terms of energy density $\epsilon(r) = \rho(r)c^2$ and expressed in dimensionless form as

$$I(R_c) = \int_0^{R_c} \left[\frac{\epsilon(r)}{\mathrm{MeVfm^{-3}}}\right] \left(\frac{r}{\mathrm{km}}\right)^6 d\left(\frac{r}{\mathrm{km}}\right) \tag{5.26}$$

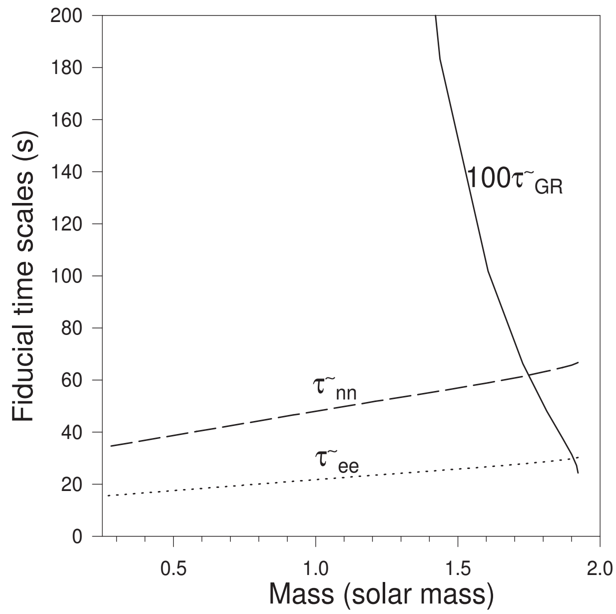

Figure 5.1: Plots of fiducial timescales with gravitational mass of neutron stars with DDM3Y EoS.

The fiducial gravitational radiation timescale $\tilde{\tau}_{GR}$ from Eq.(5.8) and Eq.(5.14), is given by

$$\tilde{\tau}_{GR} = -0.7429 \left[\frac{R}{\mathrm{km}}\right]^9 \left[\frac{1M_\odot}{M}\right]^3 [I(R_c)]^{-1}\,(\mathrm{s}) \tag{5.27}$$

where R and r are in km and M in $M_\odot$.

The fiducial shear viscous timescale $\tilde{\tau}_{SV}$ for electron-electron scattering and neutron-neutron scattering can be obtained from Eq.(5.9), Eqs.(5.11-5.13) as

$$\widetilde{\tau}_{ee} = 0.1446 \times 10^8 \left[\frac{R}{\text{km}}\right]^{3/4} \left[\frac{1M_\odot}{M}\right]^{1/4} \left[\frac{\text{km}}{R_c}\right]^6$$
$$\times \left[\frac{\text{g cm}^{-3}}{\rho_t}\right]^{1/2} \left[\frac{\text{MeVfm}^{-3}}{\epsilon_t}\right] [I(R_c)]\,(\text{s}) \tag{5.28}$$

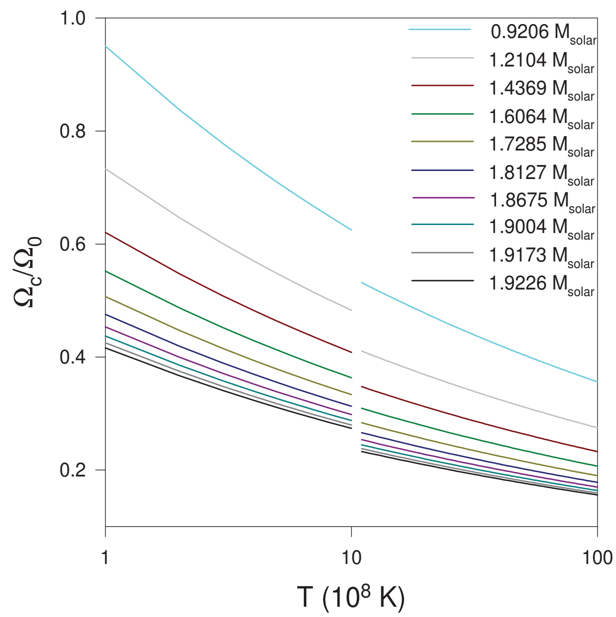

Figure 5.2: (Color online) Plots of reduced critical angular frequency with temperature for different masses of neutron stars.

$$\widetilde{\tau}_{nn} = 19 \times 10^8 \left[\frac{R}{\text{km}}\right]^{3/4} \left[\frac{1M_\odot}{M}\right]^{1/4} \left[\frac{\text{km}}{R_c}\right]^6$$
$$\times \left[\frac{\text{g cm}^{-3}}{\rho_t}\right]^{5/8} \left[\frac{\text{MeVfm}^{-3}}{\epsilon_t}\right] [I(R_c)]\,(\text{s}) \tag{5.29}$$

where the transition density ρ_t is expressed in g cm^{-3} and ϵ_t is the energy density expressed in MeV fm^{-3} at transition density.

5.3 Results and discussion

In Fig.-5.1 plots of the fiducial timescales with the gravitational masses of neutron stars are shown for the DDM3Y EoS. It is seen that the gravitational radiation timescale falls

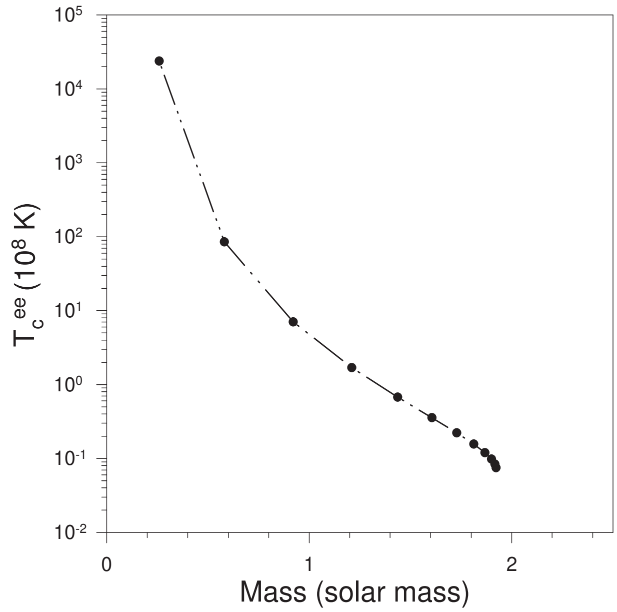

Figure 5.3: Plots of critical temperature versus mass.

rapidly with increasing mass while the viscous damping timescales increase approximately linearly. By knowing the fiducial gravitational radiation and shear viscous timescales, the temperature T dependence of the critical angular velocity Ω_c of the r-mode ($l = 2$) can be studied from Eq.(5.16). In Fig.-5.2, $\frac{\Omega_c}{\Omega_0}$ is shown as a function of temperature T for several masses of neutron stars for the DDM3Y EoS. The plots act as boundaries of the r-mode instability windows. Neutron stars lying above the plots (whose angular frequency is greater than the critical frequency) possess unstable r-modes and hence emit gravitational waves, thus reducing their angular frequencies. Once their angular velocities reach the critical frequency they enter the region below the plots, where the r-modes become stable and hence stop emitting gravitational radiation. In computing the instability windows in Fig.-5.2, the fiducial shear viscous timescale $\widetilde{\tau}_{ee}$ given in Eq.(5.28) is substituted for $\widetilde{\tau}_{SV}$ in Eq.(5.16) for temperatures T $\leq 10^9$ K and τ_{nn} from Eq.(5.29) is used for T $> 10^9$ K.

Fig.-5.3 depicts the plot of the critical temperature as a function of mass. The electron-electron scattering shear viscosity timescale is used for the calculation of T_c. We see that the critical temperature rapidly decreases with mass. The explanation is straightforward.

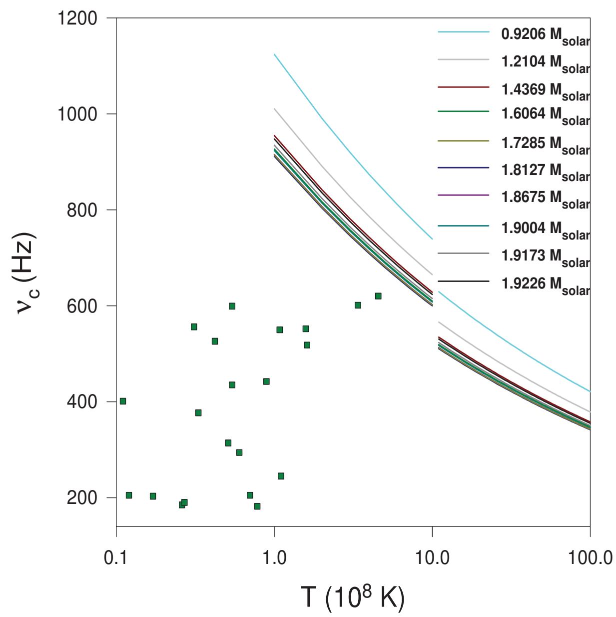

Figure 5.4: (Color online) Plots of critical frequency with temperature for different masses of neutron stars. The square dots represent observational data [164] of Table-5.1.

From Fig.-5.2 we see that for fixed T, $\frac{\Omega_c}{\Omega_0}$ rapidly decreases with increasing mass. Since $T = T_c$ when $\Omega_c = \Omega_K$ and Ω_K rapidly increases with mass and hence T_c falls, vide Eq.(5.18).

From Fig.-5.2 and Fig.-5.3 we see that the critical frequency and critical temperature decrease with mass and hence the r-mode instability window increases with the same. This means that for the same EoS and temperature, the massive configurations are more probable to r-mode instability and hence emission of gravitational waves than the less massive ones. This can be indirectly inferred from Fig.-5.1 where $\widetilde{\tau}_{GR}$ is much less than $\widetilde{\tau}_{ee}$ and $\widetilde{\tau}_{nn}$ for massive neutron stars and vice-versa for low mass neutron stars. Hence isolated young massive neutron stars have high probability for emission of gravitational waves through r-mode instability.

In Table-5.1, the spin frequencies and core temperatures (measurements and upper limits) of observed Low Mass X-ray Binaries (LMXBs) and Millisecond Radio Pulsars (MSRPs) [164] are listed and in Fig.-5.4 their positions in the critical frequency versus temperature plot are shown to compare with observational data. From Fig.-5.4, it is interesting to note that according to our model of the EoS with a rigid crust and a relatively small r-mode amplitude, all of the observed neutron stars lie in the stable r-mode region which is consistent with the lack of observation of gravitational radiation due to r-mode instability.

It is worth noting that Ω_c is dependent on the density dependence of the symmetry energy and thus on L. Again, R, R_c, $I(R_c)$ and ρ_t depend on L. Hence, for a fixed mass and temperature, Ω_c is dependent on the above parameters via the relation,

$$\Omega_c \sim \frac{R_c^{12/11}}{[I(R_c)]^{4/11}} \rho_t^{3/11} \tag{5.30}$$

In our case L, ρ_t and R_c are constants for a fixed neutron star mass and temperature. As a neutron star enters into the instability region due to accretion of mass from its companion, the amplitude of the r-mode α_r increases till reaching a saturation value. At this point the neutron star emits gravitational wave and releases its angular momentum and energy and spins down to the region of stability. Using the ideal condition that the decrease in temperature due to emission of gravitational wave is compensated by the heat produced due to viscous effects, the time evolution of spin angular velocity and spin down rate can be calculated for a neutron star from Eq.(5.22) and Eq.(5.24), respectively, provided M, T, Ω_{in} and α_r of the star is known. For the schematic values $\nu_{in} = \frac{\Omega_{in}}{2\pi} = 700$ Hz and $\alpha_r = 2 \times 10^{-7}$ used by Moustakidis [160], the evolutions of spin are calculated for various neutron star masses and shown in Fig.-5.5. In Fig.-5.6 the spin down rates has been shown for these masses. In Fig.-5.7 the spin down rates as functions of spin frequency are shown.

Some mention is to be made about the dependency of the critical frequency Ω_c on the symmetry energy slope parameter L. Although the slope L depends on the strengths and

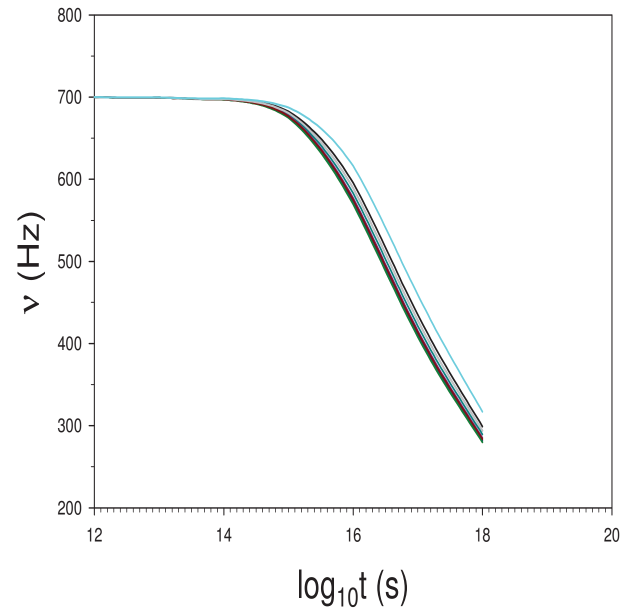

Figure 5.5: (Color online) Plots of time evolution of frequencies.

ranges of the Yukawas for the DDM3Y EoS, it does not depend on the power of the density dependence n and has a constant value of 45.1066 MeV. In a recent work, the critical frequency as a function of L of the pulsar 4U 1608-52 was plotted using an estimated core temperature $\sim 4.55 \times 10^8$ K and with different models of the EoS. In accordance with the Fig.-5.1 of [155], using the measured spin frequency and the estimated core temperature, if the mass of 4U 1608-52 is $1.4 M_\odot$ then it should marginally be unstable (Ω_c is smaller than its spin frequency), since the radius obtained from our mass-radius relation (Fig.-4.4) is $\sim$ 11.55 kms and higher than 11.5 kms. In case of the highest mass configuration of 1.9227 $M_\odot$ with a radius of $\sim$9.75 kms, it is also likely to be in the instability region as $L < 50$ MeV for our EoS. Thus we stress the fact that the r-mode instability window is enlarged for isolated neutron stars with a rigid crust if we consider the dissipation to be at the crust-core interface in agreement with [165].

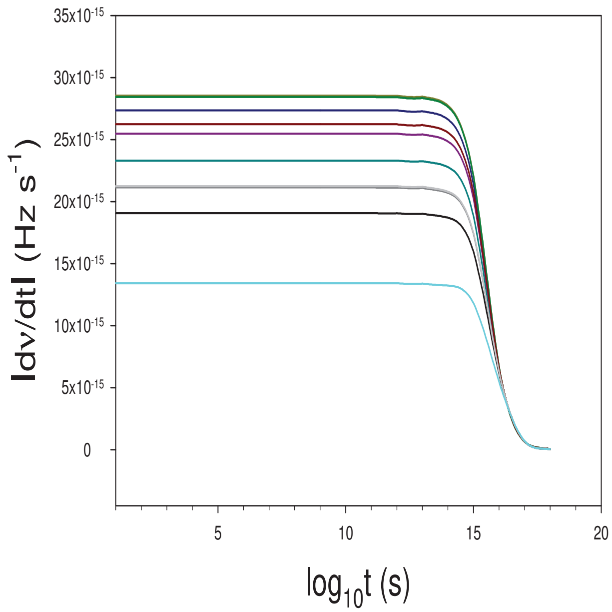

Figure 5.6: (Color online) Plots of time evolution of spin-down rates.

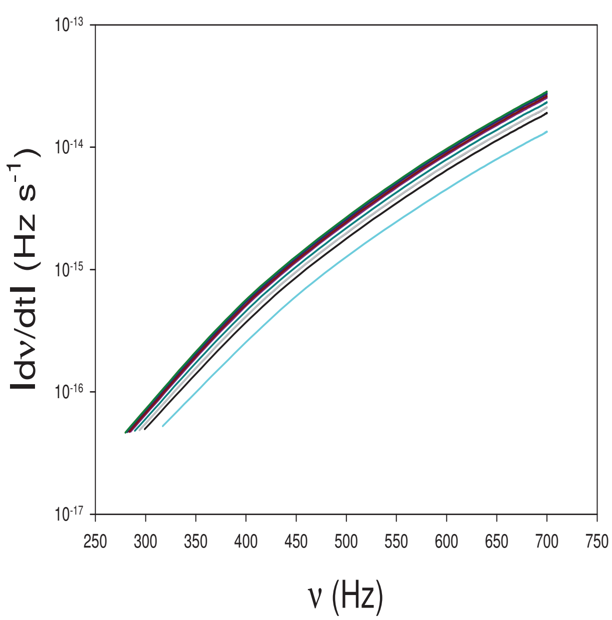

Figure 5.7: (Color online) Plots of spin-down rates versus frequencies.

Chapter 6

MASS-RADIUS RELATIONSHIP FOR NORMAL AND DARK MATTER ADMIXED NEUTRON STARS

In the universe there are large empty regions and dense regions where the galaxies are distributed. This distribution is called the cosmic web that is speculated to be governed by the action of gravity on the invisible mysterious “dark matter”. Recently, a research group led by Hiroshima University has suggested that the Cancer constellation has nine such large concentrations of dark matter, each the mass of a galaxy cluster [166].

Various theoretical models of dark matter are widespread, ranging from Cold Dark Matter to Warm Dark Matter to Hot Dark Matter and from Symmetric to Asymmetric Dark Matter [167, 168, 169, 170, 171]. Recent advances in cosmological precision tests further consolidate the minimal cosmological standard model, indicating that the universe contains 4.9% ordinary matter, 26.8% dark matter and 68.3% dark energy. Although being five times more abundant than ordinary matter, the basic properties of dark matter, such as particle mass and interactions are unsolved.

A dark star composed mostly of normal matter and dark matter may have existed early in the universe before conventional stars were able to form. Those stars generate heat via annihilation reactions between the dark matter particles. This heat prevents such stars from collapsing into the relatively compact sizes of modern stars and therefore prevent nuclear fusion among the normal matter atoms from being initiated [172].

One theory is that dark matter could be made of particles called axions. Unlike protons, neutrons and electrons that make up ordinary matter, axions can share the same quantum energy state. They also attract each other gravitationally, so they clump together. Dark matter is hard to study because it does not interact much with ordinary matter, but axion dark matter could theoretically be observed in the form of Bose stars [173]. The Bose-Einstein condensation may come from the bosonic features of dark matter models. Phase transition to condensation can occur either when the temperature cools below critical value or when the density exceeds the critical value [174].

The neutron stars could capture weakly interacting dark matter particles (WIMPs) because of their strong gravitational field, high density and finite, but very small, WIMP-to-nucleon cross section. In fact, if there is no baryon-dark matter interaction, purely baryonic neutron star would not capture dark matter at all. A dark star of comparable mass may as well accrete neutron star matter to form a dark matter dominated neutron star. In 1978, Steigman et al. [48] suggested that capture of WIMPs by individual stellar objects could affect the stellar structure and evolution. The effect of self annihilating dark matter on first-generation stars and on the evolution path of main sequence stars have been studied extensively [49, 50]. For non self-annihilating dark matter, its impact on main sequence stars [51] and neutron stars [52, 53] have been studied in different dark matter models. Gravitational effects of non self-annihilating condensate dark matter on compact stellar objects has been studied [54] assuming dark matter as ideal Fermi gas and considering the accretion process through dark matter self-interaction from the surrounding halo. The non-annihilating heavy dark matter of mass greater than 1 GeV is predicted to accumulate at the center of neutron star leading it to a possible collapse [175]. The effect of this accumulation is observable only in cases where the annihilation cross section is extremely small [176, 177]. The capture is fully efficient even for WIMP-to-nucleon cross sections (elastic or inelastic) as low as 10^{-18} mb. Moreover, a dark star of comparable mass may as well accrete neutron star matter to form a dark matter dominated neutron star. In addition to Axions and WIMPs, a general class of dark matter candidates called, Macros have been suggested that would have macroscopic size and mass [178].

Since dark matter interacts with normal baryonic matter through gravity, it is quite possible for white dwarfs and neutron stars to accrete dark matter and evolve to a dark matter admixed compact star [50, 53, 175, 179, 180, 181, 182, 183, 184]. The large baryonic density in compact stars increases the probability of dark matter capture within the star and eventually results in gravitational trapping. It may also be possible for dark matter alone to form gravitationally bound compact objects and thus mimic stellar mass black holes [185].

The hydrostatic equilibrium configuration of an admixture of degenerate dark matter and normal nuclear matter was studied by using a general relativistic two-fluid formalism taking non-self-annihilating dark matter particles of mass 1 GeV. A new class of compact stars was predicted that consisted a small normal matter core with radius of a few kilometers embedded in a ten-kilometer-sized dark matter halo [53].

Compact objects formed by non-self annihilating dark matter admixed with ordinary matter has been predicted with Earth-like masses and radii from few kms to few hundred kms for weakly interacting dark matter. For the strongly interacting dark matter case, dark compact planets are suggested to form with Jupiter-like masses and radii of few hundred kms [186]. Possible implications of asymmetric fermionic dark matter for neutron stars has been studied that applies to various dark fermion models such as mirror matter models and to other models where the dark fermions have self-interactions [187].

Although dark matter particles can have only very weak interactions with standard model states, it is an intriguing possibility that they experience much stronger self-interactions and thereby alter the behavior of dark matter on astrophysical and cosmological scales in striking ways. Recent studies [188, 189, 190, 191, 192, 193] have provided constraints on dark matter self-interaction cross-section. The constraints are based on the Cusp-core problem and the "Too big to fail" problem of galaxies. According to them the dark matter self-interaction cross-section per unit mass is about 0.1-100 $cm^2/g \sim 0.1$-1 barn/GeV, typical of the scale of strong interactions.

In this work, we consider fermionic Asymmetric Dark Matter (ADM) particles of mass 1 GeV and the self-interaction mediator mass of 100 MeV (low mass implying strong interaction), mixed with rotating and non-rotating neutron stars. ADM, like ordinary baryonic matter, is charge asymmetric with only the dark baryon (or generally only the particle) excess remains after the annihilation of most antiparticles after the Big Bang. Hence these ADM particles are non self-annihilating and behaves like ordinary free particles. The gravitational stability and mass-radius relations of static, rigid and differentially rotating neutron stars mixed with fermionic ADM are calculated using the LORENE code [194]. It is important to note that we do not allow any phase transition of the nuclear matter and the interaction between nuclear matter and dark matter is only through gravity.

6.1 Equation of state of non-interacting fermionic asymmetric dark matter

We consider the non-interacting fermionic ADM to be a completely degenerate free Fermi gas of particle mass m_χ at zero temperature. By the Pauli exclusion principle, no quantum state can be occupied by more than one fermion with an identical set of quantum numbers. Thus a non-interacting Fermi gas, unlike a Bose gas, is prohibited from condensing into a Bose-Einstein condensate. The total energy of the Fermi gas at absolute zero is larger than the sum of the single-particle ground states because the Pauli principle implies a degeneracy pressure that keeps fermions separated and moving.

The non-interacting assembly of fermions at zero temperature exerts pressure because of kinetic energy from different states filled up to Fermi level. Since pressure is force per unit area which means rate of momentum transfer per unit area, it is given by

$$P_\chi = \frac{1}{3}\int p v n_p d^3p = \frac{1}{3}\int \frac{p^2c^2}{\sqrt{(p^2c^2 + m_\chi^2 c^4)}} n_p d^3p \tag{6.1}$$

where m_χ is the rest mass of dark particles, v is the velocity of the particles with momentum $\vec{p}$ and $n_p d^3p$ is the number of particles per unit volume having momenta between $\vec{p}$ and $\vec{p}+d\vec{p}$. The factor $\frac{1}{3}$ accounts for the fact that, on average, only $\frac{1}{3}$rd of total particles $n_p d^3p$ are moving in a particular direction. For fermions having spin $\frac{1}{2}$, degeneracy = 2, $n_p d^3p = \frac{8\pi p^2 dp}{h^3}$ and hence number density $n_\chi$is given by

$$n_\chi = \int_0^{p_F} n_p d^3p = \frac{8\pi p_F^3}{3h^3} = \frac{x_F^3}{3\pi^2\lambda_\chi^3} \tag{6.2}$$

where p_F is the Fermi momentum which is maximum momentum possible at zero temperature, $x_F = \frac{p_F}{m_\chi c}$ is a dimensionless quantity and $\lambda_\chi = \frac{\hbar}{m_\chi c}$ is the Compton wavelength. The energy density ε_χ is given by

$$\varepsilon_\chi = \int_0^{p_F} E n_p d^3p = \int_0^{p_F} \sqrt{(p^2c^2 + m_\chi^2 c^4)} \frac{8\pi p^2 dp}{h^3} \tag{6.3}$$

which, along with Eq.(6.2), turns out upon integration to be

$$\varepsilon_\chi = \frac{m_\chi c^2}{\lambda_\chi^3} \chi(x_F); \qquad P_\chi = \frac{m_\chi c^2}{\lambda_\chi^3} \phi(x_F), \tag{6.4}$$

where

$$\chi(x) = \frac{1}{8\pi^2}[x\sqrt{1+x^2}(1+2x^2) - \ln(x + \sqrt{1+x^2})] \tag{6.5}$$

and

$$\phi(x) = \frac{1}{8\pi^2}[x\sqrt{1+x^2}(\frac{2x^2}{3} - 1) + \ln(x + \sqrt{1+x^2})]. \tag{6.6}$$

6.2 Equation of state of strongly self-interacting fermionic asymmetric dark matter

In order to calculate EoS of strongly interacting fermionic ADM we take course to massive vector field theory similar to the meson exchange of the nuclear interaction. The Lagrangian density (in natural units) of a massive vector field is given by

$$\mathcal{L} = -\frac{1}{4}F_{\mu\nu}F^{\mu\nu} + \frac{1}{2}m_I^2 A_\mu A^\mu - j_\mu A^\mu \tag{6.7}$$

where $F_{\mu\nu} = \partial_\mu A_\nu - \partial_\nu A_\mu$, A^μ is the 4-vector field, j^μ is the 4-current and m_I is the mass of the field quanta. The equation of motion is given by

$$(\partial_\nu \partial^\nu + m_I^2)A^\mu = j^\mu. \tag{6.8}$$

Now considering a charge of magnitude g at rest at the origin we have

$$j^0 = g\delta^3(\vec{x}) \quad \vec{j} = 0. \tag{6.9}$$

Substituting the above in the right side of Eq.(6.9) and also noting that $A^0 = V$ and $\vec{A} = 0$ we finally get

$$(\nabla^2 - m_I^2)V = -g\delta^3(\vec{x}) \tag{6.10}$$

whose solution is the Yukawa potential:

$$V(r) = g\frac{e^{-m_I r}}{4\pi r} \tag{6.11}$$

Hence the potential energy of two like charges of magnitude g is

$$V_{12}(r) = g^2\frac{e^{-m_I r}}{4\pi r} \tag{6.12}$$

and is repulsive in nature.

To proceed to the EoS, we calculate the total energy of a system of particles classically by summing over the interactions of all pairs of particles. To facilitate the calculation, we assume that the macroscopic assembly is uniformly distributed, thereby neglecting the influence of the interaction on the mean inter-particle separation. In other words, we ignore any correlations between particle positions due to their mutual interaction. Finally, we assume that the number of particles is sufficiently large that we can replace sums by integrals, and that the characteristic size of the assembly R satisfies $R >> 1/m_I$ [195].

The total Yukawa potential energy of a system of N particles in volume Ω is

$$E_\Omega = \frac{1}{2}\sum_{i\neq j} V_{ij} = \frac{1}{2}n^2 g^2 \int\int \frac{e^{-m_I r_{ij}}}{4\pi r_{ij}} d\Omega_i d\Omega_j, \tag{6.13}$$

where n is the number density.

Choosing one particle at the origin and integrating to infinity (ignoring surface terms) we get,

$$E_\Omega = \frac{1}{2m_I^2} n^2 g^2 \Omega, \tag{6.14}$$

so that the interaction energy density can be written as,

$$\varepsilon_{int} = \frac{E_\Omega}{\Omega} = \frac{1}{2m_I^2} n^2 g^2. \tag{6.15}$$

Now putting $g^2/2 = 1$ for convenience, $x_f = k_f/m_\chi$, where m_χ is the rest mass of the dark matter particle and using the relation $k_f = (3\pi^2 n)^{1/3}$ we get putting back $\hbar$ and c

$$\varepsilon_{int} = \left(\frac{1}{3\pi^2}\right)^2 \frac{x_f^6 m_\chi^6}{(\hbar c)^3 m_I^2} \tag{6.16}$$

where m_χ and m_I are expressed in MeV.

The pressure due to the interacting energy density can be computed with the help of the thermodynamic relation $P_{int} = n^2 \frac{d}{dn}\left(\frac{\varepsilon_{int}}{n}\right)$, which yields

$$P_{int} = \left(\frac{1}{3\pi^2}\right)^2 \frac{x_f^6 m_\chi^6}{(\hbar c)^3 m_I^2} \tag{6.17}$$

Hence the total energy density and pressure of self-interacting dark matter particles are given by

$$\varepsilon_{\chi int} = \varepsilon_\chi + \varepsilon_{int} = \frac{m_\chi}{\lambda_\chi^3}\chi(x_F) + \left(\frac{1}{3\pi^2}\right)^2 \frac{x_f^6 m_\chi^6}{(\hbar c)^3 m_I^2} \tag{6.18}$$

$$P_{\chi int} = P_\chi + P_{int} = \frac{m_\chi}{\lambda_\chi^3}\phi(x_F) + \left(\frac{1}{3\pi^2}\right)^2 \frac{x_f^6 m_\chi^6}{(\hbar c)^3 m_I^2} \tag{6.19}$$

The mass of the exchange boson determines the strength and range of the interaction implying lower the mass stronger the interaction and for non-interacting dark matter, m_I

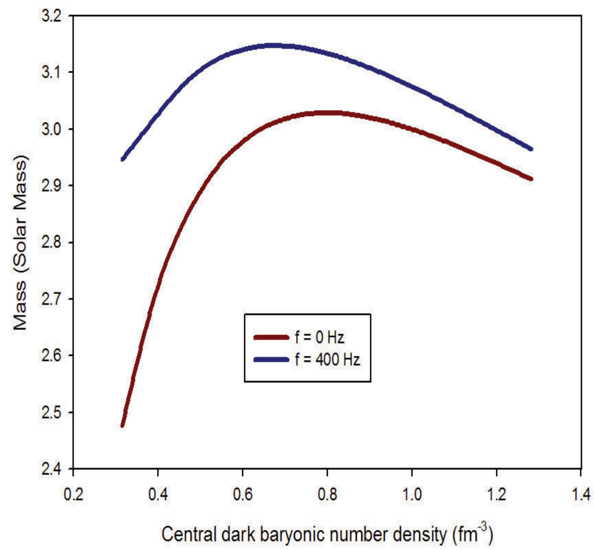

Figure 6.1: Plots of mass vs. central density for static and rotating fermionic Asymmetric Dark Matter stars.

is infinity and second terms in above equations are absent. Figs.-6.1 and 6.2 depict the plots of mass vs. central dark matter density and mass vs. equatorial radius respectively for static and rotating stars using self-interacting dark matter EoS. We see that the maximum mass for non-rotating stars goes to $3.0279 M_\odot$ with a radius of 16.2349 kms and that for rotating stars goes to $3.1460 M_\odot$ with equatorial radius of 19.2173 kms. Now, if we take the dark matter particle mass m_χ to be 0.5 GeV, then the maximum mass goes to $\sim 12.6 M_\odot$ using the relation Mass $\propto 1/m_\chi^2$ [182], thus mimicking stellar mass black holes.

6.3 Two-fluid TOV equations

We consider two ideal fluids - the nuclear matter and fermionic dark matter with the above two EoSs coupled gravitationally to form the structure of the mixed neutron star. The energy-momentum tensor of the mixed fluid can be written as [187, 196]

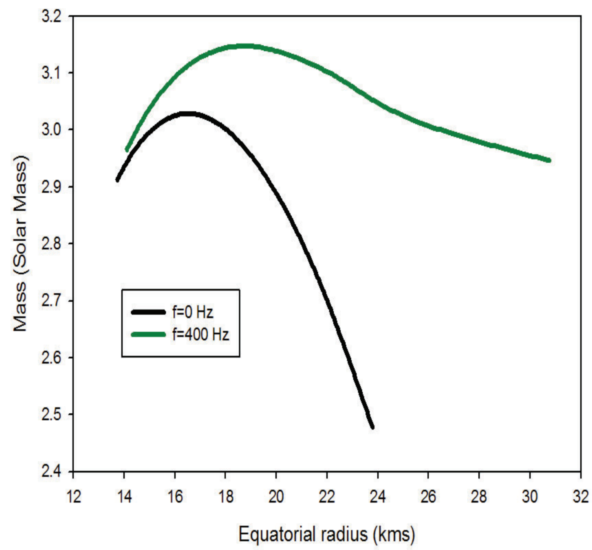

Figure 6.2: Mass-equatorial radius plots for static and rotating fermionic Asymmetric Dark Matter stars.

$$
\begin{aligned}
T^{\mu\nu} = \quad & T^{\mu\nu}_{nuc} + T^{\mu\nu}_{dark} = (\varepsilon_{nuc} + P_{nuc})u^{\mu}_1 u^{\nu}_1 - P_{nuc} g^{\mu\nu} \\
+ \quad & (\varepsilon_{dark} + P_{dark})u^{\mu}_2 u^{\nu}_2 - P_{dark} g^{\mu\nu}
\end{aligned} \tag{6.20}
$$

where u^{μ}_1, ε_{nuc} and P_{nuc} are the 4-velocity, energy density and pressure of nuclear matter respectively while the corresponding quantities in the second term are of dark matter.

For non-rotating case the metric is spherically symmetric and the hydrostatic equations of the two fluids can be written as coupled two-fluid Tolman-Oppenheimer-Volkoff (TOV) equations

$$
\begin{aligned}
\frac{dP_{nuc}(r)}{dr} &= -\frac{GM(r)\rho_{nuc}(r)}{r^2}\left(1 + \frac{P_{nuc}}{\varepsilon_{nuc}}\right) \times \\
&\left(1 + \frac{4\pi r^3 (P_{nuc} + P_{dark})}{M(r)c^2}\right)\left(1 - \frac{2GM(r)}{rc^2}\right)^{-1} \\
\frac{dP_{dark}(r)}{dr} &= -\frac{GM(r)\rho_{dark}(r)}{r^2}\left(1 + \frac{P_{dark}}{\varepsilon_{dark}}\right) \times
\end{aligned}
$$

$$\left(1+\frac{4\pi r^3(P_{nuc}+P_{dark})}{M(r)c^2}\right)\left(1-\frac{2GM(r)}{rc^2}\right)^{-1}$$

$$\frac{dM_{nuc}(r)}{dr}=4\pi r^2\rho_{nuc}(r)$$

$$\frac{dM_{dark}(r)}{dr}=4\pi r^2\rho_{dark}(r)$$

$$M(r)=M_{nuc}(r)+M_{dark}(r) \tag{6.21}$$

where $\rho_{nuc}=\varepsilon_{nuc}/c^2$, M_{nuc} is the mass density and total mass of nuclear matter while the corresponding quantities in the second equation are of dark matter. $M(r)$ is the total mass of nuclear and dark matter.

6.4 Theoretical calculations

The mass-radius relationship of non-rotating, rigidly rotating and differentially rotating neutron stars admixed with dark matter is calculated using the LORENE code. The nuclear matter and dark matter EoSs are fitted to a polytropic form $P=K\rho^\gamma$ where P is the pressure, ρ is the mass density, K the polytropic constant and γ the polytropic index for the corresponding fluid. For interacting nuclear matter $\gamma=2.03$ and $K=5.65283\times 10^{35}$ in C.G.S. units. For interacting dark matter $\gamma=1.97562$ and $K=1.33404\times 10^{36}$ in C.G.S. units. We take dark matter particle mass to be of 1 GeV and the exchange boson mass $m_I=100$ MeV, typical of strong interaction. First, we keep the dark matter central enthalpy to be $0.24c^2$ (fixed) and vary the nuclear matter central enthalpy for static, rigidly rotating and differentially rotating configurations and next we reverse the roles of nuclear and dark matter.

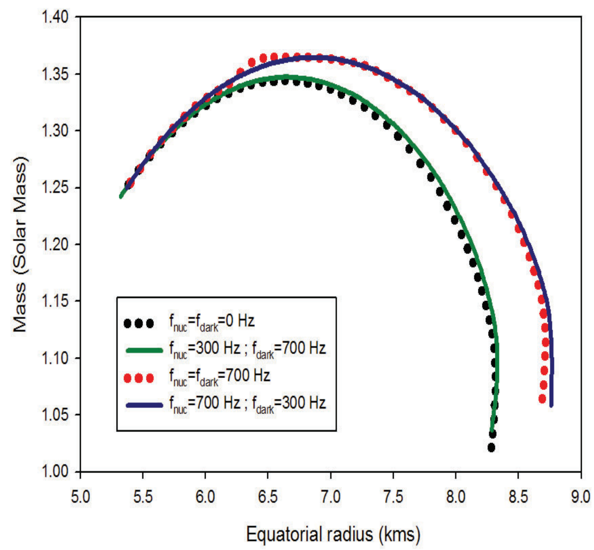

Figure 6.3: Plots of total mass vs. equatorial radius of static, rigidly rotating and differentially rotating neutron stars mixed with interacting fermionic Asymmetric Dark Matter with fixed dark matter central enthalpy ($0.24c^2$) and varying nuclear matter central enthalpies.

6.5 Results and Discussions

In Fig.-6.3 the plots of total mass vs. equatorial radius of static, rigidly and differentially rotating neutron stars mixed with fermionic self-interacting dark matter are shown for fixed dark matter central enthalpy ($0.24c^2$) and varying nuclear matter central enthalpies. In Fig.-6.4 the corresponding plots of mass vs. central baryonic number density are shown. The maximum mass of the neutron star mixed with strongly self-interacting dark matter goes to $1.3640M_\odot$ with a corresponding radius of 6.7523 kms for the case of differential rotation (frequency of dark matter to be 300 Hz and that of nuclear matter to be 700 Hz) as shown in Fig.-6.3. From Fig.-6.4 we see that the corresponding central baryonic number density is $2.1060fm^{-3}$. In this case, while the maximum gravitational mass is $1.3640M_\odot$, the corresponding matter mass is $1.5024M_\odot$ which constitutes of nuclear

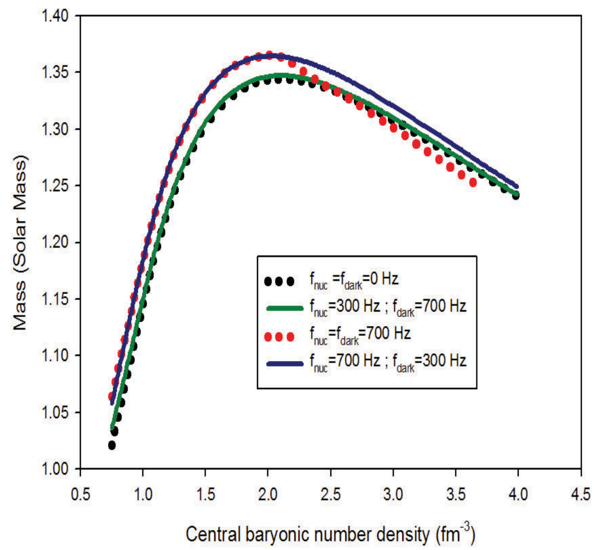

Figure 6.4: Plots of total mass vs. central baryonic density of static, rigidly rotating and differentially rotating neutron stars mixed with self-interacting fermionic Asymmetric Dark Matter with fixed dark matter central enthalpy ($0.24c^2$) and varying nuclear matter central enthalpies.

matter $1.4719M_\odot$ and dark matter $0.0305M_\odot$. In Fig.-6.5 the plots of total mass vs. equatorial radius of static, rigidly and differentially rotating neutron stars mixed with fermionic self-interacting dark matter are shown for fixed nuclear matter central enthalpy ($0.24c^2$) and varying dark matter central enthalpies. In Fig.-6.6 the corresponding plots of mass vs. central dark baryonic number density are shown. In this case the maximum mass goes to $1.9355M_\odot$ with a corresponding radius of 10.3717 kms for the case of differential rotation (frequency of dark matter to be 700 Hz and that of nuclear matter to be 300 Hz) as shown in Fig.-6.5. From Fig.-6.6 we see that the corresponding central dark baryonic number density is $1.1605fm^{-3}$. For this case, while the maximum gravitational mass is $1.9355M_\odot$, the corresponding matter mass is $2.1105M_\odot$ which constitutes of nuclear matter $0.1179M_\odot$ and dark matter $1.9926M_\odot$.

It is seen that the polytropic indices γ for nuclear and self-interacting dark matter EoSs

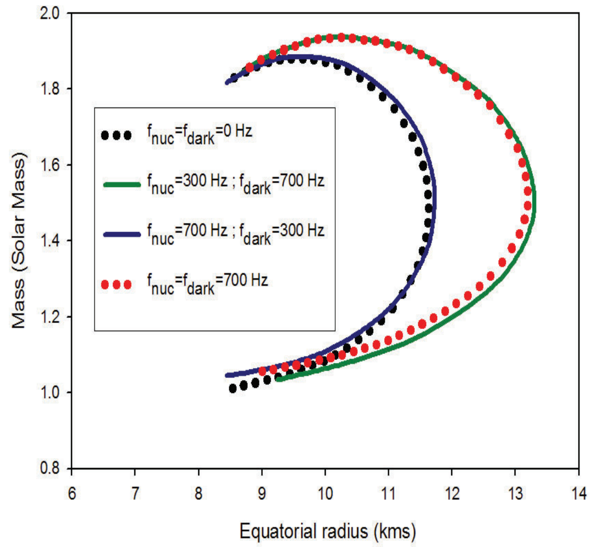

Figure 6.5: Plots of total mass vs. equatorial radius of static, rigidly rotating and differentially rotating neutron stars mixed with interacting fermionic Asymmetric Dark Matter with fixed nuclear matter central enthalpy ($0.24c^2$) and varying dark matter central enthalpies.

are approximately equal, but the polytropic coefficient K for dark matter is about 2.5 times larger than that of nuclear matter making dark matter EoS stiffer. Consequently, configurations of stars with varying dark matter central enthalpy with fixed nuclear matter central enthalpy are more massive than those obtained for the reverse case.

From Fig.-6.5 we see that the dark matter dominated neutron star behaves differently than the nuclear matter dominated one as shown in Fig.-6.3. In Fig.-6.5, the plots of low mass neutron stars admixed with dark matter typically show characteristics similar to low mass self-bound strange stars. This is because of the very strong two-body repulsive interactions of dark matter which is dominant in the configuration of Fig.-6.5 which counteracts gravity effectively for low mass region and makes radius much smaller compared to pure neutron star of similar mass (vide Fig.-4.4). Thus, while the nuclear matter dominance induces gravitational binding, dark matter dominant low mass neutron

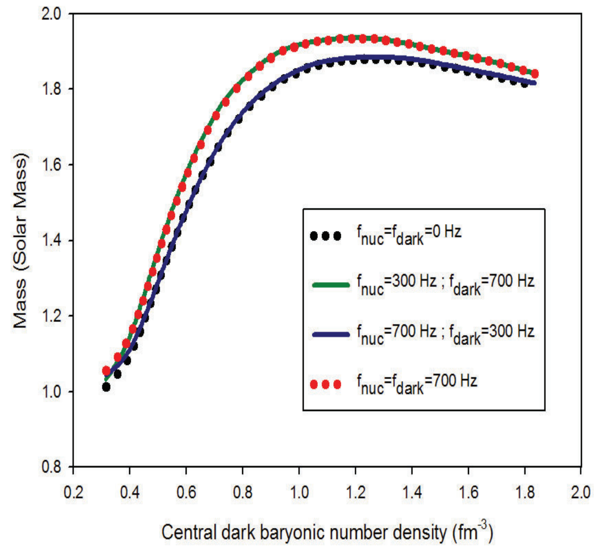

Figure 6.6: Plots of total mass vs. central dark matter density of static, rigidly rotating and differentially rotating neutron stars mixed with self-interacting fermionic Asymmetric Dark Matter with fixed nuclear matter central enthalpy ($0.24c^2$) and varying dark matter central enthalpies.

star becomes gravitationally bound at much smaller radius.

The maximum mass for non-rotating dark matter stars goes to $3.0279 M_\odot$ with a radius of 16.2349 kms for particle mass $m_\chi = 1$ GeV, and that for rotating stars it goes to $3.1460 M_\odot$ with a radius of 19.2173 kms. However, if one takes m_χ to be 0.5 GeV, then the maximum mass goes to $\sim 12.6 M_\odot$ using the relation Mass $\propto 1/m_\chi^2$ [182], thus mimicking stellar mass black holes.

Chapter 7

CONCLUDING REMARKS

In summary, we have considered a relativistic, degenerate electron gas at zero temperature under the influence of a density dependent magnetic field. Since the electrons are Landau quantized, the density of states gets modified due to the presence of the magnetic field. This, in turn, modifies the EoS of the white dwarf matter. The presence of magnetic field also gives rise to magnetic energy density and pressure which is added to those due to degenerate matter. We find that the masses of such white dwarfs increase with the magnitude of the central magnetic field. Hence we obtain a conclusive result that it is possible to have electron-degenerate magnetized white dwarfs, with masses significantly greater than the Chandrasekhar limit in the range of $\sim 3\ M_{\odot}$, provided it has an appropriate magnetic field profile with high magnitude at the centre as well as high central density.

To date there are about $\sim$250 magnetized white dwarfs with well determined fields [60] and over $\sim$600 if objects with no or uncertain field determination [197, 198] are also included. Surveys such as the SDSS, HQS and the Cape Survey have discovered these magnetized white dwarfs. The complete samples show that the field distribution of magnetized white dwarfs is in the range 10^3-10^9 gauss which basically provides the surface magnetic fields. However, the central magnetic field strength, which is presumably unobserved by the above observations, could be several orders of magnitude higher than the surface field. In fact, it is the central magnetic field which is crucial for super-Chandrasekhar magnetized white dwarfs. However, the softening of the EoS accompanying the onset of electron captures and pycnonuclear reactions in the core of these stars can lead to local instabilities which set an upper limit to the magnetic field strength at the center of the star, ranging from 10^{14}-10^{16} gauss depending on the core [68] composition.

The DDM3Y effective interaction which provides a unified description of elastic and inelastic scattering, proton-, α-, cluster- radioactivities and nuclear matter properties, also provides an excellent description of the β-equilibrated neutron star matter [115] which is stiff enough at high densities to reconcile with the recent observations of the massive compact stars [70, 71, 72] while the corresponding symmetry energy is supersoft as preferred by the FOPI/GSI experimental data [105, 199]. The experimental range of values quoted in Table-4.5 along with discussions provided above justifies the parameter set of $n = \frac{2}{3}$, C=2.2497±0.0420 and β=1.5934±0.0085 fm^2. The neutron star core-crust transition density, pressure and proton fraction determined from the thermodynamic stability condition to be $\rho_t = 0.0938$ fm^{-3}, P$_t$ = 0.5006 MeV fm^{-3} and $x_{p(t)} = 0.0308$, respectively, along with observed minimum crustal fraction of the total moment of inertia of the Vela pulsar provide a limit for its radius. It is somewhat different from the other estimates [18, 200] and imposes a constraint $R \geq 4.10+3.36M/M_\odot$ km for the mass-radius relation of Vela pulsar like neutron stars.

Next, we have studied the r-mode instability of slowly rotating neutron stars with rigid crusts with their EoS obtained from the DDM3Y effective nucleon-nucleon interaction. We have calculated the fiducial gravitational radiation and shear viscosity timescales within the DDM3Y framework for a wide range of neutron star masses. It is observed that the gravitational radiation timescale decreases rapidly with increasing neutron star mass while the viscous damping timescales exhibit an approximate linear increase. Next, we have studied the temperature dependence of the critical angular frequency for different neutron star masses. It is observed that the majority of the neutron stars do not lie in the r-mode instability region. This fact is highlighted in Fig.-5.4 where the spin frequencies and core temperatures of observed Low Mass X-ray Binaries and Millisecond Radio Pulsars [164] always lie below the region of r-mode instability. The implication is that for neutron stars rotating with frequencies greater than their corresponding critical frequencies have unstable r-modes leading to the emission of gravitational waves. Further, our study of the variation of the critical temperature as a function of mass shows that both the critical frequency and temperature decrease with increasing mass. The conclusion is that massive hot neutron stars are more susceptible to r-mode instability through gravitational radiation. Finally we have calculated the spin down rates and angular frequency evolution of the neutron stars through r-mode instability. We have also pointed out the fact that the critical frequency depends on the EoS through the radius and the symmetry energy slope parameter L. If the dissipation of r-modes from shear viscosity acts along the boundary layer of the crust-core interface then the r-mode instability region is enlarged to lower values of L. The effect of bulk viscosity and the shear viscosity in the core [201] using DDM3Y effective interaction has recently been explored [202].

Further, we have consider fermionic Asymmetric Dark Matter (ADM) particles of mass 1 GeV and the self-interaction mediator mass of 100 MeV (low mass implying strong interaction), mixed with rotating and non-rotating neutron stars. These ADM particles are non self-annihilating and behaves like ordinary free particles. We have shown that massive exotic neutron star with a strong two-body self-interacting fermionic dark matter is gravitationally stable with equal or unequal rotational frequencies of the two fluids. This provides an alternative scenario for the existence of $\sim 2M_{\odot}$ neutron stars with 'stiff' equations of states.

The mass-radius relations of pure hadronic stars mixed with self-interacting fermionic Asymmetric Dark Matter have been obtained using the LORENE code. For the case of pure dark matter stars consisting of less massive dark particles we see that the maximum masses can be comparable to that of stellar mass black holes. For the case of hadronic stars mixed with dark matter, we considered three different configurations - static, rigid rotation and differential rotation of nuclear matter and dark matter fluids. From the results, we conclude that for the dark matter dominated configurations the masses are more, *viz.* for the static case the maximum masses of these hybrid stars can reach upto $\sim 1.88 M_{\odot}$ with corresponding radii ~ 9.5 kms whereas in the rigid and differential rotational cases the maximum masses of these hybrid stars can reach upto $\sim 1.94 M_{\odot}$ with corresponding equatorial radii ~ 10.4 kms.

We also find that the dark matter dominated neutron star behaves differently than the nuclear matter dominated one that show characteristics similar to low mass self-bound strange stars. This is because of the very strong two-body repulsive interactions of dark matter which is dominant in the low mass region where it counteracts gravity effectively to make radius much smaller. Thus, while the nuclear matter dominance induces gravitational binding, dark matter dominant low mass neutron star becomes more compact. However, if the dark matter particle mass is small compared to the nucleon mass the maximum mass may well be above $2M_{\odot}$, provided no phase transition from nuclear to quark matter occurs.

In the past, phase transition and the possible existence of exotic phases like condensates or quark matter inside neutron stars have been studied extensively [203, 204, 205, 206, 207]. Since this is an era of gravitational waves, it will be interesting to find the effect of such phases on the tidal deformabilities of neutron stars in the near future. Recently crystallization of matter in white dwarfs have been observed by the Gaia satellite [208]. The upcoming gravitational wave detectors with higher sensitivities may put light on these phases of matter inside white dwarfs in the not so far future. Existence of dark matter inside compact stars also can be probed gravitationally. Such effects cannot be predicted a priori without full calculations, and we leave them for future investigation.

Bibliography

[1] S. Chandrasekhar, Mon. Not. R. Astron. Soc. **95**, 207 (1935).

[2] Ivan Marti-Vidal, Sebastien Muller, Wouter Vlemmings, Cathy Horellou and Susanne Aalto, Science **348**, 6232 (2015).

[3] M.E. Caplan and C.J. Horowitz, Rev. Mod. Phys. **89**, 041002 (2017).

[4] I. Bednarek, P. Haensel, J. L. Zdunik, M. Bejger and R. Mańka, Astron.& Astrophys. **543**, A157 (2012).

[5] G.F. Burgio, M. Baldo, P.K. Sahu and H.J. Schulze, Phys. Rev. **C 66**, 025802 (2002).

[6] P. Haensel and M. Proszynski, Astrophys. J. **258**, 306 (1982).

[7] Yeunhwan Lim, Kyujin Kwak, Chang Ho Hyun and Chang-Hwan Lee, Phys. Rev. **C 89**, 055804 (2014).

[8] R.P. Feynman, N. Metropolis and E. Teller, Phys. Rev. **75**, 1561 (1949).

[9] G. Baym, C.J. Pethick and P. Sutherland, Astrophys. J. **170**, 299 (1971).

[10] G. Baym, H.A. Bethe and C.J. Pethick, Nucl. Phys. **A 175**, 225 (1971).

[11] E. Chabanat, P. Bonche, P. Haensel, J. Meyer and R. Schaeffer, Nucl. Phys. **A 627**, 710 (1997).

[12] E. Chabanat, P. Bonche, P. Haensel, J. Meyer and R. Schaeffer, Nucl. Phys. **A 635**, 231 (1998).

[13] A. Akmal, V.R. Pandharipande and D.G. Ravenhall, Phys. Rev. **C 58**, 1804 (1998).

[14] C.J. Pethick, D.G. Ravenhall and C.R. Lorenz, Nucl. Phys. **A 584**, 675 (1995).

[15] I. Bombaci, A. Bonaccorso and A. Fabrocini, *Perspectives on Theoretical Nuclear Physics* , 229 (1995).

[16] Horst Mueller and Brian D. Serot, Nucl. Phys. **A 606**, 508 (1996).

[17] A.G. Lyne in *Pulsars: Problems and Progress*, S. Johnston, M. A. Walker and M. Bailes, eds., 73 (ASP, 1996).

[18] B. Link, R.I. Epstein and J.M. Lattimer, Phys. Rev. **Lett. 83**, 3362 (1999).

[19] R.I. Epstein and G. Baym, Astrophys. J. **387**, 276 (1992).

[20] M.A. Alpar, H.F. Chau, K.S. Cheng and D. Pines, Astrophys. J. **409**, 345 (1993).

[21] B. Link and R.I. Epstein, Astrophys. J. **457**, 844 (1996).

[22] M. Ruderman, T. Zhu and K. Chen, Astrophys. J. **492**, 267 (1998).

[23] A. Sedrakian and J.M. Cordes, Mon. Not. R. Astron. Soc. **307**, 365 (1999).

[24] G.Bertsch, J.Borysowicz, H.McManus, W.G.Love, Nucl. Phys. **A 284**, 399 (1977).

[25] G. R. Satchler and W. G. Love, Phys. Reports **55**, 183 (1979).

[26] R. G. Seyler and C. H. Blanchard, Phys. Rev. **124**, 227 (1961).

[27] R. G. Seyler and C. H. Blanchard, Phys. Rev. **131**, 355 (1963).

[28] D. Bandyopadhyay and S. K. Samaddar, Nucl. Phys. **A 484**, 315 (1988).

[29] C. Samanta, D. Bandyopadhyay and J. N. De, Phys. Lett. **B 217**, 381 (1989).

[30] D. Bandyopadhyay, C. Samanta, S. K. Samaddar and J. N. De, Nucl. Phys. **A 511**, 1 (1990).

[31] D. Vautherin and D.M. Brink, Phys. Rev. **C 5**, 626 (1972).

[32] Y.M. Engel, D.M. Brink, K. Goeke, S.J. Krieger and D. Vautherin, Nucl. Phys. **A 249**, 215 (1975).

[33] P. Bonche and D. Vautherin, Nucl. Phys. **A 372**, 496 (1981).

[34] B. Behera, T. R. Routray and R. K. Satpathy, J. Phys. **G 24**, 2073 (1998).

[35] B. Behera, T. R. Routray, B. Sahoo and R. K. Satpathy, Nucl. Phys. **A 699**, 770 (2002).

[36] T. R. Routray, X. Viñas, D. N. Basu, S. P. Pattnaik, M. Centelles, L. M. Robledo and B. Behera, J. Phys. **G 43**, 105101 (2016).

[37] P. Roy Chowdhury, D.N. Basu and C. Samanta, Phys. Rev. **C 80**, 011305(R) (2009).

[38] D.N. Basu, P. Roy Chowdhury and C. Samanta, Phys. Rev. **C 80**, 057304 (2009).

[39] Debasis Atta and D.N. Basu, Phys. Rev. **C 90**, 035802 (2014).

[40] J.M. Lattimer and M. Prakash, Phys. Rep. **442**, 109 (2007).

[41] S. Kubis, Phys. Rev. **C 70**, 065804 (2004).

[42] S. Kubis, Phys. Rev. **C 76**, 025801 (2007).

[43] A. Worley, P.G. Krastev and B.A. Li, Astrophys. J. **685**, 390 (2008).

[44] H.B. Callen, *Thermodynamics and An Introduction to Thermostatistics*, 2nd edition, John Wiley & Sons, New York (1985).

[45] R.C. Tolman, Phys. Rev. **55**, 364 (1939).

[46] J.R. Oppenheimer and G.M. Volkoff, Phys. Rev. **55**, 374 (1939).

[47] B.P. Abbott et.al., Phys. Rev. **Lett. 119**, 161101 (2017).

[48] G. Steigman, C. Sarazin, H. Quintana and J. Faulkner, Astron. J. **06**, 1050 (1978).

[49] I. Goldman and S. Nussinov, Phys. Rev. **D 40**, 3221 (1989).

[50] G. Bertone and M. Fairbairn, Phys. Rev. **D 77**, 043515 (2008).

[51] M. T. Frandsen and S. Sarkar, Phys. Rev. **105**, 011301 (2010).

[52] P. Ciarcelluti and F. Sandin, Phys. Lett. **B 695**, 19 (2011).

[53] S.-C. Leung, M.-C. Chu and L.-M. Lin, Phys. Rev. **D 84**,107301 (2011).

[54] X. Y. Li, F. Y. Wang and K. S. Cheng, JCAP **10**, 031 (2012).

[55] D. Andrew Howell et al., Nature **443**, 308 (2006).

[56] R. A. Scalzo et al., Astrophys. J. **713**, 1073 (2010).

[57] M. Hicken et al., Astrophys. J. **669**, L17 (2007).

[58] M. Yamanaka et al., Astrophys. J. **707**, L118 (2009).

[59] Jeffrey M. Silverman et al., Mon. Not. R. Astron. Soc., **410**, 1 (2011).

[60] Lilia Ferrario, Domitilla deMartino, Boris T. Gansicke, arXiv: 1504.08072v1 (2015).

[61] A. A. Sokolov and I. M. Ternov, *Synchrotron Radiation* (Pergamon, Oxford) (1968).

[62] L. D. Landau and E. M. Lifshitz, *Quantum Mechanics* (3rd. ed.; Oxford: Pergamon) (1977).

[63] V. Canuto and J. Ventura, Fundam. Cosm. Phys. **2**, 203 (1977).

[64] P. Mészáros, *High Energy Radiation from Magnetized Neutron Stars* (University of Chicago, Chicago) (1992).

[65] Dong Lai and Stuart L. Shapiro, Astrophys. J. **383**, 745 (1991).

[66] M. Rotondo et al., Phys. Rev. **C 83**, 045805 (2011).

[67] D. Bandyopadhyay, S. Chakrabarty and S. Pal, Phys. Rev. **Lett. 79**, 2176 (1997).

[68] N. Chamel, A. F. Fantina and P. J. Davis, Phys. Rev. **D 88**, 081301(R) (2013).

[69] H. Komatsu, Y. Eriguchi, I. Hachisu, Mon. Not. R. Astron. Soc. **237**, 355 (1989).

[70] P. R. Chowdhury, A. Bhattacharyya, D. N. Basu, Phys. Rev. **C 81**, 062801(R) (2010).

[71] Abhishek Mishra, P. R. Chowdhury and D. N. Basu, Astropart. Phys. **36**, 42 (2012).

[72] D. N. Basu, Partha Roy Chowdhury and Abhishek Mishra, Eur. Phys. J. **Plus 129**, 62 (2014).

[73] V. S. Uma Maheswari, D. N. Basu, J. N. De and S. K. Samaddar, Nucl. Phys. **A 615**, 516 (1997).

[74] U. Das and B. Mukhopadhyay, Phys. Rev. **D 86**, 042001 (2012).

[75] U. Das and B. Mukhopadhyay, Phys. Rev. **Lett. 110**, 071102 (2013).

[76] J. M. Dong, W. Zuo, P. Yin and J. Z. Gu, Phys. Rev. **Lett. 112**, 039001 (2014).

[77] N. Chamel, Zh. K. Stoyanov, L. M. Mihailov, Y. D. Mutafchieva, R. L. Pavlov and Ch. J. Velchev, Phys. Rev. **C 91**, 065801 (2015).

[78] G. R. Satchler, *Int. series of monographs on Physics*, Oxford University Press, *Direct Nuclear reactions*, 470 (1983).

[79] Dao T. Khoa and W. von Oertzen, Phys. Lett. **B 304**, 8 (1993).

[80] Dao T. Khoa, W. von Oertzen and A. A. Ogloblin, Nucl. Phys. **A 602**, 98 (1996).

[81] Dao T. Khoa, G. R. Satchler and W. von Oertzen, Phys. Rev. **C 56**, 954 (1997).

[82] H. Nakada, Phys. Rev. **C 68**, 014315 (2003).

[83] H. Nakada, Phys. Rev. **C 78**, 054301 (2008).

[84] H. Nakada, Phys. Rev. **C 81**, 027301 (2010).

[85] A. K. Chaudhuri, D. N. Basu and Bikash Sinha, Nucl. Phys. **A 439**, 415 (1985).

[86] D N Basu, P Roy Chowdhury and C Samanta, Nucl. Phys. **A 811**, 140 (2008).

[87] W. D. Myers, Nucl. Phys. **A 204**, 465 (1973).

[88] P Roy Chowdhury and D N Basu, Acta Phys. Pol. **B 37**,1833 (2006).

[89] G Audi, A H Wapstra and C Thibault, Nucl. Phys. **A 729**, 337 (2003).

[90] D Lunney, J M Pearson and C Thibault, Rev. Mod. Phys. **75**, 1021 (2003).

[91] G Royer and C Gautier, Phys. Rev. **C 73**, 067302 (2006).

[92] G. A. Lalazissis, J. Konig and P. Ring, Phys. Rev. **C 55**, 540 (1997).

[93] G. A. Lalazissis, S. Raman, and P. Ring, At. Data and Nucl. Data Tables **71**, 1 (1999).

[94] D. Atta, S. Mukhopadhyay and D. N. Basu, Indian J. Phys **91**, 235 (2017).

[95] P. Danielewicz, R. Lacey and W.G. Lynch, Science **298**, 1592 (2002).

[96] S Shlomo, V M Kolomietz and G Coló, Eur. Phys. J. **A 30**, 23 (2006).

[97] Y.W. Lui, D.H. Youngblood, Y. Tokimoto, H.L. Clark and B. John, Phys. Rev. **C 69**, 034611 (2004).

[98] D. H. Youngblood, Y. W. Lui, B. John, Y. Tokimoto, H. L. Clark and X. Chen, Phys. Rev. **C 69**, 054312 (2004).

[99] Y. W. Lui, D. H. Youngblood, H. L. Clark, Y. Tokimoto and B. John, Acta Phys. Pol. **B 36**, 1107 (2005).

[100] J. P. Blaizot, Phys. Rep. **64**, 171 (1980).

[101] J. P. Blaizot, J. E. Berger, J. Dechargé and M. Girod, Nucl. Phys. **A 591**, 435 (1995).

[102] D. Vretenar, T. Nikśić and P. Ring, Phys. Rev. **C 68**, 024310 (2003).

[103] M. M. Sharma, Nucl. Phys. **A 816**, 65 (2009).

[104] T. Klähn et al., Phys. Rev. **C 74**, 035802 (2006).

[105] Zhigang Xiao, Bao-An Li, Lie-Wen Chen, Gao-Chan Yong and Ming Zhang, Phys. Rev.**Lett. 102**, 062502 (2009).

[106] T. Mukhopadhyay and D.N. Basu, Nucl. Phys. **A 789**, 201 (2007).

[107] A. W. Steiner, M. Prakash, J. M. Lattimer and P. J. Ellis, Phys. Rep. **411**, 325 (2005).

[108] P. Danielewicz, Nucl. Phys. **A 727**, 233 (2003).

[109] K. Pomorski and J. Dudek, Phys. Rev. **C 67**, 044316 (2003).

[110] L. Bennour et al., Phys. Rev. **C 40**, 2834 (1989).

[111] C. J. Horowitz and J. Piekarewicz, Phys. Rev. **Lett. 86**, 5647 (2001); B. G. Todd-Rutel and J. Piekarewicz, Phys. Rev. **Lett. 95**, 122501 (2005).

[112] L. W. Chen, C. M. Ko, and B. A. Li, Phys. Rev. **Lett. 94**, 032701 (2005); Phys. Rev. **C 72**, 064309 (2005).

[113] A. W. Steiner and B. A. Li, Phys. Rev. **C 72**, 041601(R) (2005).

[114] M. Centelles, X. Roca-Maza, X. Vinas and M. Warda, Phys. Rev. **Lett. 102**, 122502 (2009).

[115] D. N. Basu, Partha Roy Chowdhury and Abhishek Mishra, Eur. Phys. J. **Plus 129**, 62 (2014).

[116] P. Roy Chowdhury, D. N. Basu and C. Samanta, Phys. Rev. **C 80**, 011305(R) (2009); D. N. Basu, P. Roy Chowdhury and C. Samanta, Phys. Rev. **C 80**, 057304 (2009).

[117] M. B. Tsang, Yingxun Zhang, P. Danielewicz, M. Famiano, Zhuxia Li, W. G. Lynch and A.W. Steiner, Phys. Rev. **Lett. 102**, 122701 (2009).

[118] J. Piekarewicz and M. Centelles, Phys. Rev. **C 79**, 054311 (2009).

[119] M. Dutra, O. Lourenco, J. S. Sa Martins, A. Delfino, J. R. Stone and P. D. Stevenson, Phys. Rev. **C 85**, 035201 (2012).

[120] Hiroyuki Sagawa, Satoshi Yoshida, Guo-Mo Zeng, Jian-Zhong Gu and Xi-Zhen Zhang, Phys. Rev. **C 76**, 034327 (2007).

[121] M. Warda, X. Viñas, X. Roca-Maza and M. Centelles, Phys. Rev. **C 80**, 024316 (2009).

[122] B. K. Agrawal, J. N. De, S. K. Samaddar, G. Colò and A. Sulaksono, Phys. Rev. **C 87**, 051306(R) (2013).

[123] Bao-An Li and Xiao Han, Phys. Lett. **B 727**, 276 (2013).

[124] C. Mondal, B. K. Agrawal, J. N. De, S. K. Samaddar, M. Centelles and X. Viñas, Phys. Rev. **C 96**, 021302(R) (2017).

[125] M. Oertel, M. Hempel, T. Klähn and S. Typel, Rev. Mod. Phys. **89**, 015007 (2017).

[126] P. Roy Chowdhury, C. Samanta and D. N. Basu, Phys. Rev. **C 73**, 014612 (2006); *ibid* Phys. Rev. **C 77**, 044603 (2008); *ibid* Atomic Data and Nuclear Data Tables **94**, 781 (2008).

[127] C. Samanta, P. Roy Chowdhury and D.N. Basu, Nucl. Phys. **A 789**, 142 (2007).

[128] De-Hua Wen, Bao-An Li and Lie-Wen Chen, Phys. Rev. **Lett. 103**, 211102 (2009).

[129] F. Gulminelli, Ad. R. Raduta, *Phys. Rev.* **C 92**, 055803 (2015).

[130] H. Pais, A. Sulaksono, B. K. Agrawal and C. Providência, *Phys. Rev.* **C 93**, 045802 (2016).

[131] C. Ducoin, J. Margueron, and P. Chomaz, *Nucl. Phys.* **A 809**, 30 (2008).

[132] C. J. Horowitz and G. Shen, *Phys. Rev.* **C 78**, 015801 (2008).

[133] C. Ducoin, J. Margueron, C. Providência and I. Vidaña, *Phys. Rev.* **C 83**, 045810 (2011).

[134] J B Hartle, Astrophys. J. **150**, 1005 (1967).

[135] W D Arnett and R L Bowers, Astrophys. J. Suppl. **33**, 415 (1977).

[136] J Xu, L W Chen, B A Li and H R Ma, Astrophys. J. **697**, 1549 (2009).

[137] T Li, U Garg, Y Liu et al., Phys. Rev. **Lett. 99**, 162503 (2007).

[138] P B Demorest, T Pennucci, S M Ransom, M S E Roberts and J W T Hessels, Nature **467**, 1081 (2010).

[139] J Antoniadis et al.,Science **340**, 6131 (2013).

[140] Doan Thi Loan, Ngo Hai Tan, Dao T Khoa and Jerome Margueron, Phys. Rev. **C 83**, 065809 (2011) and references therein.

[141] P Haensel, A Y Potekhin and D G Yakovlev, *Astrophysics and space science library*, 326 (2006).

[142] N. Andersson, Astrophys. J. **502**, 708 (1998).

[143] N. Andersson, Class. Quantum Grav. **20**, R105 (2003).

[144] J. L. Friedman and S. M. Morsink, Astrophys. J. **502**, 714 (1998).

[145] J. Provost, G. Berthomieu and A. Rocca, Astron.& Astrophys. **94**, 126 (1981).

[146] N. Andersson and K. D. Kokkotas, Int. J. Mod. Phys. **D 10**, 381 (2001).

[147] R. Bondarescu, S. A. Teukolsky, and I. Wasserman, Phys. Rev. **D 76**, 064019 (2007).

[148] N. Andersson, K. D. Kokkotas, and B. F. Schutz, Astrophys. J. **510**, 846 (1999).

[149] J. Papaloizou and J. E. Pringle, Mon. Not. R. Astron. Soc. **182**, 423 (1978).

[150] L. Lindblom, B. J. Owen, and S. M. Morsink, Phys. Rev. **Lett. 80**, 4843 (1998).

[151] C. Cutler and L. Lindblom, Astrophys. J. **314**, 234 (1987).

[152] L. Lindblom, B. J. Owen, and G. Ushomirsky, Phys. Rev. **D 62**, 084030 (2000).

[153] B. J. Owen, L. Lindblom, C. Cutler, B. F. Schutz, A. Vecchio, and N. Andersson, Phys. Rev. **D 58**, 084020 (1998).

[154] L. Lindblom, G. Mendell and B. J. Owen, Phys. Rev. **D 60**, 064006 (1999).

[155] I. Vidaña, Phys. Rev. **C 85**, 045808 (2012).

[156] K. S. Thorne, Rev. Mod. Phys. **52**, 299 (1980).

[157] J. Ipser and L. Lindblom, Astrophys. J. **373**, 213 (1991).

[158] Y. Levin and G. Ushomirsky, Mon. Not. R. Astron. Soc. **324**, 917 (2001).

[159] L. Bildsten and G. Ushomirsky, Astrophys. J. Lett. **529**, L33(2000).

[160] Ch. Moustakidis, Phys. Rev. **C 91**,035804 (2015).

[161] E. Flowers and N. Itoh, Astrophys. J. **230**, 847 (1979).

[162] C. Cutler and L. Lindblom, Astrophys. J. **314**, 234 (1987).

[163] R. Bondarescu, S. A. Teukolsky, and I. Wasserman, Phys. Rev. **D 79**, 104003 (2009).

[164] B. Haskell, N. Degenaar and W. C. G. Ho, Mon. Not. R. Astron. Soc. **424**, 93 (2012).

[165] D. H. Wen, W. G. Newton and B. A. Li, Phys. Rev. **C 85**, 025801 (2012).

[166] Y. Utsumi et al., Astrophys. J. **833**, 156 (2016).

[167] Gianfranco Bertone, Dan Hooper and Joseph Silk, Physics Reports **405**, 279 (2005).

[168] George R. Blumenthal, S. M. Faber, Joel R. Primack and Martin J. Rees, Nature **311**, 517 (1984).

[169] S. King and A. Merle, JCAP **016**, 1208 (2012).

[170] Kathryn M. Zurek, Physics Reports **537**, 91 (2014).

[171] C. S. Frenk and S. D. M. White, Ann. Phys. **524**, 507 (2012).

[172] Douglas Spolyar, Katherine Freese and Paolo Gondolo, Phys. Rev. **Lett. 100**, 051101 (2008).

[173] Alan H. Guth, Mark P. Hertzberg and C. Prescod-Weinstein, Phys. Rev. **D 92**, 103513 (2015).

[174] X. Li, T. Harko and K. Cheng, JCAP **06**, 001 (2012).

[175] A. de Lavallaz and M. Fairbairn, Phys. Rev. **D 81**, 123521 (2010).

[176] C. Kouvaris and P. Tinyakov, Phys. Rev. **D 82**, 063531 (2010).

[177] C. Kouvaris and P. Tinyakov, Phys. Rev. **D 83**, 083512 (2011).

[178] David M. Jacobs, Glenn D. Starkman and Bryan W. Lynn, Mon. Not. R. Astron. Soc. **450**, 3418 (2015).

[179] C. Kouvaris, Phys. Rev. **D 77**, 023006 (2008).

[180] M. McCullough and M. Fairbairn, Phys. Rev. **D 81**, 083520 (2010).

[181] M. Ángeles Pérez-García and J. Silk, Phys. Lett. **B 711**, 6 (2012).

[182] Gaurav Narain, Jürgen Schaffner-Bielich and Igor N. Mishustin, Phys. Rev. **D 74**, 063003 (2006).

[183] Ang Li, Feng Huang and Ren-Xin Xu, Astroparticle Physics **37**, 70 (2012).

[184] Qian-Fei Xiang, Wei-Zhou Jiang, Dong-Rui Zhang and Rong-Yao Yang, Phys. Rev. **C 89**, 025803 (2014).

[185] M. R. S. Hawkins, Mon. Not. R. Astron. Soc. **415**, 2744 (2011).

[186] Laura Tolos and Jürgen Schaffner-Bielich, Phys.Rev. **D 92**, 123002 (2015).

[187] I. Goldman, R. N. Mohapatra, S. Nussinov, D. Rosenbaum and V. Teplitz, Phys. Lett. **B 725**, 200 (2013).

[188] Jason Pollack, David N. Spergel and Paul J. Steinhardt, Astrophys. J. **804**, 131 (2015).

[189] Yonit Hochberg, Eric Kuflik, Hitoshi Murayama, Tomer Volansky and Jay G. Wacker, Phys. Rev. **Lett. 115**, 021301 (2015).

[190] Chian-Shu Chen, Guey-Lin Lin and Yen-Hsun Lin, JCAP **01**, 013 (2016).

[191] James M. Cline, Zuowei Liu, Guy D. Moore, and Wei Xue, Phys. Rev. **D 90**, 015023 (2014).

[192] Kimberly K. Boddy, Jonathan L. Feng, Manoj Kaplinghat, and Tim M.P. Tait, Phys. Rev. **D 89**, 115017 (2014).

[193] Miguel Rocha, Annika H. G. Peter, James S. Bullock, Manoj Kaplinghat, Shea Garrison-Kimmel, Jose Oñorbe and Leonidas A. Moustakas, Mon. Not. R. Astron. Soc. **430**, 81 (2013).

[194] Eric Gourgoulhon arXiv:1003.5015v2 (2011).

[195] Stuart L. Shapiro and Saul A. Teukolsky, *Black Holes, White Dwarfs and Neutron Stars: The Physics of Compact Objects* (1983).

[196] F. Sandin and P. Ciarcelluti, Astroparticle Physics **32**, 278 (2009).

[197] S. O. Kepler, I. Pelisoli, S. Jordan, S. J. Kleinman, D. Koester, B. Külebi, V. Pecanha, B. G. Castanheira, A. Nitta, J. E. S. Costa, D. E. Winget, A Kanaan, and L. Fraga, Mon. Not. R. Astron. Soc. **429**, 2934 (2013).

[198] S. O. Kepler, I. Pelisoli, D. Koester, G. Ourique, S. J. Kleinman, A. D. Romero, A. Nitta, D. J. Eisenstein, J. E. S. Costa, B. Külebi, S. Jordan, P. Dufour, P. Giommi and A. Rebassa-Mansergas, Mon. Not. R. Astron. Soc. **446**, 4078 (2015).

[199] W Reisdorf et al., Nucl. Phys. **A 781**, 459 (2007).

[200] Jun Xu, Lie-Wen Chen, Bao-An Li and Hong-Ru Ma, Phys. Rev. **C 79**, 035802 (2009).

[201] S. P. Pattnaik, T. R. Routray, X. Viñas, D. N. Basu, M. Centelles, K. Madhuri and B. Behera, J. Phys. **G 45**, 055202 (2018).

[202] Sujan Roy, Somnath Mukhopadhyay, Joydev Lahiri, Debasis Atta, Partha Roy Chowdhury and D.N. Basu, arXiv:1905.06158 (2019).

[203] B. Kämpfer, J. Phys. **A 14**, L471 (1981).

[204] B. Kämpfer, J. Phys. **G 9**, 1487 (1983).

[205] Jean Macher and Jürgen Schaffner-Beilich, Eur. J. Phys. **26**, 341 (2005).

[206] B. K. Sharma, P. K. Panda, and S. K. Patra, Phys. Rev. **C 75**, 035808 (2007).

[207] J. L. Zdunik and P. Haensel, Astron.& Astrophys. **551**, A61 (2013).

[208] Pier-Emmanuel Tremblay et al., Nature **565**, 202-205 (2019).